JPL NO. 9950 – 1096

December 15, 1983

Final Report
Covering the Period: 1 May 1980 through 31 October 1983

HOMOGENEOUS AND HETEROGENEOUS PROCESSES OF ATMOSPHERIC INTEREST

By: Michel J. Rossi, John R. Barker, and David M. Golden
Department of Chemical Kinetics

Prepared for:

NATIONAL AERONAUTICS AND SPACE ADMINISTRATION
UPPER ATMOSPHERE RESEARCH OFFICE, CODE SU
600 Independence Avenue, SE
Washington, DC 20546

Attention: R. T. Watson
Manager, Upper Atmospheric Research Program
EPM-20

SRI Project PYU-6534
Contract No. JPL ~~9545815~~ 954815

Approved:

M. E. Hill, Laboratory Director
Chemistry Laboratory

G. R. Abrahamson, Vice President
Physical Sciences Division

SRI International
333 Ravenswood Ave. • Menlo Park, CA 94025
415 326-6200 • TWX: 910-373-2046 • Telex: 334-486

INTRODUCTION

This Final Report contains the following papers and reports written during the course of JPL/NASA-sponsored upper atmospheric research program in the Department of Chemical Kinetics at SRI International for the contract period.

Chapter

This report was prepared for the Jet Propulsion Laboratory, California Institute of Technology, sponsored by the National Aeronautics and Space Administration.

Chapter I

THIRD-ORDER RATE CONSTANTS OF ATMOSPHERIC IMPORTANCE

Roger Patrick, and David M. Golden

(International Journal of Chemical Kinetics, 1983, 15, 1189-1227)

Third-Order Rate Constants of Atmospheric Importance

ROGER PATRICK* and DAVID M. GOLDEN
Department of Chemical Kinetics, SRI International, Menlo Park, California 94025

Abstract

Input data and results are presented for the calculation of a number of third-order rate constants of atmospheric interest using Troe's approximate method. A comparison with experimental data indicates that this approach provides a reliable method for predicting unknown rate constants and estimating temperature dependences. These calculations form the basis of the recommendations of the NASA review panel for third-order rate constants to be used in atmospheric modeling.

Introduction

Quantitative modeling of the atmosphere requires a comprehensive set of rate constants for a number of chemical reactions. Many of the most important reactions are association reactions which are either at or close to their limiting third-order kinetic behavior under atmospheric conditions. The review of laboratory measured rate constants for these processes is currently undertaken by a number of panels, and their recommendations appear at regular intervals. Unfortunately few measurements have been made at stratospheric temperatures close to 200 K, and so it is necessary to extrapolate from data obtained at room temperature and above in order to obtain the relevant rate constants. In the past this has been done by assuming that the experimental rate constant data followed either Arrhenius, that is, $k = A \exp(-E/RT)$, or T^n type behavior. Neither of these forms has any real theoretical basis, and although each may fit experimental data equally well, extrapolation at 200 K using the two equations may give differing results.

In principle unimolecular rate theory offers a sounder theoretical basis on which to fit data and formulate extrapolations. However, rigorous use of detailed theory presents a formidable computational problem, especially when the evaluation of large numbers of rate constants is required.

* Postdoctoral Research Associate.

International Journal of Chemical Kinetics, Vol. 15, 1189–1227 (1983)
 CCC 0538-8066/83/111189-39$04.90

Troe [4,5] nas recently suggested simplified equations, based on RRKM theory, allowing the quantitative estimation of second-order rate constants for unimolecular decomposition which may be related through the equilibrium constant to the rate constants for the reverse third-order association reactions. In a further paper [6] he discusses treatment of rate constants in the fall-off region. This method has been adopted by the NASA and CODATA review panels [1,2] to estimate theoretically the temperature and pressure dependence of key atmospheric reactions, and on this basis, to evaluate and rationalize laboratory measurements. The details of these calculations, along with the required thermodynamic and spectroscopic input data, are given in this paper.

In addition to providing an improved method for extrapolating experimental data, these calculations allow a thorough testing of Troe's formalism for a wide variety of molecules, many of which are larger than those that have been treated by this approach before.

The formalism also provides a useful method of highlighting uncertainties and ambiguities in the experimental data.

Theoretical Formalism

The rate of dissociation in the low-pressure second-order regime is given by the rate of energization of molecules above the dissociation threshold E_0. If the molecular energies are separated into their vibrational and rotational contributions, then the strong collision rate constant may be expressed as

$$k^{sc}_{diss,0} = Z_{LJ} \int_0^\infty \int_{E_0}^\infty f(E,J)\, dE\, dJ \tag{1}$$

where Z_{LJ} is the Lennard–Jones collision frequency, and $f(E,J)$ is the distribution of molecules among the available rovibrational states. Troe's [4,5] formalism starts from eq. (1) and by a series of approximations factors out contribution to $f(E,J)$ by differing degrees of freedom:

$$k^{sc}_{diss,0} = Z_{LJ} \frac{\rho(E_0)RT}{Q_{vib}} \exp\left(\frac{-E_0}{RT}\right) F_E F_{anh} F_{rot} F_{corr} \tag{2}$$

where $\rho(E_0)$ is the density of states at the critical energy E_0; F_E, F_{anh}, and F_{rot} are the correction terms for the energy dependence of the density of states, anharmonicity, and rotation, respectively; and Q_{vib} is the vibrational partition function.

Following Troe, Z_{LJ} is given by

$$(3)\quad Z_{LJ} = 8.09 \times 10^{-10}/\mathrm{cm^3\ molecule^{-1}\ s^{-1}} \times \sqrt{(T/1000\ \mathrm{K})(20\ \mathrm{g\ mol^{-1}}/\mu_{AM})}\ (\sigma_{AM}/5\ \text{Å})^2 \Omega^{2,2}_{AM}$$

where the collision integral is approximated by

$$(4)\quad \Omega^{2,2}_{AM} \simeq [0.697 + 0.5185 \log(kT/\epsilon_{AM})]^{-1}$$

In this expression the reduced mass μ_{AM} is given by $m_A m_M/(m_A + m_M)$, the Lennard–Jones collision diameter σ_{AM} is given by $(\sigma_A + \sigma_M)/2$, and the Lennard–Jones well depth ϵ_{AM} is given by $\sqrt{\epsilon_{AA}\epsilon_{MM}}$.

$\rho(E_0)$ is calculated according to the Whitten–Rabinovitch approximation, and F_E and F_{anh} are given by

$$(5)\quad F_E \simeq \sum_{v=0}^{s-1} \frac{(s-1)!}{(s-1-v)!} \left(\frac{RT}{E_0 + aE_z}\right)^v$$

with a the Whitten–Rabinovitch parameter and E_z the zero-point energy,

$$(6)\quad F_{anh} \simeq \left(\frac{s-1}{s-3/2}\right)^m$$

with s the total number of oscillators and m equal to the difference in the number of oscillators in the reactant and product molecules.

The barrier to association for the reactions discussed here is likely to be negligible, and so the critical energy E_0 may be identified with ΔH^0_0, the enthalpy change for the reaction at 0 K. Under these circumstances the relevant expression for F_{rot} is

$$(7)\quad F_{rot} = \frac{(s-1)!}{(s+1/2)!} \left(\frac{E_0 + aE_z}{RT}\right)^{3/2} \times \left[\frac{2.15(E_0/RT)^{1/3}}{2.15(E_0/RT)^{1/3} - 1 + (E_0 + aE_z)/(s+1/2)RT}\right]$$

The treatment of internal rotors presents some difficulties, since for many of the molecules considered here, barriers to rotation are not known. Consequently all internal rotors are treated as low-frequency torsional vibrations. At the low temperatures relevant to these calculations, the difference in the heat capacity of these types of motion is not significant.

The term F_{corr} is not calculable and represents a correction term to account for coupling between the different types of degress of freedom.

Following Troe, this was set equal to unity. This step may be justified *a posteriori* by the good agreement with experimental measurements found in most cases.

The association rate constant $k^{sc}_{rec,0}$ may be easily obtained from $k^{sc}_{diss,0}$ via the equilibrium constant K_{eq}:

$$k^{sc}_{rec,0} = k^{sc}_{diss,0} K_{eq} \tag{8}$$

$k^{sc}_{rec,0}$ represents an upper limit for the rate constant and must be multiplied by a collisional deactivation efficiency β_c ($0 < \beta_c < 1$) to obtain a value that can be compared to experiment. The temperature dependence of β_c is given by

$$\frac{\beta_c}{1 - \beta_c^{1/2}} = \frac{\langle \Delta E \rangle}{F_E RT} \tag{9}$$

where $\langle \Delta E \rangle$ is the average energy removed per collision.

In the fall-off region of transition from high-pressure second-order to low-pressure third-order kinetics the pressure dependence of association reactions can show considerable deviation from classical Lindemann behavior. Luther and Troe [6] have developed a simplified equation which accommodates this deviation in a parameter F, the broadening parameter,

$$k(M) = \frac{k_\infty k_0[M]}{k_\infty + k_0[M]} F \exp\left[1 + \left(\log\left\{\frac{k_0[M]}{k_\infty}\right\}\right)^2\right]^{-1} \tag{10}$$

where k_0 and k_∞ are the low- and high-pressure limiting rate constants, respectively. Where $F = 1$, Lindemann behavior operates. F is made up of the product of two terms: a strong collision, F_{sc} and a weak collision F_{wc} broadening parameter. F_{sc} is dependent on the molecular structure and in general becomes smaller as molecular complexity increases. It may be calculated according to rules derived by Luther and Troe [5]. F_{wc} is given approximately by

$$F_{wc} \simeq \beta^{0.14} \tag{11}$$

For most of the molecules encountered here, a value of $F \sim 0.6$ is found, although for some of the larger species it may be considerably less.

Table Format and Input Data

The following units are used throughout the tables: ν/cm^{-1}; I/amu·Å^2; T/K, ΔH°_f/kJ/mol; S°/J/mol·K; K_{eq}/molecule/cm^{-3}; σ_{LJ}/Å; ϵ_{LJ}/K; ρ/cm;

Z_{LJ}/cm^3/molecule·s; $k_{diss,0}$/cm^3/molecule·s; $k_{rec,0}$/cm^6/molecule^2·s; $\langle \Delta E \rangle$/kJ/mol.

Thermochemical data are generally taken from JANAF tables [7], except where footnoted. Data in parentheses are estimated either on the basis of known thermochemistry and spectroscopic parameters or from additivity rules [8]. Spectroscopic parameters ν and I are also generally taken from JANAF. If frequencies are estimated, they are chosen so as to give the correct entropy for the molecule. Unknown moments of inertia are calculated on the basis of reasonable or known molecular structures using the method of Thompson [9].

Equilibrium constants are calculated from both the thermodynamic data K_{eq}^{Trd} and the spectroscopic data K_{eq}^{SP} in order to check the internal consistency of the input data. Agreement between these values is generally very good. Where there is disagreement, this usually results from the neglect of states other than the ground state in the calculation of the electronic partition function. For this reason the thermodynamic equilibrium constant is always preferred.

The Lennard–Jones parameters, σ and ϵ/k are generally not available for the molecules of interest. These are estimated from the relations [10]

$$\sigma = 1.18 V_b^{1/3} \tag{12}$$

$$\epsilon/k = 1.21 T_b \tag{13}$$

where T_b is the normal boiling temperature (K) and V_b is the LeBas value obtained from tables of atomic volumes. Where T_b is unknown, it is estimated on the basis of analogous molecules. In all the calculations, the third-body M is taken to be nitrogen for which the values σ = 3.61 Å and ϵ/k = 91.5 K are used [9].

The value for $k_{rec,0}^{wc}$ at 300 K is generally the one recommended by the NASA review panel, and β_c is derived by comparing this with the calculated value of the strong collision rate constant k_{rec}^{sc}. $\langle \Delta E \rangle$ is then obtained from eq. (7). Following Troe [4] and assuming $\langle \Delta E \rangle$ is temperature independent allows β_c at 200 K to be calculated and combined with $k_{rec,0}^{sc}$ to give the predicted value of $k_{rec,0}^{wc}$ at 200 K. (In those instances where no experimental data exist for a reaction, a typical value of 0.3 is assumed for β_c at 300 K.)

The temperature dependence of $k_{rec,0}^{wc}$ may be cast in the form

$$k_{rec,0} = k_{rec,0}^{300}(T/300)^{-n} \tag{14}$$

The appropriate values of n are given in the tables.

Sensitivity and Accuracy of Calculation

The sensitivity calculations refer to the $HO_2NO_2 \rightleftharpoons HO_2 + NO_2$ system which is fairly representative of the moderately complex species considered here.

Variation of ΔH_0^0

Since the exponential terms in eq. (2) and the equilibrium constant cancel when $k_{rec,0}^{sc}$ is calculated, its dependence on the dissociation energy is relatively weak. An increase in ΔH_0^0 of 10% is reflected in a factor of 2 increase in $k_{rec,0}^{sc}$. This arises almost entirely from an increase in the density of states at the dissociation limit $\rho(E_0)$. Since HO_2NO_2 has a number of low frequencies (125, 200 cm^{-1}), the dependence of $\rho(E_0)$ on ΔH_0^0 is more pronounced than it would be if all the frequencies were high.

Variation of Vibrational Frequencies

$\rho(E_0)$ is the term which is most affected by changes in the vibrational frequencies. The extent of the variation depends greatly on the size of the frequency under consideration. Variation of frequencies close to 1000 cm^{-1} by a factor of 2 gives rise to a variation in $k_{rec,0}^{wc}$ of ~20%, while a similar uncertainty in frequencies ~200 cm^{-1} gives rise to a change by a factor of 2. In most cases the vibrational frequencies of the molecules are well known. Where they have to be estimated, the assigned values can be checked for consistency by calculating the overall entropy of the molecule and comparing this, via group additivity, to other species.

Variation of Lennard–Jones Parameters

These are the most uncertain of the input parameters. However, the values estimated from eqs. (12) and (13) are unlikely to be in error by more than ~20%. An error of 20% in ϵ/k only leads to a 3% error in $k_{rec,0}^{wc}$ for $HO_2 + NO_2$, while a similar error in σ is propagated more directly as a 23% error in the rate constant, assuming no errors in the corresponding values for N_2.

Thus it can be seen that $k_{rec,0}^{wc}$ is comparatively insensitive to most of the input parameters and so, even when data are estimated rather than known, little error should be introduced into the calculation, provided reasonable choices are made.

Accuracy of Eq. (2)

In addition to considering the uncertainties introduced into the calculations via the input data, it is useful to try to assess the magnitude of the uncertainty associated with the approximations in eq. (2) itself. It can be shown [11] that eq. (1) may be written as

$$k^{sc}_{diss,0} = \frac{Q_r^{\dagger}}{Q_r Q_v} \int_{E_0}^{\infty} \gamma(E)\rho(E) \exp\left(\frac{-E}{RT}\right) dE \tag{15}$$

where $Q_r^{\dagger}$ and Q_r are the rotational partition functions for the transition state and the molecule, respectively, Q_v is the vibrational partition function for the molecule, $\rho(E)$ is the harmonic density of states at energy E, and $\gamma(E)$ is the appropriate correction for anharmonicity. The factor $Q_r^{\dagger}/Q_r$ represents a correction for rotational effects and depends sensitively on the form chosen to represent the potential surface. The corresponding factor F_{rot} in the Troe formalism is derived for a Lennard–Jones interaction potential with a centrifugal barrier, and following this assumption, it can be shown [8] that for the diatomic approximation

$$\frac{Q_r^{\dagger}}{Q_r} = \left(\frac{6D_0}{RT}\right)^{1/3} \tag{16}$$

where D_0 is the potential energy of interaction.

Equation (15) was integrated directly using numerical integration techniques and input data for the dissociation reactions of HO_2NO_2 and $ClNO_2$. The strong collision rate constants thus calculated were 5.8×10^{-21} and 1.6×10^{-29} cm^3/molecule-s, and these may be compared with the values of 1.2×10^{-20} and 3.2×10^{-29} cm^3/molecule-s given by eq. (2). Thus the rate constants calculated by the different techniques agree to within a factor of 2, although it should be borne in mind that neither eq. (2) nor eq. (15) correctly addresses the equation of rovibrational coupling.

Notes on the Tables

These notes referring to Tables I–XIII. address specific points raised by the calculations for some of the reactions.

Table II: $N_2O = N_2 + O^1D$

The rate constant [12] for this association of N_2 and O^1D is extremely low compared to the prediction for k^{sc}_{rec}. This is a consequence of intersystem crossing to the lower energy $N_2 + O^3P$ curve, providing an additional

dissociation channel. This channel cannot be accommodated by the simple Troe model, and so the β_c value derived here does not represent a simple collisional deactivation efficiency as in the other examples. It was assumed to be temperature independent in deriving the suggested value for $k^{wc}_{rec,0}$ at 200 K.

Table V: $NO_2 \rightleftharpoons NO + O$

Third-order calculations by both Troe [4] and Michael and Lee [13] also give rise to values of $k^{sc}_{rec,0}$ that are smaller than the recommended experimental value. The reason for the implied β_c value > 1 is not clear since both the spectroscopy and the thermodynamics of this system are well defined.

Table VII: $HONO \rightleftharpoons OH + NO$

The recommended experimental value for the rate constant for the association reaction is 6.7×10^{-21} cm^6/molecule^2·s. In order to reproduce this value correctly using the Troe formalism, it is necessary to take account of the formation of both the *cis* and the *trans* isomers of HONO. The value of β_c was assumed to be the same for each of the channels.

Table IX: $HO_2NO_2 \rightleftharpoons HO_2 + NO_2$

The vibrational frequencies assigned to HO_2NO_2 are those recommended by Baldwin and Golden [14]. The first five frequencies are obtained from work of Niki et al. [15], while the remaining ones are based on those for FNO_3, I_2O_2, and HNO_3, with the low-frequency torsion adjusted to give the correct entropy for the molecule. The entropy of HO_2NO_2 is based on a measured value for $MeONO_2$ [16], corrected for the change of internal rotor from a methyl to an OH group. The bond dissociation energy at 0 K is that recommended by Baldwin and Golden [12].

Table XII: $ClNO_2 \rightleftharpoons Cl + NO_2$; $ClONO \rightleftharpoons Cl + NO_2$

The calculated strong association rate constant for the formation of $ClNO_2$ is 7.71×10^{-31} cm^6/molecule^2·s, which when compared to the experimental rate constant for the disappearance of Cl, 1.8×10^{-30} cm^6/molecule^2·s [1], would lead to $\beta_c = 2.35$ if this were the only product. This value for the deactivation efficiency is some eight times larger than might

be expected and well outside the uncertainties of the calculation. However, Niki et al. [17] observed that ClONO is in fact the major product and that the two isomers are formed in the approximate ratio 4–1 ClONO–$ClNO_2$. The strong collision rate constant for ClONO formation is calculated to be 2.83×10^{-30} cm^6/molecule^2·s, based on vibrational frequencies reported by Janowski et al. [18] and a value for ΔH_f(ClONO) given by Rohlack et al. [19]. But as in the case of HONO, *cis* and *trans* forms of ClONO would be expected, and so, to a good approximation, the rate of Cl consumption by this channel would be doubled, that is, $k^{sc}_{rec,0} = 5.66 \times 10^{-30}$ cm^6/molecule^2·s. The experimental rate constant thus represents the sum of the rate constants for the individual channels. The quoted value of $\beta_c = 0.28$ is assumed to be the same for each of the reactions.

Table XIII: ClOO = Cl + O_2

The thermochemistry of ClOO obtained from the CODATA review of Baulch et al. [2].

Table XIV: $ClONO_2$ = ClO + NO_2; ClOONO = ClO + NO_2

As indicated in the NASA review [1], experimental data for this association reaction fall into two sets that are in substantial disagreement. Several low-pressure measurements [20–23] of the rate of ClO disappearance in the presence of NO_2 are in good agreement and yield an average rate constant $k_0 = 1.8 \times 10^{-31}$ cm^6/molecule^2·s. No product identification was carried out and it was assumed that the reaction gave $ClONO_2$. However, direct measurements [24,25] of the rate of thermal decomposition of $ClONO_2$ ($k_{diss} = 6.2 \times 10^{-23}$ cm^3/molecule·s at 300 K) combined with the measured equilibrium constant gave $k_0 = 4.5 \times 10^{-32}$ cm^6/molecule^2·s. In Table XIV (a) the vibrational frequencies used for $ClONO_2$ are those given by Miller et al. [26], while the dissociation enthalpy $\Delta H^0_0(ClONO_2)$ was taken from the study of Schonle et al. [25]. If $ClONO_2$ is the sole product of the reaction, then to match the experimentally determined rate of ClO disappearance would require a large value of $\beta_c = 0.86$. Chang et al. [3] have pointed out that this apparent disagreement can be resolved if it is assumed that an additional product, ClOONO, is formed in the reaction of ClO with NO_2. The difference between the measured rate of ClO disappearance and the value of Schonle et al. for the rate constant for $ClONO_2$ production, that is, 1.3×10^{-31} cm^6/molecule^2·s, is now identified as the rate of formation of ClOONO. The frequencies and thermochemistry of

ClOONO given in Table XIV(b) are those estimated by Chang et al. [3]. The Troe calculations are consistent with the suggestion that two isomers are formed since the necessary rate constants are predicted with reasonable values of β_c.

However, recent studies of the rate of formation of $ClONO_2$ from the ClO + NO_2 reaction using diode laser spectroscopy [27] and of the Cl atom yield from photolysis of the products of this reaction [28] indicate that there is only one isomer of chlorine nitrate. This suggests that the most likely reason for the apparent discrepancy in the forward and reverse rate constants is the uncertainty in the thermochemistry of $ClONO_2$. On the basis of the rate constant measurements, a "kinetic" equilibrium constant of 3.4×10^6 molecules/cm^3 may be calculated, and this leads to $\Delta H_f(ClONO_2)$ = 22.8 kJ/mol (cf. 26.4 kJ/mol as measured by Knauth [24]). In Table XIV(c) a calculation is presented based on this thermochemistry. The strong collision rate constant k_{rec}^{sc} is calculated to be 2.24×10^{-31} cm^6/molecule^2·s, and so a β_c of 0.8 is required to match the experimental rate constant for loss of ClO.

Table XV: $BrONO_2 \rightleftharpoons BrO + NO_2$

The vibrational frequencies given for $BrONO_2$ are those estimated by Sander et al. [29]. The thermochemistry of $BrONO_2$ is not known, but if it is assumed that $\Delta H_0^0(BrO\text{-}NO_2) \sim \Delta H_0^0(ClO\text{-}NO_2)$, the strong collision rate constant is then calculated to be 2.76×10^{-31} cm^6/molecule^2·s at 300 K. Thus in order to reproduce the experimentally determined value of 5.0×10^{-31} cm^6/molecule^2·s for BrO disappearance, a β_c of 1.8 is required. As in the case of chlorine nitrate, this large value of β_c would be explained in terms of a less stable isomer BrOONO, but there is no evidence for this species. Alternatively, the estimated thermochemistry of $BrONO_2$ may be in error. It should be pointed out that Baulch et al. [2] recommend an estimated $\Delta H_f(BrONO_2) = 20 \pm 30$ kJ/mol $\approx \Delta H_f(ClONO_2)$, but additivity arguments require that $BrONO_2$ be substantially less stable than $ClONO_2$.

Table XVI

It should be noted that there is a large discrepancy between the values of $\Delta H_{f,300}$ for FOO quoted by JANAF (12.55 kJ/mol) and the CODATA report (50 kJ/mol). For the purposes of this calculation, the JANAF value was used. If the heat of formation were indeed as high as 50 kJ/mol, then

$\Delta H(F - O_2)$ would be 28.91 kJ/mol and k_{rec}^{sc} would be reduced to 1.14×10^{-33} cm^6/molecule^2-s, requiring a β_c value of 14 to match the experimental rate constant. The results of the calculation presented here agree with those given by Jubert [30] who also used the JANAF thermochemistry.

Table XVIII: $FNO_2 \rightleftharpoons F + NO_2$; $FONO \rightleftharpoons F + NO_2$

Since there is some evidence suggest that less stable isomers may be a common occurrence among the halogen nitrites, calculations were performed for the corresponding fluorine analogs. The thermochemistry and spectroscopic parameters were estimated on the basis of similar molecules. The results indicate that the formation of the less stable species can easily be 2–3 times faster than that of the other isomer, largely as a result of its increased entropy. In the case of FONO, *cis* and *trans* forms need also be included. The possibility of isomers of fluorine compounds should therefore be noted by modelers and suggests a need for further experimental work in this area.

Table XX: $CH_3O_2 \rightleftharpoons CH_3 + O_2$

The frequencies assigned to CH_3O_2 were fixed so as to give an entropy consistent with that derived from group additivity. The small value of β_c required to match the recommendation may be a consequence of incorrectly assuming $F_{corr} = 1$. However, recent data [31] for this reaction suggest that it may be more complex at low pressures than believed at the time the experimental data were evaluated.

Conclusion

It may be noted that for most of the reactions considered here, the value of β_c required to give agreement between the calculated strong collision rate constant and the recommended experimental value lies in the range 0.1–0.5. This is the range that might be considered reasonable on the basis of studies of energy transfer [32]. Some calculations require a β_c value <0.1, which may indicate that the implicit neglect of coupling between rotation vibration involved in setting F_{corr} may not be totally satisfactory. However, the general conclusion is that in the majority of cases this approximate method of calculating third-order rate constants performs remarkably well.

TABLE I

REACTION:		O_3		‡		O_2		+		O					
ν	I	T	ΔH_f	S°	ν	I	ΔH_f	S°	ν	I	ΔH_f	S°	ΔH	ΔS	K_{eq}^{TH}	K_{eq}^{SP}
1110.0	42.4	0	145.60	0	1580.3	11.5	0	0	-	-	246.81	0	101.21	0	-	-
1043.0	37.6					11.5										
705.0	4.7	200	143.30	224.10			0	193.38			248.45	152.05	105.15	121.33	2.76×10^{-2}	1.37×10^{-2}
		300	143.09	238.82			0	205.02			249.20	160.96	106.11	127.16	3.57×10^{7}	1.35×10^{7}
															σ_{LJ}	ϵ_{LJ}/k
															3.43	161.2

$\rho(E_o)$ / $a(E_o)$ / F_{anh}	T	Z_{LJ}	F_E / Q_{vib}	F_{rot}	k_{diss}^{ac}	k_{rec}^{ac} / k^{uc} / β_c	$\langle \Delta E \rangle$	n	F_{ac} / F_{uc} / F
5.99×10^{-2}	200	2.41×10^{-10}	1.03	31.49	3.63×10^{-34}	1.32×10^{-32}	0.31	2.36	0.98
0.984			1.00			1.56×10^{-33}			0.74
1.78						0.12			0.73
	300	2.65×10^{-10}	1.04	20.87	2.64×10^{-25}	7.35×10^{-33}	0.31		0.93
			1.05			6.00×10^{-34}			0.70
						0.08			0.65

TABLE II

REACTION:	N_2O				+	N_2			+	$O(^1D)$							
ν	I	T	ΔH_f	S°	ν	I	ΔH_f	S°	ν	I	ΔH_f	S°	ΔH	ΔS	k^{TH}_{eq}	k^{SP}_{eq}
2221.7	39.8	0	85.48	0	2357.5	8.4	0	0	-	-	436.56	0	351.08	0	-	-
1276.5	39.8					8.4										
589.2		200	82.78	205.47			0	179.88			437.81	135.14	355.03	109.55	3.61×10^{-68}	3.65×10^{-68}
		300	82.05	219.87			0	191.50			438.90	143.43	356.85	115.06	1.82×10^{-37}	2.35×10^{-37}

$\rho(\xi_0)$	T	λ_{LJ}	F_E	F_{rot}	k^{sc}_{diss}	k^{sc}_{rec}	$\langle \Delta E \rangle$	n	F_{sc}	σ_{LJ}	ϵ_{LJ}/k
$a(\xi_0)$						k^{wc}			F_{wc}		
F_{anh}			Q_{vib}			β_c			F		
2.94×10^{-1}	200.0	2.89×10^{-10}	1.01	98.01	4.11×10^{-98}	1.13×10^{-30}	$< 1.05 \times 10^{-6} >$	0.59	0.91	220.0	3.88
0.993			1.01			4.44×10^{-37}			-		
1.78						3.9×10^{-7}			-		
	300.0	3.16×10^{-10}	1.01	66.88	1.62×10^{-67}	8.91×10^{-31}			0.87		
			1.07			3.50×10^{-37}			-		
						3.9×10^{-7}			-		

TABLE III

REACTION:		HO_2			‡	O_2			+	H						
ν	I	T	ΔH_f	S°	ν	I	ΔH_f	S°	ν	I	ΔH_f	S°	ΔH	ΔS	K_{eq}^{TH}	K_{eq}^{SP}
1389.4	0.8	0	13.39	0	1580.3	11.5	0	0	-	-	216.02	0	202.63	0	-	-
1101.0	15.8					11.5										
3414.0	15.0	200	11.38	214.87			0	193.38			217.32	106.31	205.94	84.82	1.62×10^{-30}	1.50×10^{-30}
		300	10.46	229.0			0	205.2			218.00	114.74	207.54	90.94	1.00×10^{-12}	9.78×10^{-13}
															σ_{LJ}	ϵ_{LJ}/k
															3.43	289.3

$\nu(E_o)$ / $n(E_o)$ / F_{anh}	T	Z_{LJ}	F_E / Q_{vib}	F_{rot}	k_{diss}^{sc}	k_{rec}^{sc} / k^{wc} / β_c	$\langle \Delta E \rangle$	n	F_{sc} / F_{wc} / F
3.76×10^{-2}	200	2.83×10^{-10}	1.01	62.02	1.98×10^{-60}	1.32×10^{-30}	0.19	1.59	0.99
0.98			1.00			1.05×10^{-31}			0.70
1.78						0.08			0.70
	300	3.09×10^{-10}	1.02	41.94	9.58×10^{-43}	9.80×10^{-31}	0.19		0.98
			1.00			5.50×10^{-32}			0.67
						0.06			0.66

TABLE IV

REACTION:		H_2O_2			+			OH									
ν	I	T	ΔH_f	S°	ν	I	ΔH_f	S°	ν	I	ΔH_f	S°	ΔH	ΔS	k^{TB}_{eq}	k^{SP}_{eq}
3774.0	20.1	0	-129.81	0	3735.2	0.9	38.87	0	3735.2	0.9	38.87	0	207.55	0	-	-
1380.0	19.3					0.9				0.9						
3788.0	1.7	200	134.14	210.52			39.30	171.48			39.30	171.48	212.74	132.44	8.22×10^{-30}	2.64×10^{-30}
1266.0																
880.0		300	-136.11	232.88			39.46	183.59			39.46	183.59	215.03	134.30	9.11×10^{-12}	5.65×10^{-12}
225.0																
															σ_{LJ}	ϵ_{LJ}/k
															4.20	289.30

$\rho(E_o)$	T	Z_{LJ}	F_E	F_{rot}	k^{sc}_{diss}	k^{sc}_{rec}	$\langle \Delta E \rangle$	n	F_{sc}
$a(E_o)$						k^{sc}			F_{sc}
F_{anh}			Q_{vib}			β_c			F
10.19	200.0	3.33×10^{-10}	1.03	41.25	1.5×10^{-59}	1.84×10^{-30}	2.84	0.75	0.85
0.95			1.25			9.34×10^{-31}			0.90
1.52						0.49			0.76
	300.0	3.64×10^{-10}	1.05	27.21	1.58×10^{-41}	1.73×10^{-30}	2.84		0.82
			1.54			6.90×10^{-31}			0.88
						0.40			0.72

TABLE V

REACTION:		NO_2		‡	NO		+		O						
ν	I	T	ΔH_f	S°	ν	I	ΔH_f	S°	ν	I	ΔH_f	S°	ΔH	ΔS	K_{eq}^{TH}	K_{eq}^{SP}
1357.8	40.8	0	35.92	0	1903.6	9.8	89.79	0	-	-	246.81	0	300.68	0	-	-
1665.5	38.6					9.8										
756.8	2.1	200	33.89	225.74			90.20	198.64			248.45	152.15	304.76	125.05	3.11×10^{-54}	1.78×10^{-54}
		300	33.08	239.91			90.29	210.65			249.20	160.96	306.41	131.70	8.22×10^{-28}	3.91×10^{-28}

σ_{LJ}	ϵ_{LJ}/k
3.46	356.9

$\rho(E_o)$ / $a(E_o)$ / F_{anh}	T	Z_{LJ}	F_E / Q_{vib}	F_{rot}	k_{diss}^{ac}	k_{rec}^{ac} / k^{uc} / β_c	$\langle \Delta E \rangle$	n	F_{ac} / F_{uc} / F
2.97×10^{-1}	200.0	2.74×10^{-10}	1.01	84.56	5.05×10^{-85}	1.63×10^{-31}	-	1.21	0.96
0.99			1.00			1.96×10^{-31}			1.0
1.78						1.20			0.96
	300.0	2.98×10^{-10}	1.02	57.48	8.26×10^{-58}	1.00×10^{-31}	-		0.90
			1.03			1.20×10^{-31}			1.0
						1.20			0.90

TABLE VI

REACTION:			NO_3		‡	NO_2			+		O					
ν	I	T	ΔH_f	S°	ν	I	ΔH_f	S°	ν	I	ΔH_f	S°	ΔH	ΔS	K_{eq}^{TH}	K_{eq}^{SP}
1158.0	76.8	0	77.52	0	1357.8	40.8	35.92	0	-	-	246.81	0	205.21	0	-	-
1158.0	38.4				1665.5	38.6										
940.0	38.4	200	72.70	235.79	756.8	2.1	33.89	225.74			248.45	152.15	209.64	142.10	1.72×10^{-28}	8.41×10^{-29}
704.0																
704.0		300	71.13	252.71			33.08	239.91			249.20	150.96	211.15	148.16	2.28×10^{-10}	1.06×10^{-10}
765.0																

σ_{LJ}	ϵ_{LJ}/k
3.77	395.0

$\rho(E_o)$ / $a(E_o)$ / F_{anh}	T	Z_{LJ}	F_E / Q_{vib}	F_{rot}	k_{diss}^{ac}	k_{rec}^{ac} / k^{uc} / β_c	$\langle \Delta E \rangle$	n	F_{ac} / F_{uc} / F
53.36	200.0	2.86×10^{-10}	1.04	36.93	2.75×10^{-58}	1.60×10^{-30}	0.39	2.27	0.96
0.981			1.02			2.26×10^{-31}			0.76
1.37						0.14			0.73
	300.0	3.15×10^{-10}	1.05	24.19	2.03×10^{-40}	8.89×10^{-31}	0.39		0.87
			1.12			9.00×10^{-32}			0.72
						0.10			0.63

TABLE VIIa

REACTION:			HONO (cis)				OH			NO					
ν	I	T	ΔH_f	S°	ν	I	ΔH_f	S°	ν	I	ΔH_f	S°	ΔH	ΔS	K_{eq}^{TH}	K_{eq}^{SP}
3462.0	6.1	0	-70.50	0	3735.2	0.9	38.87	0	1903.6	9.8	89.79	0	199.16	0	-	-
1639.0	46.9					0.9				9.8						
1330.0	40.8	200	-75.19	232.61			39.30	171.48			90.20	198.64	204.69	137.51	1.92×10^{-27}	9.34×10^{-28}
855.0																
525.0		300	-76.73	249.31			39.46	183.59			90.29	210.65	206.48	144.93	1.01×10^{-9}	4.09×10^{-10}
638.0																

															σ_{LJ}	ϵ_{LJ}/k
															3.60	273.5
$\rho(E_o)$	T	Z_{LJ}	F_E	F_{rot}	k_{diss}^{ac}	k_{rec}^{ac}			<ΔE>	n	F_{ac}					
$a(E_o)$						k^{uc}					F_{uc}					
F_{anh}			Q_{vib}			β_c					F					
16.05	200	2.73×10^{-10}	1.03	37.98	3.09×10^{-57}	1.59×10^{-30}			4.14	2.66	0.93					
0.957			1.04			9.20×10^{-31}					0.93					
1.52						0.58					0.86					
	300	2.98×10^{-10}	1.05	24.90	6.58×10^{-40}	6.49×10^{-31}			4.14		0.86					
			1.17			3.13×10^{-31}					0.90					
						0.48					0.78					

TABLE VIIb

REACTION:		HONO (trans)			:	OH			+	NO						
ν	I	T	ΔH_f	$S°$	ν	I	ΔH_f	$S°$	ν	I	ΔH_f	$S°$	ΔH	ΔS	K_{eq}^{TH}	K_{eq}^{SP}
3590.0	4.7	0	-72.67	0	1903.6	0.9	38.87	0	3735.2	9.8	89.79	0	201.33	0	-	-
1696.0	49.7					0.9				9.8						
1260.0	45.0	200	-77.34	232.23			39.30	171.48			90.20	198.64	206.84	137.89	5.50×10^{-28}	2.68×10^{-28}
794.0																
598.0		300	-78.85	249.42			39.46	183.59			90.29	210.65	208.60	144.82	4.25×10^{-10}	1.80×10^{-10}
543.0																
															σ_{LJ}	ϵ_{LJ}/k
															3.60	273.5

$\rho(E_o)$ / $a(E_o)$ / F_{anh}	T	Z_{LJ}	F_E / Q_{vib}	F_{rot}	k_{diss}^{sc}	k_{rec}^{sc} / k^{wc} / β_c	$\langle \Delta E \rangle$	n	F_{sc} / F_{wc} / F
16.78	200	2.73×10^{-10}	1.03	38.36	9.68×10^{-58}	1.75×10^{-30}	4.14	2.57	0.93
0.957			1.04			1.01×10^{-30}			0.93
1.52						0.58			0.86
	300	2.98×10^{-10}	1.05	25.21	3.15×10^{-40}	7.38×10^{-31}	4.[illegible]4		0.85
			1.17			3.56×10^{-31}			0.90
						0.48			0.77

TABLE VIII

REACTION:		$HONO_2$		‡	NO_2			+	OH						
ν	I	T	ΔH_f	S°	ν	I	ΔH_f	S°	ν	I	ΔH_f	S°	ΔH	ΔS	E_{eq}^{TH}	E_{eq}^{SP}
3550.0	38.43	0	-124.52	0	1357.8	40.8	35.92	0	3735.2	0.9	38.87	0	199.33	0	-	-
1708.0	42.03				1665.5	38.6				0.9						
1331.0	80.46	200	-131.91	247.40	756.8	2.1	33.89	225.74			39.30	171.48	205.10	149.82	6.76×10^{-27}	4.56×10^{-27}
1325.0																
879.0		300	-134.31	266.35			33.08	239.91			39.46	183.59	206.85	157.15	3.77×10^{-9}	2.38×10^{-9}
762.0																
579.0																
647.0																
465.0																
															σ_{LJ}	ϵ_{LJ}/k
															3.91	390.0

$\rho(E_o)$	T	Z_{LJ}	F_E	F_{rot}	k_{diss}^{uc}	k_{rec}^{uc}	<ΔE>	n	F_{uc}
$a(E_o)$						k^{uc}			F_{uc}
F_{anh}			Q_{vib}			β_c			F
1.08×10^3	200	2.99×10^{-10}	1.05	28.56	1.42×10^{-55}	2.14×10^{-29}	2.30	3.18	0.91
0.944			1.07			9.44×10^{-30}			0.89
1.38						0.44			0.81
	300	3.24×10^{-10}	1.08	18.42	2.82×10^{-38}	7.44×10^{-30}	2.30		0.81
			1.31			2.60×10^{-30}			0.86
						0.35			0.70

TABLE IX

REACTION:	HO_2NO_2			:	NO_2			+	NO_2								
ν	I	T	ΔH_f°	S°	ν	I	ΔH_f°	S°	ν	I	ΔH_f°	S°	ΔH	ΔS	E_{eq}^{TH}	E_{eq}^{SP}
3540.0	128.4	0	-46.92	0	1357.8	40.8	35.92	0	1389.4	0.8	13.39	0	96.23	0	- -	- -
1748.0	100.6				1665.5	38.6			1101.0	15.8					- -	- -
1304.0	50.8	200	-55.23	273.31	756.8	2.1	33.89	225.74	3414.0	15.0	11.38	214.87	100.50	167.28	1.13×10^2	1.14×10^2
1396.0																
803.0		300	-57.24	300.12			33.08	239.91			10.46	229.00	100.78	168.49	4.39×10^{10}	4.47×10^{10}
633.0																
560.0																
735.0																
125.0																
400.0																
880.0																
200.0																

$\rho(E_o)$	T	Z_{LJ}	F_E	F_{rot}	k_{diss}^{sc}	k_{rec}^{sc}	$\langle \Delta E \rangle$	n	F_{sc}
$\sigma(E_o)$						k^{uc}			F_{uc}
F_{anh}			Q_{vib}			β_c			F
3.50×10^3	200	3.67×10^{-10}	1.13	12.25	9.72×10^{-29}	8.31×10^{-30}	37.2	3.00	0.73
0.879			2.46			7.75×10^{-31}			0.99
1.322						0.91			0.72
	300	3.97×10^{-10}	1.20	7.48	1.19×10^{-28}	2.46×10^{-31}	37.2		0.62
			5.22			2.30×10^{-31}			0.98
						0.87			0.61

σ_{LJ}	ϵ_{LJ}/k
4.16	422.8

TABLE X

REACTION:	N_2O_5				⇌ NO_3				+ NO_2							
ν	I	T	ΔH_f	$S°$	ν	I	ΔH_f	$S°$	ν	I	ΔH_f	$S°$	ΔH	ΔS	K_{eq}^{TH}	K_{eq}^{SP}
1728.0	239.9	0	21.44	0	1158.0	76.8	77.40	0	1357.8	40.8	35.92	0	91.88	0	—	—
1338.0	182.9				1158.0	38.4			1665.5	38.6						
743.0	100.5	200	12.70	311.73	940.0	38.4	72.70	235.79	756.8	2.1	33.89	225.74	93.89	149.80	7.37×10^2	7.70×10^2
614.0					704.0											
353.0		300	11.30	346.43	704.0		71.13	252.71			33.08	239.91	92.91	146.19	6.95×10^{10}	6.95×10^{10}
614.0					765.0											
577.0																
85.0																
55.0																
55.0																
1728.0																
1247.0																
860.0																
743.0																
353.0																
															σ_{LJ}	ϵ_{LJ}/k
															4.57	450.0

$\rho(E_0)$ / $a(E_0)$ / F_{anh}	T	Z_{LJ}	F_E / Q_{vib}	F_{rot}	k_{diss}^{oc}	k_{rec}^{oc} / k^{uc} / β_c	$\langle \Delta E \rangle$	n	F_{oc} / F_{uc} / F
1.88×10^6	200.0	3.37×10^{-10}	1.18	9.15	4.69×10^{-26}	6.34×10^{-28}	0.63	4.12	0.53
0.897			25.43			1.17×10^{-29}			0.79
1.24						0.18			0.42
	300.0	3.65×10^{-10}	1.29	5.64	1.22×10^{-18}	1.74×10^{-29}	0.63		0.44
			107.38			2.20×10^{-30}			0.75
						0.33			0.33

TABLE XI

REACTION:		ClHO	:	NO	+	Cl						
ν	I	T	ΔH_f	S°	ν	I	ΔH_f	S°	ν	I	ΔH_f	S°	ΔH	ΔS	E_{eq}^{TR}	E_{eq}^{SP}
1799.7	93.8	0	53.64	0	1903.6	9.8	89.79	0	-	-	119.33	0	155.48	0	-	-
595.6	88.0					9.8										
330.9	5.9	200	51.59	244.52			90.20	198.64			120.52	156.53	158.73	110.65	7.62×10^{-17}	5.4×10^{-17}
		300	51.80	261.58			90.29	210.66			121.02	165.10	159.51	114.18	3.79×10^{-3}	2.34×10^{-3}
															σ_{LJ}	ϵ_{LJ}/k
															4.02	323.7

$\rho(E_o)$ / $\sigma(E_o)$ / F_{anh}	T	λ_{LJ}	F_E / Q_{vib}	F_{rot}	k_{diss}^{ac}	k_{rec}^{ac} / k^{uc} / β_c	$\langle \Delta E \rangle$	n	F_{ac} / F_{uc} / F
2.90×10^{-1}	200	3.06×10^{-10}	1.02	46.08	3.07×10^{-47}	2.96×10^{-31}	3.99	1.57	0.86
0.986			1.12			1.70×10^{-31}			0.92
1.78						0.57			0.79
	300	3.32×10^{-10}	1.03	30.83	7.18×10^{-34}	1.88×10^{-31}	3.99		0.82
			1.33			9.00×10^{-32}			0.90
						0.48			0.74

TABLE XIIa

REACTION:	$ClNO_2$				:	NO_2			+	Cl								
ν	I	T	ΔH_f°	S°	ν	I	ΔH_f°	S°	ν	I	ΔH_f°	S°	ΔH	ΔS	E_{eq}^{TR}	E_{eq}^{SP}
1685.0	135.8	0	17.54	0	1357.0	40.0	35.92	0	-	-	119.33	0	137.71	0	-	-
1293.0	97.8				1665.5	38.6										
794.0	38.0	200	13.20	252.52	756.8	2.1	33.89	225.74			120.52	156.53	141.21	129.75	2.07×10^{-11}	2.94×10^{-11}
411.0																
631.0		300	12.12	271.96			33.08	239.91			121.02	165.10	141.98	133.05	4.12×10^{1}	4.14×10^{1}
367.0																

$\sigma(E_g)$	T	k_{LJ}	P_E	P_{rot}	k_{diss}^{SC}	k_{rec}^{SC}	$\langle \Delta E \rangle$	n	P_{SC}
$\sigma(E_g')$						k^{SC}			P_{SC}
P_{esh}			Q_{vib}			β_c			r
26.67	200	3.07×10^{-10}	1.05	25.49	3.95×10^{-41}	1.37×10^{-30}	1.60	2.05	0.86
0.568			1.15			6.58×10^{-31}			0.87
1.37						0.36			0.75
	300	3.35×10^{-10}	1.07	16.52	3.19×10^{-29}	7.71×10^{-31}	1.60		0.79
			1.31			2.17×10^{-31}			0.84
						0.28			0.66

σ_{LJ}	ϵ_{LJ}/k
4.26	336.4

TABLE XIIb

REACTION:			ClONO		:	NO_2		+	Cl						
ν	I	T	ΔH_f	S°	ν	I	ΔH_f	S°	ν	I	ΔH_f	S°	ΔH	ΔS	K_{eq}^{TH}	K_{eq}^{SP}
1715.0	130.8	0	58.85	0	1357.8	40.8	35.92	0	-	-	119.33	0	96.42	0	-	-
858.0	98.7				1665.5	38.6										
644.0	32.1	200	55.88	269.65	756.8	2.1	33.89	225.74			120.52	156.53	98.58	112.62	0.50	0.48
406.0																
258.0		300	55.65	293.06			33.08	239.91			121.02	165.10	98.45	111.95	1.24×10^{8}	1.22×10^{8}
108.0																
															σ_{LJ}	ϵ_{LJ}/k
															4.26	336.4

$\rho(E_o)$	T	Z_{LJ}	F_E	F_{rot}	k_{diss}^{ac}	k_{rec}^{ac}	$\langle \Delta E \rangle$	n	F_{ac}
$a(E_o)$						k^{wc}			F_{wc}
F_{anh}			Q_{vib}			β_c			F
76.46	200	3.07×10^{-10}	1.07	17.65	2.37×10^{-30}	4.92×10^{-30}	1.67	2.02	0.74
0.96			2.35			1.81×10^{-30}			0.87
1.37						0.37			0.64
	300	3.35×10^{-10}	1.12	11.31	3.46×10^{-22}	2.83×10^{-30}	1.67		0.67
			4.33			7.97×10^{-31}			0.84
						0.28			0.56

TABLE XIII

REACTION:		ClOO	ΔH_f	S°		O_2	ΔH_f	S°		Cl	ΔH_f	S°	ΔH	ΔS	k_{eq}^{TH}	k_{eq}^{SP}
ν	I	T			ν	I			ν	I						
1440.8	8.8	0	90.79	0	1580.3	11.5	0	0	-	-	119.33	0	28.53	0	-	-
407.0	72.0					11.5										
372.0	80.8	200	89.26	245.37			0	193.38			120.52	156.53	31.26	104.54	7.26×10^{16}	6.94×10^{16}
		300	89.12	263.59			0	205.20			121.02	165.10	31.90	106.52	2.50×10^{19}	2.57×10^{19}
															σ_{LJ}	ϵ_{LJ}/k
															3.91	342.3

$\nu(E_o)$	T	Z_{LJ}	F_E	F_{rot}	k_{diss}^{ac}	k_{rec}^{ac}	$\langle \Delta E \rangle$	n	F_{ac}
$a(E_o)$						k^{uc}			F_{uc}
F_{anh}			Q_{vib}			β_c			F
2.71×10^{-2}	200	2.89×10^{-10}	1.08	10.13	6.64×10^{-16}	9.57×10^{-33}	1.73	1.43	0.92
0.948			1.13			3.57×10^{-33}			0.87
1.78						0.37			0.80
	300	3.15×10^{-10}	1.13	6.54	1.79×10^{-13}	6.99×10^{-33}	1.73		0.87
			1.40			2.0×10^{-33}			0.80
						0.29			0.73

TABLE XIVa

REACTION:			$ClONO_2$		‡	NO_2		+	ClO							
ν	I	T	ΔH_f	S°	ν	I	ΔH_f	S°	ν	I	ΔH_f	S°	ΔH	ΔS	k_{eq}^{TH}	k_{eq}^{SP}
1735.4	187.0	0	33.92	0	1357.8	40.8	35.92	0	866.0	26.0	101.30	0	103.30	0	-	-
1291.9	165.0				1665.5	38.6				26.0						
809.3	55.5	200	27.51	277.19	756.8	2.1	33.89	225.74			101.25	214.33	107.63	162.88	9.25×10^{-1}	1.19
780.2																
710.8		300	26.40	302.62			33.08	239.91			101.22	226.74	107.30	164.03	1.47×10^{9}	1.74×10^{9}
560.0																
434.1																
270.0																
121.0																
															σ_{LJ}	ϵ_{LJ}/k
															4.47	364.7

$\rho(E_o)$	T	τ_{LJ}	F_E	F_{rot}	k_{diss}^{ac}	k_{rec}^{ac}	$\langle \Delta E \rangle$	n	F_{ac}
$\omega(E_o)$						k^{wc}			F_{wc}
F_{anh}			Q_{vib}			β_c			F
1.16×10^{3}	200.0	3.22×10^{10}	1.10	14.40	5.52×10^{-31}	5.97×10^{-31}	1.17	3.34	0.75
0.942			2.17			1.74×10^{-31}			0.85
1.38						0.29			0.64
	300.0	3.50×10^{-10}	1.16	9.09	3.07×10^{22}	2.09×10^{-31}	1.17		0.65
			4.16			4.50×10^{32}			0.82
						0.22			0.53

TABLE XIVb

REACTION:			ClOONO		:	NO_2		+		ClO					
ν	I	T	ΔH_f	S°	ν	I	ΔH_f	S°	ν	I	ΔH_f	S°	ΔH	ΔS	k_{eq}^{TH}	k_{eq}^{SP}
1735.0	187.0	0	53.12	0	1357.8	40.8	35.92	0	866.0	26.0	101.30	0	84.10	0	-	-
500.0	165.0				1665.5	38.6				26.0						
880.0	55.6	200	48.26	287.24	756.8	2.1	33.89	225.74			101.25	214.33	86.88	152.83	4.79×10^{4}	6.86×10^{4}
858.0																
710.0		300	48.11	315.44			33.08	239.91			101.22	226.74	86.19	151.21	1.90×10^{12}	1.64×10^{12}
500.0																
125.0																
270.0																
108.0																
															σ_{LJ}	ϵ_{LJ}/k
															4.47	364.7

$\rho(E_o)$	T	Z_{LJ}	F_E	F_{rot}	k_{diss}^{sc}	k_{rec}^{sc}	<ΔE>	n	F_{sc}
$a(E_o)$						k^{uc}			F_{uc}
F_{anh}			Q_{vib}			β_c			F
2.26×10^{3}	200.0	3.22×10^{-10}	1.13	11.52	5.05×10^{-26}	7.37×10^{-31}	3.72	2.93	0.67
0.933			3.89			3.94×10^{-31}			0.91
1.38									
	300.0	3.50×10^{-10}	1.20	7.22	4.60×10^{-19}	2.80×10^{-31}	3.72		0.58
			9.76			1.20×10^{-31}			0.89
						0.43			0.52

TABLE XIVc

REACTION:	$ClONO_2$			‡	NO_2			+	ClO							
ν	I	T	ΔH_f°	S°	ν	I	ΔH_f°	S°	ν	I	ΔH_f°	S°	ΔH	ΔS	K_{eq}^{TH}	K_{eq}^{SP}
1735.4	187.0	0	29.85	0	1357.8	40.8	35.92	0	866.0	26.0	101.30	0	107.37	0	-	-
1291.9	165.0				1665.5	38.6				26.0						
809.3	55.5	200	23.91	277.19	756.8	2.1	33.89	225.74			101.25	214.33	111.21	162.88	1.06×10^{-1}	1.02×10^{-1}
780.2																
710.8		300	22.80	302.62			33.08	239.91			101.22	226.74	111.50	164.03	3.47×10^{8}	3.41×10^{8}
560.0																
434.1																
270.0																
121.0																

$\rho(E_o)$	T	Z_{LJ}	F_E	F_{rot}	k_{diss}^{sc}	k_{rec}^{sc}	$\langle \Delta E \rangle$	n	σ_{LJ}	ϵ_{LJ}/k
$a(E_o)$						k^{sc}				
F_{anh}			(F_{vib})			β_c			4.47	364.7
1.48×10^3	200.0	3.22×10^{-16}	1.10	14.90	6.20×10^{-32}	5.84×10^{-31}	22.16	2.54		
0.942			2.17			1.74×10^{-31}				
1.38						0.86				
	300.0	3.50×10^{-10}	1.16	9.41	7.79×10^{-23}	2.24×10^{-31}	22.16			
			4.16			1.89×10^{-31}				
						0.8				

F_{sc}	0.75
F_{nc}	0.73
F	0.55
	0.65
	0.63
	0.41

TABLE XV

REACTION:			$BrOhO_2$		‡	NO_2		+		BrO					
ν	I	T	ΔH_f	S°	ν	I	ΔH_f	S°	ν	I	ΔH_f	S°	ΔH	ΔS	K_{eq}^{TH}	K_{eq}^{SP}
1711.0	271.3	0	54.26	0	1357.8	40.8	35.92	0	718.7	39.3	125.71	0	107.37	0	-	-
1285.0	251.3				1665.5	38.6				39.3						
802.0	57.6	200	48.02	289.03	756.8	2.1	33.89	225.74			125.55	225.33	111.42	162.04	1.15×10^{-1}	1.15×10^{-1}
720.0																
690.0		300	46.94	315.08			33.08	239.91			125.52	238.05	111.66	162.88	3.60×10^{8}	3.60×10^{8}
560.0																
390.0																
240.0																
90.0																
															σ_{LJ}	ϵ_{LJ}/k
															4.60	369.4

$\rho(E_o)$	T	Z_{LJ}	F_E	F_{rot}	k_{diss}^{ac}	k_{rec}^{ac}	<ΔE>	n	F_{ac}
$a(E_o)$						k^{uc}			F_{uc}
F_{anh}			Q_{vib}			β_c			F
2.65×10^{3}	200.0	3.20×10^{-10}	1.10	14.48	8.52×10^{-32}	7.42×10^{-31}	- - -	2.43	0.72
0.942			2.81			1.34×10^{-30}			1.00
1.38						1.81			0.72
	300.0	3.48×10^{-10}	1.16	9.33	9.92×10^{-23}	2.76×10^{-31}	- - -		0.63
			5.81			5.00×10^{-31}			1.00
						1.81			0.63

TABLE XVI

REACTION:			FO_2		‡		J_2		+		F							
ν	I	T	ΔH_f°	S°	ν	I	ΔH_f°	S°	ν	I	ΔH_f°	S°	ΔH	ΔS	E_{eq}^{TH}	E_{eq}^{SF}
1495.0	6.6	0	14.22	0	1580.3	11.5	0	0	-	-	76.82	0	62.59	0	-	-
584.5	53.4					11.5										
376.0	46.7	200	12.75	242.10			0	193.38			78.17	149.56	65.43	100.83	5.52×10^7	4.78×10^7
		300	12.55	258.99			0	205.02			78.91	158.64	66.36	104.68	2.00×10^{13}	1.72×10^{13}

$\rho(E_o)$	T	Z_{LJ}	F_E	F_{vib}	F_{rot}	k_{diss}^{sc}	k_{rec}^{sc}	k^{sc}	β_c	$\langle \Delta E \rangle$	n	σ_{LJ}	ϵ_{LJ}/k	F_{sc}
$\alpha(E_o)$														F_{sc}
F_{anh}														F
6.28×10^{-2}	200	2.53×10^{-10}	1.04		20.10	3.41×10^{-24}	6.15×10^{-32}			2.38	1.35			0.90
0.972			1.09				2.77×10^{-32}							0.89
1.78							0.45							0.80
	300	2.77×10^{-10}	1.07		13.17	8.96×10^{-19}	4.47×10^{-32}			2.38				0.85
			1.28				1.60×10^{-32}							0.87
							0.36							0.74

TABLE XVII

REACTION:			FNO ‡			NO + F									
ν	I	T	ΔH_f	S°	ν	I	ΔH_f	S°	ν	I	ΔH_f	S°	ΔH	ΔS	K_{eq}^{TH}	K_{eq}^{SP}
1844.0	47.7	0	-63.18	0	1903.6	9.8	89.79	0	-	-	76.82	0	229.79	0	-	-
521.0	42.3					9.8										
765.0	5.3	200	-65.20	232.36			90.20	198.64			78.17	149.56	233.57	115.84	4.05×10^{-36}	2.96×10^{-36}
		300	-65.69	248.03			90.29	210.66			78.91	158.66	234.89	121.29	6.64×10^{-16}	4.14×10^{-16}

σ_{LJ}	ϵ_{LJ}/k
3.52	262.6

$\rho(E_o)$ / $a(E_o)$ / F_{anh}	T	Z_{LJ}	F_E / Q_{vib}	F_{rot}	k_{diss}^{ac}	k_{rec}^{ac} / k^{uc} / β_c	<ΔE>	n	F_{ac} / F_{uc} / F
2.93×10^{-1}	200.0	2.79×10^{-10}	1.01	66.20	$1.2(\times 10^{-66}$	3.11×10^{-31}	1.69	1.74	0.90
0.991			1.03			1.19×10^{-32}			0.87
1.78						0.38			0.79
	300.0	3.03×10^{-10}	1.02	44.73	$1.31. \times 10^{-46}$	1.96×10^{-31}	1.69		0.86
			1.12			5.88×10^{-32}			0.84
						0.30			0.73

TABLE XVIIIa

REACTION:			FNO_2		:	NO_2		+	F						
ν	I	T	ΔH_f	S°	ν	I	ΔH_f	S°	ν	I	ΔH_f	S°	ΔH	ΔS	k_{eq}^{TH}	k_{eq}^{SP}
1793.0	38.0	0	-102.93	0	1357.8	40.8	35.92	0	-	-	76.82	0	215.67	0	-	-
1312.0	81.9				1665.5	38.6										
822.0	43.9	200	-107.49	242.03	756.8	2.1	33.89	225.74			78.17	149.56	219.55	133.27	1.52×10^{-31}	2.90×10^{-31}
570.0																
742.0		300	-108.78	260.24			33.08	239.91			78.91	158.66	220.77	138.33	1.47×10^{-12}	2.76×10^{-12}
460.0																

															σ_{LJ}	ϵ_{LJ}/k
															3.82	253.5

$\rho(E_o)$	T	Z_{LJ}	F_E	F_{rot}	k_{diss}^{ac}	k_{rec}^{ac}	$\langle \Delta E \rangle$	n	F_{ac}
$\omega(E_o)$						k^{wc}			F_{wc}
F_{anh}			Q_{vib}			β_c			F
8.67×10^1	200.0	2.71×10^{-10}	1.03	38.84	7.91×10^{-61}	5.18×10^{-30}	1.74	2.00	0.89
0.978			1.06			1.99×10^{-30}			0.87
1.37						0.38			0.78
	300.0	2.96×10^{-10}	1.05	25.48	4.34×10^{-42}	2.96×10^{-30}	1.74		0.82
			1.26			8.86×10^{-31}			0.84
						0.30			0.69

TABLE XVIIIb

REACTION:			FONO		:	NO_2		+	F							
ν	I	T	ΔH_f	S°	ν	I	ΔH_f	S°	ν	I	ΔH_f	S°	ΔH	ΔS	K_{eq}^{TH}	K_{eq}^{SP}
1825.0	103.03	0	-61.59	0	1357.8	40.8	35.92	0	-	-	76.82	0	174.33	0	-	-
870.0	73.10				1665.5	38.6										
670.0	29.94	200	-63.91	254.54	756.8	2.1	33.89	225.74			78.17	149.56	175.97	120.76	8.16×10^{-21}	8.16×10^{-21}
560.0																
310.0		300	-63.76	276.88			33.08	239.91			78.91	158.66	175.75	121.69	1.39×10^{-5}	1.39×10^{-5}
135.0																

							σ_{LJ}	ϵ_{LJ}/k	
							3.82	253.5	

$\rho(E_o)$ / $\omega(E_o)$ / F_{anh}	T	Z_{LJ}	F_E / Q_{vib}	F_{rot}	k_{diss}^{ac}	k_{rec}^{ac} / k^{uc} / β_c	$\langle \Delta E \rangle$	n	F_{ac} / F_{uc} / F
4.34×10^2	200.0	2.71×10^{-10}	1.04	30.99	1.15×10^{-49}	1.41×10^{-29}	1.74	1.96	0.76
0.973			1.85			5.39×10^{-30}			0.87
1.37						0.38			0.66
	300.0	2.96×10^{-10}	1.07	20.18	1.14×10^{-34}	8.16×10^{-30}	1.74		0.69
			3.08			2.43×10^{-30}			0.84
						0.30			0.58

TABLE XIX

REACTION:	$FONO_2$				+	NO_2			+	FO							
ν	I	T	ΔH_f	S°	ν	I	ΔH_f	S°	ν	I	ΔH_f	S°	ΔH	ΔS	k^{TB}_{eq}	k^{SP}_{eq}
1759.1	52.96	0	18.05	0	1337.8	40.8	35.92	0	1056.0	14.7	108.76	0	126.63	0	-	-
1300.9	111.01				1665.5	38.6				14.7						
927.7	141.17	200	11.83	269.26	756.8	2.1	33.89	225.74			108.77	204.64	130.08	161.12	6.44×10^{-7}	6.61×10^{-7}
803.7																
708.5		300	10.44	293.23			33.08	239.91			105.78	216.77	131.42	163.45	1.12×10^{-7}	1.14×10^{-7}
633.0																
454.5																
302.6																
151.6															σ_{LJ}	ϵ_{LJ}/k
															4.08	274.8

$\rho(E_0)$	T	Z_{LJ}	F_E	F_{rot}	k^{sc}_{diss}	k^{sc}_{rec}	$\langle \Delta E \rangle$	n	F_{sc}
$\alpha(E_0)$						k^{sc}			F_{sc}
F_{anh}			Q_{vib}			β_c			F
2.21×10^3	200.0	2.85×10^{-10}	1.09	17.44	1.03×10^{-36}	1.59×10^{-30}	1.88	3.18	0.77
0.949			1.90			6.20×10^{-30}			0.88
1.38						0.39			0.67
	300.0	3.11×10^{-10}	1.38	11.06	6.73×10^{-25}	5.96×10^{-30}	1.88		0.67
			3.21			1.79×10^{-31}			0.84
						0.30			0.57

TABLE XX

REACTION: CH_3O_2 ⇌ CH_3 + O_2

ν	I	T	ΔH_f	S°	ν	I	ΔH_f	S°	ν	I	ΔH_f	S°	ΔH	ΔS	K_{eq}^{TH}	K_{eq}^{SP}
3006.0	48.2	0	26.47	0	3044.0	1.8	149.04	0	1580.3	11.5	0	0	122.57	0	-	-
3006.0	41.7				3162.0	1.8				11.5						
1050.0	9.7	200	19.92	251.78	1396.0	3.6	146.87	179.27			0	193.38	126.95	120.87	5.30×10^{-8}	5.20×10^{-8}
2930.0					3162.0											
1467.0		300	17.15	272.47	1396.0		145.66	194.30			0	205.20	128.51	127.03	4.45×10^{3}	4.47×10^{3}
1464.0					580.0											
1464.0																
1182.0																
1049.0																
928.0																
303.0																
120.0																
															σ_{LJ}	ϵ_{LJ}/k
															4.02	360.0

$\rho(E_o)$ / $\omega(E_c)$ / F_{anh}	T	Z_{LJ}	F_E / Q_{vib}	F_{rot}	k_{diss}^{sc}	k_{rec}^{sc} / k^{uc} / β_c	$\langle \Delta E \rangle$	n	F_{sc} / F_{uc} / F
5.24×10^{2}	200	3.16×10^{-10}	1.09	17.12	2.69×10^{-36}	5.20×10^{-29}	0.11	3.42	0.79
0.895			1.96			2.40×10^{-30}			0.66
1.26						0.05			0.52
	300	3.43×10^{-10}	1.14	10.87	8.67×10^{-26}	1.94×10^{-29}	0.11		0.75
			3.08			6.0×10^{-31}			0.61
						0.03			0.46

TABLE XXI

REACTION:	$CH_3O_2NO_2$				+	CH_3O_2			+	NO_2								
ν	I	T	ΔH_f°	S°	ν	I	ΔH_f°	S°	ν	I	ΔH_f°	S°	ΔH	ΔS	E_{eq}^{TB}	E_{eq}^{SP}
2004.0	1048.0	230.7	5	-28.33	0	3008.0	48.2	26.47	0	1357.8	40.8	35.92	0	90.72	0	-	-
3008.0	928.0	202.5				2004.0	41.7			1665.5	38.6						
2930.0	876.0	52.1	200	-40.22	315.36	1050.0	9.7	19.92	251.78	756.0	2.1	33.89	225.74	94.03	162.16	3.00×10^3	3.04×10^3
2000.0	709.0					2930.0											
1756.0	455.0		300	-44.27	348.38	1467.0		17.15	272.47			33.08	239.91	94.50	164.0	3.18×10^{11}	3.20×10^{11}
1467.0	450.0					1444.0											
1467.0	303.0					1444.0											
1444.0	120.0					1182.0											
1301.0	40.0					1049.0											
1182.0	40.0					928.0											
1050.0						303.0											
						120.0											

$\rho(E_c)$	T	Z_{LJ}	F_E	F_{rot}	k_{diss}^{sc}	k_{rec}^{sc}	$\langle \Delta E \rangle$	n	F_{sc}	σ_{LJ}	ϵ_{LJ}/k
$\omega(E_c)$						k^{sc}			F_{sc}		
F_{anh}			Q_{vib}			β_c			F		
2.00×10^6	200.0	3.63×10^{-10}	1.18	9.39	7.68×10^{-26}	2.52×10^{-29}	2.07	4.66	0.54	4.76	490.00
0.83			34.16			9.84×10^{-30}			0.88		
1.16						0.39			0.47		
	300.0	3.92×10^{-10}	1.29	5.81	1.67×10^{-18}	5.10×10^{-30}	2.07		0.46		
			136.38			1.50×10^{-30}			0.84		
						0.29			0.39		

TABLE XXII

REACTION:		SO_3H			:	SO_2			+		OH					
ν	I	T	ΔH_f	S°	ν	I	ΔH_f	S°	ν	I	ΔH_f	S°	ΔH	ΔS	k_{eq}^{TH}	k_{eq}^{SP}
1068.0	101.0	0	-399.52	0	1151.4	57.0	-296.31	0	3735.2	0.9	38.87	0	144.08	0	-	-
1391.0	52.7				517.7	48.6				0.9						
1391.0	49.9	200	-406.15	260.21	1361.8	8.3	-295.65	232.92			39.30	171.48	149.80	144.19	6.25×10^{-13}	6.15×10^{-13}
495.0																
529.0		300	-410.03	280.82			-296.86	248.35			39.46	183.53	152.63	151.12	5.09	4.86
529.0																
3550.0																
1396.0																
500.0																
															σ_{LJ}	ϵ_{LJ}/k
															4.39	384.5

$\rho(E_o)$ / $\sigma(E_o)$ / F_{anh}	T	Z_{LJ}	F_E / Q_{vib}	F_{rot}	k_{diss}^{uc}	k_{rec}^{uc} / k^{uc} / β_c	<ΔE>	n	F_{uc} / F_{uc} / F
2.53×10^2	200.0	3.25×10^{-10}	1.07	21.49	7.63×10^{-42}	1.24×10^{-29}	0.24	3.38	0.89
0.927			1.11			1.18×10^{-30}			0.72
1.38						0.10			0.64
	300.0	3.54×10^{-10}	1.11	13.76	2.22×10^{-29}	4.56×10^{-30}	0.24		0.79
			1.44			3.00×10^{-31}			0.69
						0.07			0.54

Acknowledgment

This work was supported in part by the National Aeronautics and Space Administration under contract DNA001-81-E-0146 (JPL 954815).

Bibliogrpahy

[1] Chemical Kinetic and Photochemical Data for Use in Stratospheric Modelling, JPL Pub. 81–3, 1981.
[2] D. L. Baulch, R. A. Cox, R. F. Hampson, J. A. Kerr, J. Troe, and R. T. Watson, *J. Phys. Chem. Ref. Data*, **9**, 295 (1980).
[3] J. S. Chang, A. C. Baldwin, and D. M. Golden, *J. Chem. Phys.*, **71**, 2021 (1979).
[4] J. Troe, *J. Chem. Phys.*, **66**, 4745 (1977).
[5] J. Troe, *J. Chem. Phys.*, **66**, 4758 (1977).
[6] K. Luther and J. Troe, "Proc. 17th Int. Symposium on Combustion," 1979, p. 535.
[7] "JANAF Thermochemical Tables," 2nd ed., 1970.
[8] S. W. Benson, "Thermochemical Kinetics," 2nd ed., Wiley, New York, 1976.
[9] H. B. Thompson, *J. Chem. Phys.*, **47**, 3407 (1967).
[10] R. C. Reid and T. K. Sherwood, "Properties of Gases and Liquids," McGraw-Hill, New York, 1958.
[11] P. J. Robinson and K. A. Holbrook, "Unimolecular Reactions," Wiley, New York, 1972.
[12] O. Kajimoto and R. J. Cvetanovic, *J. Chem. Phys.*, **64**, 1005 (1976).
[13] J. V. Michael and J. H. Lee, *J. Phys. Chem.*, **83**, 10 (1979).
[14] A. C. Baldwin and D. M. Golden, *J. Phys. Chem.*, **82**, 644 (1978).
[15] H. Niki, P. D. Maker, C. M. Savage, and L. P. Breitenbach, *Chem. Phys. Lett.*, **45**, 564 (1977).
[16] D. R. Stull, E. F. Westrum, and G. C. Sinke, "The Chemical Thermodynamics of Organic Compounds," Wiley, New York, 1969.
[17] H. Niki, P. D. Maker, C. M. Savage, and L. P. Breitenbach, *Chem. Phys. Lett.*, **59**, 78 (1978).
[18] B. Janowski, H. D. Knauth, and H. Martin, *Ber. Bunsenges. Phys. Chem.*, **81**, 1262 (1977).
[19] D. Rohlack, H. D. Knauth, and A. Guarnieri, private communication.
[20] M. S. Zahniser, J. S. Chang, and F. Kaufman, *J. Chem. Phys.*, **67**, 997 (1977).
[21] J. W. Birks, B. Shoemaker, T. J. Leck, R. A. Borders, and L. J. Hart, *J. Chem. Phys.*, **66**, 4591 (1977).
[22] M. T. Leu, C. L. Lin, and W. B. DeMore, *J. Phys. Chem.*, **81**, 190 (1967).
[23] Y. P. Lee, R. M. Stimpfle, R. A. Perry, J. A. Mucha, K. M. Evenson, D. A. Jennings, and C. J. Howard, *Int. J. Chem. Kinet.*, **14**, 711 (1982).
[24] H. D. Knauth, *Ber. Bunsenges. Phys. Chem.*, **82**, 212 (1978).
[25] G. Schonle. H. D. Knauth, and R. N. Schindler, *J. Phys. Chem.*, **83**, 3297 (1979).
[26] R. H. Miller, D. L. Bernitt, and I. C. Hisatune, *Spectrosc. Acta*, **23A**, 223 (1967).
[27] R. A. Cox, J. P. Burrows, and G. B. Coker, unpublished.
[28] J. J. Margitan, *J. Geophys. Res.*, unpublished.
[29] S. P. Sander, G. W. Ray, and R. T. Watson, *J. Phys. Chem.*, **85**, 199 (1981).
[30] A. H. Jubert, *Z. Naturforsch.*, **35A**, 1071 (1980).
[31] E. A. Selzer and K. D. Bayes, *J. Phys. Chem.*, **87**, 392 (1983).
[32] D. C. Tardy and B. S. Rabinovitch, *Chem. Rev.*, **77**, 369 (1977).

Received November 22, 1982
Accepted April 25, 1983

Chapter II

A COMPUTATIONAL STUDY OF THE $HO_2 + HO_2$ AND $DO_2 + DO_2$ REACTIONS

Roger Patrick, John R. Barker, and David M. Golden

(Accepted for publication in
the Journal of Physical Chemistry)

A COMPUTATIONAL STUDY OF THE $HO_2 + HO_2$ AND $DO_2 + DO_2$ REACTIONS

Roger Patrick, John R. Barker and David M. Golden
Department of Chemical Kinetics
SRI International, Menlo Park, CA 94025

ABSTRACT

Experimental data concerning the title reactions are reviewed. An attempt was made to model the unusual pressure and temperature dependences of the rate constants within the framework of conventional RRKM theory. It was possible to fit all the experimental data with a single model but in order to do so, it was necessary to postulate a very loose, highly entropic, H_2O_4 intermediate. Projections based on this model are made for the variation of the rate constant over wide ranges of temperature and pressure.

*This work was supported, in part, by Contract DNA001-81-E-0146 (JPL 954815) with the National Aeronautics and Space Administration.

March 1983; rev, May 1983

Submitted to J. Phys. Chem.

INTRODUCTION

As a result of its importance to atmospheric and combustion chemistry the disproportionation reaction of gas phase HO_2 radicals has recently been studied by a number of groups.

$$HO_2 + HO_2 \rightarrow H_2O_2 + O_2 \qquad (1)$$

This work has indicated that the reaction rate shows marked pressure[1-3] and temperature dependences[1,4-6] which are inconsistent with the original view that the reaction involved a simple metathesis in which one HO_2 radical simply abstracts a H atom from the other to give the products H_2O_2 and O_2. Instead a mechanism involving the formation of an intermediate H_2O_4 species is now favored:

$$HO_2 + HO_2 \rightleftarrows H_2O_4 \rightarrow H_2O_2 + O_2 \qquad (2)$$

To date little attempt has been made to analyze this type of mechanism in detail to see if it can account for the observed kinetics or to make predictions of the rate constant at high pressures or temperatures. In addition to accurate rate data, it is necessary to have information on the spectroscopic and thermodynamic parameters of the H_2O_4 intermediate in order to carry out

the required calculations. The available experimental data relevant to the problem are briefly reviewed in the following sections. Throughout this discussion, the rate constant for self-reactions, such as (1), is defined by

$$k = -\tfrac{1}{2} \frac{d[R]}{dt} \frac{1}{[R]^2} .$$

(a) Kinetic Data

Cox and Burrows[1] and Thrush and Wilkinson[2] first demonstrated that the rate constant for reaction (1) was pressure dependent. More recently Sander et al[3] used flash photolysis/UV detection methods to show that the rate constant is linearly dependent on pressure in a variety of diluent gases and varies from (1.91 ± 0.29) x 10^{-12} cm^3 $molecule^{-1}$ s^{-1} at 100 Torr to (2.97 ± 0.45) x 10^{-12} cm^3 $molecule^{-1}$ s^{-1} at 700 Torr in nitrogen. Extrapolation of their data to zero pressure suggests a pressure independent contribution to the reaction with a rate constant of 1.75 x 10^{-12} cm^3 $molecule^{-1}$ s^{-1}. The form of the pressure dependence has been subsequently confirmed by Simonaitis and Heicklen,[7] who also used flash photolysis/UV-detection techniques. (There is a small systematic difference in the rate constants reported by the two groups but this can be accounted for by the differences in the extinction coefficients assumed for the HO_2 radical.) The extrapolation leading to a zero pressure contribution to the rate constant has been supported by the low pressure studies of Thrush and Tyndall[6,8] who reported a rate constant of (1.6 ± 0.1) x 10^{-12} cm^3 $molecule^{-1}$ s^{-1} between 7 and 20 Torr, using diode laser spectroscopy.

The pressure dependence of the rate constant for

$$DO_2 + DO_2 \rightarrow D_2O_2 + O_2 \qquad (3)$$

has also been investigated by Sander et al.[3] They found the rate constant to be less dependent on pressure than the corresponding HO_2 reaction, varying from an extrapolated 5×10^{-13} cm^3 $molecule^{-1}$ s^{-1} at zero pressure to 9×10^{-13} cm^{-3} $molecule^{-1}$ s^{-1} at 700 Torr of nitrogen.

The temperature dependence of reaction 1 at pressures of 700 Torr or greater has been investigated by several groups, and these studies all report strong negative temperature dependences. Cox and Burrows[1] generated HO_2 by the modulated photolysis of $H_2/O_2/Cl_2$ mixtures in a variety of diluents at a total pressure of 760 Torr, and they observed a temperature dependence of k_1, between 275 and 339 K, which could be expressed as $(3.8 \pm 1.4) \times 10^{-14}$ $\exp[(1250 \pm 250)/T]$ cm^3 $molecule^{-1}$ s^{-1}. Lii et al[4] used pulse radiolysis of H_2/O_2 mixtures at a total pressure of 2 atm and found a temperature dependence between 276 and 400 K which they expressed as $(1.14 \pm 0.16) \times 10^{-13}$ $\exp[(1057 \pm 45)/T]$ cm^{-3} $molecule^{-1}$ s^{-1}. Patrick and Pilling[5] used flash photolysis of $Cl_2/O_2/CH_3OH$ mixtures at a total pressure of 700 ± 10 Torr to generate HO_2 and found k to be given by $(4.14 \pm 1.15) \times 10^{-13}$ $\exp[(630 \pm 115)/T]$ cm^{-3} $molecule^{-1}$ s^{-1} between 298 and 510 K. Even at low pressure, the temperature dependence was found to be strongly negative by Thrush and Tyndall[6] who reported a rate constant of 2.4×10^{-13} $\exp(560/T)$ cm^3 $molecule^{-1}$ s^{-1} between 298 and 358 K at pressures of between 7 and 20 Torr.

Very recently, Sander[9] has also reported the temperature dependence of the $HO_2 + HO_2$ and $DO_2 + DO_2$ reactions, both determined by flash photolysis/UV spectroscopy over the range 290–450 K. At zero pressure, the rate constants are given by:

$$k_1 = 2.3 \times 10^{-13} \exp(600/T), \qquad k_3 = 2.2 \times 10^{-14} \exp(900/T)$$

while at 700 Torr, the bimolecular rate constants may be expressed as:

$$k_1 = 1.8 \times 10^{-13} \exp(824/T), \qquad k_3 = 1.7 \times 10^{-14} \exp(1201/T)$$

The temperature dependence of k_1 is in quite good agreement with the previous data of Patrick and Pilling[5] and Thrush and Tyndall.[6]

(b) Structure of H_2O_4

The molecular parameters of HO_2[10] are well established and the values used in the subsequent calculation are given in Table 1. By contrast even the structure of the postulated H_2O_4 intermediate is open to speculation. At low temperatures, in matrix isolation studies, a number of workers[11-14] have identified infrared and Raman spectra of the products of electrical discharge passed through water vapor, which they associate with a linear HOOOOH molecule. Only the skeletal motions of the O_4 chain have been identified in this way and there is substantial disagreement over the actual frequencies: O-O stretches are reported to be typically in the range 700-1000 cm^{-1}, while O-O-O bends are in the range 400-600 cm^{-1}. The actual values reported by Giguere and coworkers are given in Table 1 and these were used in some of the following calculations.

Supportive evidence for the formation of tetroxides with O_4 chain structures in the self reactions of peroxy radicals is provided by the observed products of the reaction of two CH_3O_2 radicals:[15]

$$2CH_3O_2 \rightarrow HCHO + CH_3OH + O_2 \qquad (4a)$$

$$\rightarrow 2CH_3O + O_2 \qquad (4b)$$

$$\rightarrow CH_3OOCH_3 + O_2 \qquad (4c)$$

Table 1 MOLECULAR PARAMETERS FOR H_2O_4, D_2O_4, HO_2, and DO_2

Vibrational Frequencies

H_2O_4	ω/cm^{-1}	Type	Ref.	D_2O_4	ω/cm^{-1}
ν_1	3599	O-H stretch	38		2416
ν_2	3608	O-H stretch	38		2029
ν_3	855	O-O stretch	11		855
ν_4	764	O-O stretch	11		764
ν_5	450	OOO bend	11		450
ν_6	175	HOOO torsion	(assumed)		124
ν_7	175	HOOO torsion	(assumed)		124
ν_8	1402	O-H bend	38		1015
ν_9	1266	O-H bend	38		966
ν_{10}	823	O-O stretch	11		823
ν_{11}	430	OOO bend	11		430
ν_{12}	100	OOOO torsion	(assumed)		100

HO_2	ω/cm^{-1}	Type	Ref.	DO_2
ν_1	3410	O-H stretch	10	2411
ν_2	1390	bend	10	947
ν_3	1095	O-O stretch	10	1095

Moments of inertia I/amu A^{-2} [39]

H_2O_4	HO_2	D_2O_4	DO_2
16.6	0.82	18.3	1.22
113.2	14.97	120.0	15.88
114.5	15.84	122.3	17.04

Lennard-Jones Parameters[40]

	ε/k /K	σ/A
H_2O_4	577.0	4.55
N_2	71.4	3.68

Each of the sets of products is consistent with the initial formation of a $CH_3O_4CH_3$ intermediate.

The HO_2 radical has a large dipole moment (2.1 Debye),[16] and it has been suggested[16] that the intermediate in the disproportion reaction is in fact hydrogen bonded with a structure OOH-OOH or even a doubly hydrogen bonded cyclic species:

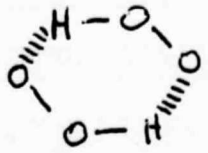

(I)

Lee and coworkers[17] have used FTIR spectroscopy to investigate the products of the UV photolysis of a dilute matrix sample of H_2CO or glyoxal in O_2 at 12-20 K. They observed the IR peaks associated with HO_2 radicals and also other peaks at 3323, 1416 and 1108 cm^{-1}, somewhat displaced from those of HO_2, which they ascribe to a hydrogen-bonded HO_2 dimer. Since Lee and coworkers did not study the spectrum at longer wavelengths, it is not clear whether they were observing the same species as Giguere; their reported frequency shifts are consistent with those expected upon forming hydrogen bonds but, in addition, they are not inconsistent with some of those frequencies expected for a linear HOOOH species.

An experiment by Niki and coworkers[18] has at least placed some restrictions on the nature of the transition state involved in the conversion of H_2O_4 to the final reaction products. Using FTIR detection they observed the isotope distribution in product H_2O_2 formed from a mixture of $H^{18}O^{18}O$ and $H^{16}O^{16}O$ radicals. Since a mixed product of the form $H^{16}O^{18}OH$ was never observed they were able to rule out (II) as a possible transition state.

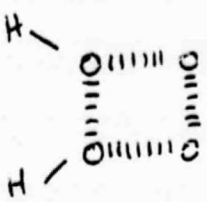

(II)

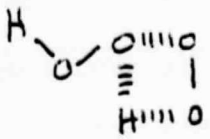

(III)

This experiment also excludes the possibility of a cyclic O_4 structure for H_2O_4 but unfortunately, it cannot distinguish between a linear HOOOOH molecule leading to a transition state such as (III) or a hydrogen bonded intermediate.

An additional unresolved question concerns the electronic state of the H_2O_4 intermediate. Two HO_2 radicals in their ground state ($^2A''$) can combine on either a triplet or a singlet surface but, if a linear HOOOOH intermediate is involved, the triplet surface is likely to be repulsive. However, the assumed products H_2O_2 and $O_2(^3\Sigma_g^-)$ can only be reached on the triplet surface. This raises the question of whether H_2O_4 is a bound triplet state species, which may be possible for a hydrogen bonded species where the unpaired electrons would not be required for bonding, or whether the first formed products are the thermochemically accessible H_2O_2 and $O_2(^1\Delta_g)$ (Figure 1).

(c) Thermochemical Data

The heat formation of HO_2 has recently been redetermined by Howard[19] who obtained it from a study of the $HO_2 + NO \rightleftarrows HO + NO_2$ equilibrium. The reported value was $\Delta H_f^{298} = 10.5 \pm 2.5$ kJ mol^{-1}.

The heat of formation for H_2O_4 depends on its structure and the nature of the bonding between the two HO_2 fragments. Two independent investigations by Adamic et al.[20] and Bennet et al.[21] have been made into the low temperature (140 K) equilibrium in solution between t-butyl peroxy radicals and an assumed

tetroxide species using ESR techniques. On the basis of these results, Nangia and Benson[22] obtained a value for ΔH for the gas-phase reaction at 300 K:

$$2HO_2 \rightarrow HOOOOH$$

This was $\Delta H = -34.3 \pm 4.2$ kJ mol^{-1}. Benson and Shaw[23] estimated the corresponding entropy change on the basis of model structures as $\Delta S = -143.1$ J mol^{-1} K^{-1}. The correction of the measured enthalpy change at 140 K in the liquid phase to the gas phase at 300 K was recalculated here (see appendix) and the corresponding entropy change was also derived. The values found were $\Delta H = -58.6$ kJ mol^{-1} and $\Delta S = -237.7$ J mol^{-1} K^{-1}. The origin of the difference between this value for ΔH and that reported by Nangia and Benson lies in the different assumptions made in estimating heats of vaporization. This shows that there is a large uncertainty in deriving the thermochemistry of gas phase HOOOOH.

It is unlikely that a singly hydrogen bonded intermediate would be more strongly bound than Benson's estimate for HOOOOH, indeed a value of about 21 kJ mol^{-1} is often suggested. This may presumably be doubled in the case of the cyclic species.

REACTION MECHANISM

The form of the pressure and temperature dependences for reaction (1) seem to be well established.

The potential energy surface over which the reaction occurs may be considered in terms of two limiting cases, illustrated in Figure 1, both of which could, in principle, account for the observed pressure dependence of the rate constant, k_1.

Type (a): Here two essentially independent channels are operative (5,6). The zero pressure rate constant of 1.75×10^{-12} cm^3 molecule^{-1} s^{-1} represents an abstraction reaction leading directly to products. The pressure dependence of the experimentally determined rate constant, k_{obs}, is represented by a pressure-dependent approach to equilibrium between HO_2 and H_2O_4, the only loss process for H_2O_4 being redissociation:

$$HO_2 + HO_2 \rightarrow H_2O_2 + O_2 \qquad (5)$$

$$HO_2 + HO_2 \overset{[M]}{\rightleftarrows} H_2O_4 \qquad (6, -6)$$

If H_2O_4 redissociates rapidly, then an equilibrium is set up and the observed rate constant for loss of HO_2 is simply k_5. On the other hand, if k_{-6} is very slow, the H_2O_4 is essentially stable and k_{obs} is given by $k_5 + k_6[M]$. In the intermediate region, at high pressures, substantial amounts of the H_2O_4 complex will be formed and the observed rate constant will be given by

$$k_{obs} = k_5 + \left\{k_6 - k_{-6} \frac{[H_2O_4]}{[HO_2]^2}\right\}[M] \qquad (7)$$

Under such conditions, k_{obs} is not a true rate constant since it will be time dependent, but if k_{-6} is sufficiently small, then this would not be apparent on the timescale of experiments, such as those of Sander et al.,[3] i.e., ~ 20 ms. Similarly, deviations from second-order kinetics in the observed loss of HO_2 radicals would be small. Reaction (6) may be assumed to be at its low-pressure limit in view of the weak bonding in H_2O_4, and its relatively low density of states if the frequencies in Table 1 are used. The rate constants k_6 and k_{-6} can then be calculated using approximate methods developed by Troe.[24,25] Taking k_5 to be given by the experimentally determined 1.75×10^{-12} cm^3 $molecule^{-1}$ s^{-1}, it is then possible to simulate the time dependence of HO_2 over a timescale of 20 ms using numerical integration techniques, and hence extract the apparent second order rate constant for loss of HO_2 as a function of pressure. Adopting this procedure, it was found that if Benson's suggested bond strength of 34.3 kJ is assumed for a HOOOOH species with the parameters given in Table 1, then the lifetime of the HOOOOH molecule is too short to affect the observed HO_2 kinetics and k_{obs} simply equals k_5, which is independent of pressure. In order to increase the lifetime of HOOOH sufficiently to account for the experimental pressure dependence in k_{obs}, it is necessary to raise the bond strength to around 77 kJ mol^{-1}.

An additional problem for this model, even if a stronger bond is assumed, is presented by the temperature dependence. As the temperature is raised, the lifetime of such a HOOOOH intermediate decreases rapidly until by 400 K the only loss of HO_2 is once again by reaction (5). Thus at temperatures greater than 300 K, the temperature dependence of k_{obs} would be essentially that of k_5, and it is unlikely that the rate constant for a disproportionation reaction would have such a strong negative temperature dependence as that observed experimentally.

The same behavior would be expected if hydrogen bonded HOOHOO intermediate were assumed, and in this case it would probably be more difficult to justify the increase in bond strength.

Type (b): In this model it is assumed that there is no direct disproportionation reaction at all. Instead, the reaction products H_2O_2 and O_2 are formed by a molecular elimination from an HOOOOH intermediate. The mechanism may be represented by:

$$HO_2 + HO_2 \underset{k_{-a}}{\overset{k_1}{\rightleftharpoons}} H_2O_4^* \xrightarrow{k_r} H_2O_2 + O_2 \qquad (8)$$

$$k_s[M] \quad \downarrow\uparrow \quad k_{-s}[M]$$

$$H_2O_4$$

From this, k_{obs} may be derived as

$$k_{obs} = \frac{k_1 k_r + k_r k_{-s}[M][H_2O_4]/[HO_2]^2}{k_s[M] + k_{-a} + k_r} \qquad (9)$$

where the rate constants k_1, k_r, k_{-a}, k_s, and k_{-s} are defined above. The zero pressure contribution arises from those vibrationally excited $H_2O_4^*$ molecules which rearrange to give H_2O_2 and O_2 directly, while the pressure dependence is a result of the stabilization of some $H_2O_4^*$ into the well. The stablized H_2O_4 molecules may or may not subsequently decompose thermally depending upon the depth that is assumed for the well; the thermal decomposition products can be HO_2 radicals or $H_2O_2 + O_2$, depending upon the relative barrier heights and A-factors.

This kind of model is more difficult to test numerically than type (a) and a two-channel RRKM model was developed in order to make the necessary simulations. The calculation method is described below.

CALCULATIONAL METHOD

$H_2O_4^*$ is formed by a chemical activation process with a rate constant k_1^∞ in highly vibrationally excited states from which it may be stabilized by collision, decompose back to reactants with a rate constant $k_{-a}(E)$ or eliminate H_2O_2 and O_2 with a rate constant $k_r(E)$. If the thermalized H_2O_4 does not decompose on the experimental timescale, then the rate constant for the loss of HO_2 radicals is given by

$$k_{obs} = k_1^\infty \int_{E_1}^\infty \frac{k_r(E) + \beta Z[M]}{k_{-a}(E) + k_r(E) + \beta Z[M]} f(E)dE \qquad (10)$$

This expression is derived in the same way as in the usual strong-collider RRKM theory, where a steady-state treatment for $H_2O_4^*(E)$ is used. E_1 is the barrier to redissociation, k_1^∞ is the high-pressure limiting rate constant for reaction (1), Z is the Lennard-Jones collision frequency, β is the collisional deactivation efficiency, and f(E) is the chemical activation distribution[29]

$$f(E) = \frac{k_{-a}(E)N(E)\ \exp(-E/kT)}{\int_{E_1}^\infty k_{-a}(E)N(E)\ \exp(-E/kT)\ dE} \qquad (11)$$

where N(E) is the density of states of H_2O_4 at energy E.

However, if the bonding in H_2O_4 is sufficiently weak, molecules deactivated into the well may decompose either back to HO_2 radicals or to products on the experimental timescale. Monte Carlo calculations[26] showed that the chemical activation process in the subsequent models at pressures of 100 Torr and greater leads to the rapid (< 5 ns) thermalization of those H_2O_4 molecules that survive until the first collision occurs . The secondary (thermal) decomposition of stabilized H_2O_4 may therefore be treated by a conventional

two-channel thermal decomposition mechanism. The rate constants for the decomposition of thermalized molecules are given by:[27]

$$k_{-a} = \int_{E_1}^{\infty} \frac{k_{-a}(E)\ \beta Z[M]}{k_{-a}(E) + k_r(E) + \beta Z[M]}\ f'(E)dE \qquad (12)$$

and

$$k_r = \int_{E_2}^{\infty} \frac{k_r(E)\ \beta Z[M]}{k_{-a}(E) + k_r(E) + \beta Z[M]}\ f'(E)dE \qquad (13)$$

where f'(E) is the thermal distribution function:

$$f'(E) = \frac{N(E)\ \exp(-E/kT)}{Q_{vib}} \qquad (14)$$

and E_2 is the activation barrier for the molecular elimination channel.

The probability, p, of thermal decomposition leading to $H_2O_2 + O_2$ rather than back to HO_2 radicals is then given by:

$$p = \frac{k_r}{k_{-a} + k_r} \qquad (15)$$

If the thermal reaction is fast compared to the experimental timescale, then the overall rate constant for loss of HO_2 may be expressed in a modified version of (8):

$$k_{obs} = k_1^{\infty} \int_{E_1}^{\infty} \frac{k_r(E) + \beta Z[M]p}{k_{-a}(E) + k_r(E) + \beta Z[M]}\ f(E)dE \qquad (16)$$

The microscopic rate constants $k_{-a}(E)$ and $k_r(E)$ were calculated using RRKM theory and assuming fixed transition states. Exact state counting[28] was used to determine the sums of states for the activated complexes and the Whitten-Rabinovitch[29] approximation was used to obtain the density of states of the molecule. Anharmonic corrections to the densities of states were made according to the Haarhof's procedure.[30]

The value of the high pressure rate constant k_1^∞, for this reaction is not known experimentally, and for the purposes of this calculation it was assumed equal to 1.4×10^{-11} cm^3 molecule^{-1} s^{-1} by analogy with the value for the recombination of the isoelectronic ethyl radical.[31] This may be an underestimate since using the isoelectronic argument predicts that the high pressure rate for OH + HO_2 would be the same as CH_3 + C_2H_5, i.e., ~ 2.5×10^{-11} cm^3 molecule^{-1} s^{-1}, (obtained by the cross-combination rule based on rate constants for C_2H_5 + C_2H_5[31] and CH_3 + CH_3[32]), whereas at 1 atm DeMore[33] reports the rate constant to be $(1.2 \pm 0.4) \times 10^{-10}$ cm^3 molecule^{-1} s^{-1} and pressure dependent. The high-pressure rate constant for the DO_2 + DO_2 reaction was also taken as 1.4×10^{-11} cm^3 molecule^{-1} s^{-1}, and both high-pressure rate constants were assumed to be independent of temperature.

Following Troe[25] the collision rate constant Z was set equal to the Lennard-Jones collision rate constant given by:

$$Z = N_A \sigma_{A-M}^2 \left(8RT/\pi\mu_{A-M} \right)^{1/2} \Omega^{2,2}(A-M) \qquad (17)$$

where N_A is the Avogadro number, μ_{A-M} is the reduced molar mass, and σ_{A-M} is the average Lennard-Jones collision diameter given by $(\sigma_A + \sigma_M)/2$. The reduced collision integral $\Omega^{2,2}(A-M)$ may be expressed as an approximate function of kT/ε_{A-M}, where ε_{A-M} is the Lennard-Jones well-depth defined by $\varepsilon_{A-M} = (\varepsilon_{AA}\varepsilon_{MM})^{1/2}$:

$$\Omega^{2,2}(A-M) = [0.697 + 0.5185 \log(kT/\varepsilon_{A-M})]^{-1} \qquad (18)$$

The relevant Lennard-Jones parameters are given in Table 1. The temperature dependence of β, the deactivation efficiency, was described by the approximate equation of Troe:[25]

$$\frac{\beta}{1 - \beta^{1/2}} = \frac{\langle \Delta E \rangle}{F_E kT} \qquad (19)$$

where $\langle \Delta E \rangle$, the average energy removed by collision, was taken to be 1.88 kJ mol^{-1} and independent of temperature, and F_E is the energy dependence of the density of states.

This treatment of "weak" collision effects is perhaps not as realistic as the Monte Carlo calculations incorporating an exponential model for energy transfer, as described by Barker.[26] However, a comparison was made, for a simple chemical activation case, between the results of a stochastic calculation with starting energies selected from the chemical activation distribution function (equation 11) by Monte Carlo techniques and the results obtained by numerical integration of equation (10). These results were in complete agreement, which justifies the use of the simplified treatment of the energy transfer process (equation 10). The direct integration of equations (10) and (16) was found to be more efficient computationally than the equivalent Monte Carlo technique, which required large numbers of trajectories and long running times for systems in which the subsequent decomposition of thermalized molecules was important.

The transition state parameters used in the first calculations, assuming a linear HOOOOH structure for the adduct are given in Table 2. The frequencies and structure of the transition state leading back to HO_2 fragments, $H_2O_4^{\dagger}$ (1), were chosen so as to be consistent with the high pressure limit rate constant. In order to ensure that k_1^{∞} was temperature independent some of the modes in this transition state were systematically tightened as the temperature increased. The structure of the second transition state, $H_2O_4^{\dagger}$ (2), was assumed to be like (III) and the frequencies chosen were based on those of hydrogen peroxide with additional modes assigned according to

Benson's methods.[34] The structure and frequencies of the corresponding deuterated species were based on the original protonated ones and chosen so as to be consistent with the Teller-Redlich product rule.[29]

Calculations were performed for three kinds of linear HOOOOH molecule in an attempt to account for the observed pressure dependences of the $HO_2 + HO_2$ and $DO_2 + DO_2$ reaction and the temperature dependence of the $HO_2 + HO_2$ reaction. The first of the species had frequencies as reported by Giguere and a dissociation energy $\Delta H(HO_2 - O_2H)$ as given by Benson, the second had the same frequencies but was more strongly bound and the third had looser frequencies and a weak bond.

Table 2. TRANSITION STATE FREQUENCIES

$H_2O_4^{\dagger}(1)$		$H_2O_4^{\dagger}(2)$		$D_2O_4^{\dagger}(1)$	$D_2O_4^{\dagger}(2)$
ω/cm^{-1}	Type	ω/cm^{-1}	Type	ω/cm^{-1}	ω/cm^{-1}
3500(2)	O-H stretch	3774	O-H stretch	2475(2)	2800
1390(2)	O ^{O} O bend	3788	O-H stretch	980(2)	2800
1000(2)	O-O stretch	1266	H·O ÷ O bend	1000(2)	1025
60(2)	pseudo vibrations	1380	OOH bend	60(2)	1025
45(2)	correlating with	880	O-O stretch	23(2)	880
25	translation	1580	O —·— O stretch	32	1580
	and rotation	300	O·O stretch		300
		300	O.O —·— O bend		300
		225	torsion		175
		150	O·H·O bend		113
		150	O·O·H bend		113

A potential surface intermediate between (a) and (b) was also considered where some, but not all, of the experimentally observed zero-pressure rate constant may be ascribed to a direct disproportionation reaction.

The additional uncertainties associated with possible hydrogen-bonded intermediates precluded any detailed calculations, but some conclusions can be drawn on the basis of the results of the calculations involving HOOOOH intermediates.

RESULTS

(i) Tight molecule, weak bond: Using the frequencies and bond strength in Table 1 for the HOOOOH molecule and the transition state parameters given in Table 2, it was possible to obtain the observed zero pressure rate constant if the barrier to the decomposition of HOOOOH to products, E_2, was set at 10.0 kJ mol^{-1}. However, no pressure dependence is predicted when the pressure is raised to 700 Torr. Within this model the microscopic rate constants for back dissociation, $k_{-a}(E)$, are too fast for competition by collisional stabilization to occur. It was found that the zero pressure rate constant is determined primarily by the difference in energy between the two barriers, E_1 and E_2, for the decomposition of the intermediate molecule, while the pressure dependence is determined by the density of states of the molecule at energy E_1. In order to obtain the observed experimental pressure dependence, it is necessary to either increase the well depth over the value suggested by Benson or increase the entropy of the molecule by reducing some of its vibrational frequencies from the values reported by Giguere. These options were investigated in turn.

(ii) Tight molecule, strong bond: If E_1 is increased to 140.0 kJ mol^{-1} and E_2 is set at 116.0 kJ mol^{-1}, then it is possible to obtain the experimental values of k_1 at zero and higher pressures, as shown in Figure 2, using equation (10). With this deep a well, the lifetime of stabilized HOOOOH is $\sim 2 \times 10^5$ s for unimolecular decomposition at 700 Torr, which is much longer

than the experimental timescale. However, it is known that H_2O_3 has a very similar absorption spectrum to H_2O_2,[35] and so it may be expected that the spectrum of H_2O_4 would also resemble that of H_2O_2. Thus the residual absorption observed after the disappearance of the HO_2 radicals in the flash photolysis experiments[3] might have been due to H_2O_4 rather than to H_2O_2.

The predicted temperature dependence for this model is illustrated in Figure 3 along with available experimental results. The prediction is based only on the room temperature data of Sander et al.,[3] and there are small systematic differences between that data set and the other temperature-dependent data. Variation of the frequencies for $H_2O_4^{\dagger}(2)$ indicated that any loosening of the transition state would change the temperature dependence from negative to positive which would then be in disagreement with the experimental data.

The remaining data which have to be taken into account within the model are those for the pressure and temperature dependence of the $DO_2 + DO_2$ reaction. By making a suitable choice of frequencies, consistent with the Teller-Redlich relation, for the transition state for decomposition to products it is possible to arrive at values of E_1 and E_2, based on the protonated case, but corrected for zero point energy differences, which lead to the experimental value for k_3 at zero pressure. E_1 is then 140.8 kJ mol^{-1} and E_2 is 128.8 kJ mol^{-1}. Thus although E_1 is not affected greatly by deuteration, E_2 is substantially raised when deuterium is substituted for hydrogen. However, it can be seen from Figure 2 that the pressure-dependence predicted by this model is too steep, with k_3 predicted to be 2.9×10^{-12} cm^3 $molecule^{-1}$ s^{-1} at 700 Torr. The enhanced pressure dependence arises because the density of states of DOOOOD at E_1 is greater than that of HOOOOH, and this reduces the

redissociation rate of the first formed DOOOOD* and enables collisional stabilization to compete more effectively.. Within this model, the only way in which the pressure dependence of the $DO_2 + DO_2$ reaction could be less than that for $HO_2 + HO_2$ would be if the well were sufficiently shallow that the stabilized molecules also decompose on the experimental timescale. The product distribution of this later decomposition would be determined largely by the relative barrier heights and since E_2 is higher for the deuterated case, back decomposition might be more favored than in the corresponding protonated case. This "loose molecule-weak bond" model is investigated in the next section.

(iii) Loose molecule, weak bond: If the value of E_1 is taken to be that suggested by Benson, then it is necessary to reduce some of the frequencies of the HOOOOH molecule from the values reported by Giguere in order to match the experimental pressure dependence (Table 3). In addition, as E_1 is reduced, it is necessary to take account of the thermal decomposition of stabilized HOOOOH by using equation (16) to calculate k_1. The lifetime of thermalized "loose" HOOOOH is $\sim 2 \times 10^{-9}$ s at 700 Torr and 300 K. With this model it is possible to reproduce the experimental pressure dependence for the $HO_2 + HO_2$ reaction with $E_1 = 34.3$ kJ mol^{-1} and $E_2 = 10.0$ kJ mol^{-1} using the molecular parameters in Table 3 and the previous transition state parameters given in Table 2. It can be seen that it was necessary to increase the entropy of the molecule quite drastically with the O-O stretching frequencies reduced to 100 cm^{-1} and the O-O-O bending frequencies reduced to 95 cm^{-1}. The realism of this step is open to question. The predicted temperature dependence for this model at zero pressure and 700 Torr is similar to that calculated in (ii) and presented in Figure 3. It can be seen thac the temperature dependence of the rate constant

is somewhat underestimated by these calculations. The agreement can be improved if it is assumed that k_1^∞ has some negative temperature dependence and the result for the case when $k_1^\infty \propto T^{-2}$ is also illustrated in Figure 3. The true temperature dependence of k_1^∞ is, of course, unknown but by analogy with alkyl radical recombination[31] is might be expected to be slightly negative.

As in (ii), using the same frequencies for the transition state leading to products, $D_2O_4^\dagger(2)$, it is possible to fit the zero-pressure rate constant for the $DO_2 + DO_2$ reaction (Table 3). The corresponding values of E_1 and

Table 3. MOLECULAR FREQUENCIES FOR "LOOSE" HOOOOH MODEL

H_2O_4 ω/cm^{-1}	D_2O_4 ω/cm^{-1}
3600(2)	2546(2)
1500(2)	1060(2)
100(3)	100(3)
95(3)	95(2)
80(2)	72(2)
60	42

of E_1 and E_2 are 35.1 and 22.8 kJ mol^{-1}, respectively. When the pressure is raised to 700 Torr, k_3 increases to 1.2×10^{-12} cm^3 $molecule^{-1}$ s^{-1}, in good agreement with the experimental value. The pressure dependence of k_3 is

moderated by the thermal reaction and so, in this way, it is possible for the pressure dependence of k_3 to be less than that of k_1.

The predicted temperature dependence of k_3 at zero pressure and 700 Torr is given in Figure 4 along with the recent data of Sander.[9] This prediction is based only on the room temperature pressure dependence for the $HO_2 + HO_2$ reaction and the assumption that k_3^∞ independent of temperature, and not optimized for the $DO_2 + DO_2$ reaction, but even so the agreement is quite good. The results of a calculation in which k_3^∞ is arbitrarily assigned a T^{-2} dependence are also illustrated.

It is possible to obtain the same agreement with experiment for increased values of E_1, up to ~ 60 kJ mol^{-1} if the frequencies of the HOOOOH molecule are raised accordingly. For well depths greater than 60 kJ mol^{-1}, the lifetime of H_2O_4 becomes too long for thermal decomposition of the stabilized species to play a role, and the predicted pressure dependence for reaction (3) is then too great to give agreement with experiment, as in (i). Molecular parameters which give satisfactory fits to all the experimental data are given in Table 4, along with those for a model based on Giguere's frequencies which fits only the HO_2 data.

TABLE 4. MOLECULAR PARAMETERS FOR HOOOOH USED IN FITTING KINETIC DATA

E_1/kJ mol^{-1}	E_2/kJ mol^{-1}	ω_{O-O}/cm^{-1}	ω_{OOO}/cm^{-1}	S/J mol^{-1} K^{-1}
34.3	10.0	100	95	379.5
40.0	15.7	145	100	369.7
60.0	35.7	300	150	346.5
140.0	116.0	Giguere Model		298.9

Figure 5 shows an extended projection of the temperature dependence of reaction (1) from stratospherically important temperatures to those more relevant to combustion processes. Above ~ 1000 K, it can be seen that the reaction rate is predicted to be independent of pressure and begins to increase with temperature, with a rate constant of ~ 3×10^{-12} cm^3 $molecule^{-1}$ s^{-1} at 3000 K. The same temperature dependence is obtained for all values of E_1 up to 60 kJ mol^{-1}. Figure 6 examines the pressure dependence of k_1 at 300 K up to pressures near the high pressure limit. In the loose molecule-weak bond case, it can be seen that the high pressure limit for k_1 is not k_1^∞ but $p^\infty k_1^\infty$, where p^∞ is given by equation (15), when k_r and k_{-a} have their limiting high pressure values. However, in this instance, p^∞ is ~ 0.94, and so the results for models (ii) and (iii) are essentially the same. Below 1 atm the pressure dependence is linear, but curvature becomes apparent at only a few atmospheres, and this pressure regime should be easily accessible experimentally.

In addition to type (a) and (b) potential surfaces, it is possible to envisage an intermediate case where some, but not all, of the zero-pressure rate constant may be ascribed to a direct disproportionation reaction. This possibility is more difficult to assess since the magnitude of this direct contribution to the zero-pressure rate constant, k_d, not known. However, if k_d is assumed to be temperature-independent, it must be less than 8×10^{-13} cm^3 $molecule^{-1}$ s^{-1}, the slowest experimentally observed value for the zero-pressure rate constant at 450 K.[9] Taking $k_d = 7 \times 10^{-13}$ cm^3 $molecule^{-1}$ s^{-1}, and assuming a 60 kJ mol^{-1} bond for HOOOOH, it was possible to fit the experimental pressure dependence of the $HO_2 + HO_2$ reaction with O-O stretches of 300 cm^{-1}, $0\ ^0\ 0$ bends of 180 cm^{-1} and $E_2 = 40.0$ kJ mol^{-1}. The temperature

dependence of the rate constant at 700 Torr was calculated to be the same as the case where $k_d = 0$, however, the temperature dependence at zero pressure is somewhat less marked than in the latter case. Thus, it appears that it is not possible to rule out the possibility that some contribution to the total rate constant is due to a direct disproportionation reaction.

(iv) Hydrogen-bonded intermediates: Due to the additional uncertainty associated with this kind of molecule, extensive detailed calculations were not attempted. However, on the basis of the previous results and some limited calculations on this model, it is possible to draw some useful conclusions.

For a linear hydrogen bonded species, HOOHOO, the binding between the radical fragments is unlikely to be stronger than the 34.3 kJ mol^{-1} assumed by Benson for HOOOOH, indeed it may be substantially less. Thus, in order to achieve a high enough density of states to account for the pressure dependence of the reaction, it too would be required to have a number of very low frequencies. In addition, the transition state for product formation will be much looser than that for the previous model and will resemble more closely that for back decomposition to reactants. Consequently, the values of $k_r(E)$ will be much faster, and it will be necessary to raise E_2 relative to E_1 in order to obtain the correct zero pressure rate constant. Depending on the exact nature of this transition state, it may even be necessary for E_2 to be greater than E_1, in which case the temperature dependence of the zero pressure rate constant will no longer be negative, and hence will be at variance with experimental results.

It has been suggested[16] that a doubly hydrogen bonded intermediate may be formed. However, these two bonds would have to be formed consecutively and, given the weakness of the first hydrogen bond and the lower A-factor for

cyclization compared to redissociation, this process is not likely to be favored. Even if cyclization should occur, the concomitant reduction in the density of states at an albeit greater value of E_1 would make it difficult to accommodate the observed pressure dependence.

CONCLUSION

The calculations presented here indicate that any model based on a type (b) potential surface is quite heavily constrained in terms of the molecular and transition state properties, required to reproduce the experimental pressure and temperature dependences of the $HO_2 + HO_2$ and $DO_2 + DO_2$ reactions. The observation that the pressure dependence of the $DO_2 + DO_2$ reaction is less than that of the $HO_2 + HO_2$ reaction, requires that the interfragment bonding be weak (30-60 kJ mol^{-1}), but in this case, the H_2O_4 molecule must be allowed a higher entropy than Giguere's frequency assignment permits in order for any pressure dependence to be predicted at all. In addition, in order to get a negative temperature dependence for either reaction, the transition state leading to products must be made very tight. Even so, the temperature dependence is underestimated unless k_1^{∞} is also assumed to have a negative temperature dependence. This problem cannot be overcome by further tightening the transition state since it is then becomes necessary to reduce E_2 in order to reproduce the zero pressure rate constant, and under these conditions the barrier leading to products is so low that the rate constant is no longer pressure dependent.

It is not clear from the current literature whether a very loose structure for H_2O_4 is possible or not. The frequencies assigned by Giguere and coworkers to HOOOOH observed in a matrix are certainly consistent with those that might be expected on the basis of analogous molecules, such as H_2O_2 or H_2S_4, assuming similar bonding. However, the bond strengths in these stable molecules are substantially greater than that in any of the H_2O_4 species

listed in Table 4 (e.g., $\Delta H(HO-OH) = 215$ kJ mol^{-1}), and arguments may be made based on Badger's rule to support the suggestion that the O-O frequencies should be less than those in H_2O_2. Also, in addition to possible problems involved in assigning frequencies in a complex system such as that analyzed by Giguere, it is not clear that the intermediates they observed at low temperatures in a matrix are necessarily the same as that formed in reaction (1) in the gas phase.

It is also difficult to find any potential problems with the experimental data on the kinetics of reaction (1). All the rate data which display a pressure dependence were obtained using UV spectrometry to detect the HO_2 radical, but the reported gas phase and solution spectra for HO_2 are very similar,[1,35] and so it is unlikely that any unexpected pressure dependence in the spectrum is possible. However, confirmation of the pressure dependence of the rate constant by some other technique would be valuable. It would also be useful if more kinetic data were available at very high pressures or in non-polar solvents to validate the pressure dependence and provide a measure of the high-pressure limit rate constant. In aqueous media, the $HO_2 + HO_2$ reaction is very slow, 1.26×10^{-15} cm^3 $molecule^{-1}$ s^{-1},[36] presumably due to solvent effects. By contrast, studies by Howard and Ingold[37] suggest that in tetrachloromethane the rate constant may be as fast as 9×10^{-12} cm^3 $molecule^{-1}$ s^{-1}, although this value was determined in an indirect experiment. It is always necessary to use fairly complex chemical systems to generate HO_2 radicals, but sufficient cross-checks seem to have been made to confirm the expected chemistry. Even so, it is somewhat unexpected that the ratio k_3/k_1 is independent of pressure.[3]

In view of the expected weak bonding in H_2O_4, and because when it is first formed, energy is already in the reaction coordinate for redissociation, it might

be suggested that a statistical RRKM calculation of $k_{-a}(E)$ may be inappropriate. But if the statistical assumption does break down, $k_{-a}(E)$ would be faster than calculated by RRKM techniques, and it would be correspondingly more difficult to account for the experimental pressure dependence.

Further experimental work is required in order to clarify the mechanism of this reaction, although it is unlikely that any single experiment will yield sufficient information. In addition to offering an opportunity to measure k_1^{∞}, studies in solution may lead to improved spectroscopic characterization of H_2O_4. It may also prove fruitful to investigate the electronic state of the oxygen molecule produced in this reaction. If $O_2(^1\Delta)$ is formed, then following the time dependence of its production may lead to information on the lifetime of H_2O_4.

The main conclusion of this study is that either H_2O_4 indeed has a very loose structure or that some other mechanism, rather than one involving associative complex formation, is required to account for the experimental data.

Acknowledgement

The authors would like to thank Dr. M. Mozurkewich for helpful discussions.

Appendix

BOND DISSOCIATION ENTHALPY FOR $tBuO_2-O_2tBu$

Following Nangia and Benson,[22] the experimentally determined thermochemistry for the equilibrium:

$$tBuO_2-O_2tBu \rightleftarrows 2\ tBuO_2$$

in solution at 140 K is taken as a starting point:[20,21]

$$\Delta H^+_{\ell,140} = 36.8 \pm 4.2 \text{ kJ mol}^{-1}$$

$$\Delta S^+_{\ell,140} = 142.3 \pm 25.1 \text{ J mol}^{-1} \text{ K}^{-1}$$

The superscript (+) refers to measurements in liquid-phase systems (hydrocarbon solvents) at 140 K with the standard state of 1 Molar.

In order to translate these data to thermodynamic quantities for the gas phase at 300 K, it is first necessary to "correct" the liquid phase data to 300 K, and then to transpose them to the gas phase.

The appropriate quantity required to correct the enthalpy and entropy to 300 K is the liquid-phase heat capacity as a function of temperature. To approximate this quantity estimates of the heat capacities of 2,2,7,7-tetramethyloctane and 2,2-dimethyl butane were used as surrogates for ditertiary butyl tetroxide and the tertiary butyl peroxy radical, respectively. Using the group additivity methods of Luria and Benson,[41] ΔC_p is found to vary from 25.5 J mol^{-1} K^{-1} at 140

K to 7.8 J mol^{-1} K^{-1} at 300 K. In view of the other approximations involved, it is reasonable to use the average value, $\Delta C_p \sim 18.8$ J mol^{-1} K^{-1}, at all temperatures. Thus the liquid-phase parameters at 300 K may be calculated as:

$$\Delta H^+_{\ell,300} = \Delta H^+_{\ell,140} + \Delta C_p(300-140)\ 10^{-3} = 39.7 \text{ kJ mol}^{-1}$$

$$\Delta S^+_{\ell,300} = \Delta S^+_{\ell,140} + \Delta C_p \ln(300/140) = 156.5 \text{ J mol}^{-1}\ K^{-1}$$

In order to convert these values to the corresponding gas-phase quantities, the methods of Mendenhall and Benson[42] were used which lead to:

$$\Delta H^o_{g,T} = \Delta H^+_{\ell,T} + 2\,\Delta H^{T_B}_{vap}(tBuO_2) - \Delta H^{T_B}_{vap}(O_4) + \Delta C_{vap}[T - T_o - 2T_B]$$

$$\Delta S^o_{g,T} = \Delta S^+_{\ell,T} + R\ln(V_s) + TC + \Delta C_{vap} \ln\left(\frac{T\,T_o}{T_B^2}\right)$$

where the superscript (o) indicates the 1 atm standard state, T_B is the boiling point of $tBuO_2$, T_o is the boiling point of $tBuO_4tBu$, $\Delta H^{T_B}_{vap}(tBuO_2)$ and $\Delta H^{T_o}_{vap}(O_4)$ are the heats of vaporization at the boiling points, V_s is the molar volume of the solvent, and TC is Trouton's constant.

It is observed empirically[41,43] that $\Delta C_{vap} \sim 50.2$ J mol^{-1} K^{-1} and so it was estimated that $\Delta H^{T_o}_{vap}(O_4) = 41.8$ kJ mol^{-1} with $T_o = 467$ K (based on an average of values for dodecane and di-t-amyl peroxide) and $\Delta H^{T_B}_{vap}(tBuO_2) = 27.2$ kJ mol^{-1} with $T_B = 323$ K (based on the values for 2,2-dimethyl butane). $R\ln(V_s) \sim 20.9$ J mol^{-1} K^{-1} for many solvents, and so

$$\Delta H^o_{g,300} = \Delta H^+_{\ell,300} + 18.8 = 58.6 \text{ kJ mol}^{-1}$$

$$\Delta S^o_{g,300} = \Delta S^+_{\ell,300} + 83.7 = 238.5 \text{ J mol}^{-1}\ K^{-1}$$

The value for $\Delta H^o_{g,300}$ is almost a factor of 2 larger than that deduced by Nangia and Benson[22] from the same experimental data. This discrepancy arises from the

use of different hydrocarbon species as models for $tBuO_2$ and tBu_2O_4 and different methods of correcting ΔH_{vap} from the boiling point of the liquids to 300 K. This indicates that the real uncertainty in the bond dissociation enthalpy at 300 K in the gas phase is at least ± 24 kJ mol^{-1}.

The value for $\Delta S^{o}_{g,300}$ = 238.5 J mol^{-1} K^{-1} is substantially greater than the value of 150.6 J mol^{-1} K^{-1} obtained by additivity methods where group values were estimated assuming a "normal" structure and frequencies. On the basis of this value of $\Delta S^{o}_{g,300}$, the entropy of H_2O_4 would be only 217.6 J mol^{-1} K^{-1} which implies a tighter molecule than even that suggested by Giguere (Table 4).

If, on the other hand, the additivity value of $\Delta S^{o}_{g,300}$ is assumed correct and converted to $\Delta S^{+}_{\ell,140}$, then a value of 220.0 J mol^{-1} is obtained. This may be combined with the experimental value of $\Delta G^{+}_{\ell,140}$ = 16.7 kJ mol^{-1} to yield $\Delta H^{+}_{\ell,140}$ = 47.7 kJ mol^{-1}. However, these parameters are not consistent with the reported temperature dependence of the equilibrium constant. It thus appears that while a looser H_2O_4 species than expected from additivity methods is required by the kinetic data, a tighter one is needed to fit the equilibrium data. However, it should be borne in mind that the uncertainties in this kind of analysis are large and so the reliability of the gas-phase thermodynamic parameters is difficult to assess.

REFERENCES

1. R. A. Cox and J. P. Burrows, J. Phys. Chem., 83, 2560 (1979).

2. B. A. Thrush and J.P.T. Wilkinson, Chem. Phys. Lett., 66, 441 (1979).

3. S. P. Sander, M. Peterson, R. T. Watson, and R. Patrick, J. Phys. Chem., 86, 1236 (1982).

4. R. R. Lii, R. A. Gorse, M. C. Sauer, and S. Gordon, J. Phys. Chem., 83, 1803 (1979).

5. R. Patrick and M. J. Pilling, Chem. Phys. Lett., 91, 343 (1982).

6. B. A. Thrush and G. S. Tyndall, Chem. Phys. Lett., 92, 232 (1982).

7. R. Simonaitis and J. Heicklen, J. Phys. Chem., 86, 5416 (1982).

8. B. A. Thrush and G. S. Tyndall, J.C.S., Faraday II, 78, 1469 (1982).

9. S. P. Sander, to be published.

10. T. T. Paukert and H. S. Johnston, J. Chem. Phys., 56, 2834 (1972).

11. P. A. Giguere and K. Herman, Can. J. Chem., 48, 3473 (1970).

12. P. A. Giguere, Trans. NY Acad. Sci., 343, 334 (1972).

13. J. L. Arnau and P. A. Giguere, J. Chem. Phys., 60, 270 (1974).

14. T. V. Yagodovskaya and L. I. Nekvasov, Zh. Fiz. Khim., 51, 2434 (1977), and references therein.

15. D. L. Baulch, R. A. Cox, P. J. Crutzen, R. F Hampson, J. A. Kerr, J. Troe, and R. T. Watson, J. Phys. Chem. Ref. Data, 11, 327 (1982).

16. C. J. Howard, Proc. NATO Adv. St. Inst. Atmos. Ozone, 409 (1979).

17. M. Diem, T-Y Tso, and E.K.C. Lee, J. Chem. Phys., 64, 6452 (1982).

18. H. Niki, P. D. Maker, C. M. Savage, and L. P. Breitenbach, Chem. Phys. Lett., 73, 43 (1980).

19. C. J. Howard, J. Am. Chem. Soc., 102, 6937 (1980).

20. K. Adamic, J. A. Howard, and K. U. Ingold, Chem. Comm., 505 (1969).

21. J. E. Bennet, D. M. Brown, and B. Mile, Chem. Comm., 504 (1969).

22. P. S. Nangia and S. W. Benson, J. Phys. Chem., 83, 1138 (1979).

23. S. W. Benson and R. Shaw, "Thermochemistry of Organic Peroxides, Hydroperoxides, Polyoxides, and their Radicals," in Organic Peroxides, Vol. I, (ed. D. Swern), Wiley Interscience, New York (1970).

24. J. Troe, J. Chem. Phys., 66, 4745 (1977).

25. J. Troe, J. Chem. Phys., 66, 4758 (1977).

26. (a) J. R. Barker, Chem. Phys., accepted for publication;
(b) J. R. Barker, paper presented at Symposium on Reaction Kinetics Related to Atmospheric Chemistry, Tsukuba, Japan, 1982.

27. Th. Just and J. Troe, J. Phys. Chem., 84, 3068 (1980).

28. S. E. Stein and B. S. Rabinovitch, J. Chem. Phys., 58, 2438 (1973).

29. P. J. Robinson and K. A. Holbrook, Unimolecular Reactions, Wiley-Interscience, New York (1972).

30. P. C. Haarhof, Mol. Phys., 6, 101 (1963).

31. D. A. Parkes and C. P. Quinn, J.C.S., Faraday I, 72, 1952 (1976).

32. M. Quack and J. Troe, Gas Kinetics and Energy Transfer, Vol. 2, 175 (1977).

33. W. B. DeMore, J. Phys. Chem., 86, 121 (1982).

34. S. W. Benson and H. E. O'Neal, NSRDS-NBS 21 (1970).

35. B.H.J. Bielski and H. A. Schwarz, J. Phys. Chem., 72, 3836 (1968).

36. B.H.J. Bielski and A. D. Allen, J. Phys. Chem., 81, 1046 (1977).

37. J. A. Howard and K. U. Ingold, Can. J. Chem., 45, 785 (1967).

38. G. Herzberg, "Molecule Spectra and Molecular Structure," in Molecular Spectra and Molecular Structure, Vol. 2, Van Nostrand, Princeton (1945).

39. H. B. Thompson, J. Chem. Phys., 47, 3407 (1967).

40. R. C. Reid and T. K. Sherwood, The Properties of Gases and Liquids, (2nd ed.) McGraw Hill, New York (1966).

41. M. Luria and S. W. Benson, J. Chem. Eng. Data 22, 90 (1977).

42. S. W. Benson and G. D. Mendenhall, J. Am. Chem. Soc., 98, 2046 (1976).

43. R. Shaw, J. Chem Eng. Data, 14, 461 (1969).

CAPTIONS

Figure 1 Energetics of the HO_2, H_2O_4, H_2O_2 System

Figure 2 Experimental and Calculated Pressure Dependences for k_1 and k_3

- ⊖, ⊟ Sander et al. (3),
- ⧫ Simonaitis and Heicklen (7),
- ——— Calculated pressure dependence for k_1 (models ii and iii),
- —·— calculated pressure dependence for k_3 (model ii),
- – – – calculated pressure dependence for k_3 (model iii).

Figure 3 Experimental and Calculated Temperature Dependences for k_1

- ⧫ data of Patrick and Pilling (5)
- ⧫ data of Thrush and Tyndall (8),
- ⧫, ⊖ data of Sander (9) at 700 Torr and at zero pressure
- —·—·— calculated temperature dependence at 700 Torr and zero pressure, model ii, k_1^∞ assumed T independent
- – – – – calculated temperature dependence model iii, k_1^∞ assumed T independent.
- ——— calculated temperature dependence model iii, k_1^∞ assumed $\propto T^{-2}$

Figure 4 Experimental and Calculated Temperature Dependence for k_3

- ⧫, ⊖ data of Sander (9) at 700 Torr and at zero pressure
- – – – – calculated temperature dependence, k_3^∞ assumed T independent
- ——— calculated temperature dependence, k_3^∞ assumed $\propto T^{-2}$

Figure 5 Calculated Temperature Dependence for k_1 from 150–3000 K

- ——— 700 Torr pressure
- – – – zero pressure

Figure 6 Calculated Pressure Dependence for k_1 Over Range 0 - 50 atm

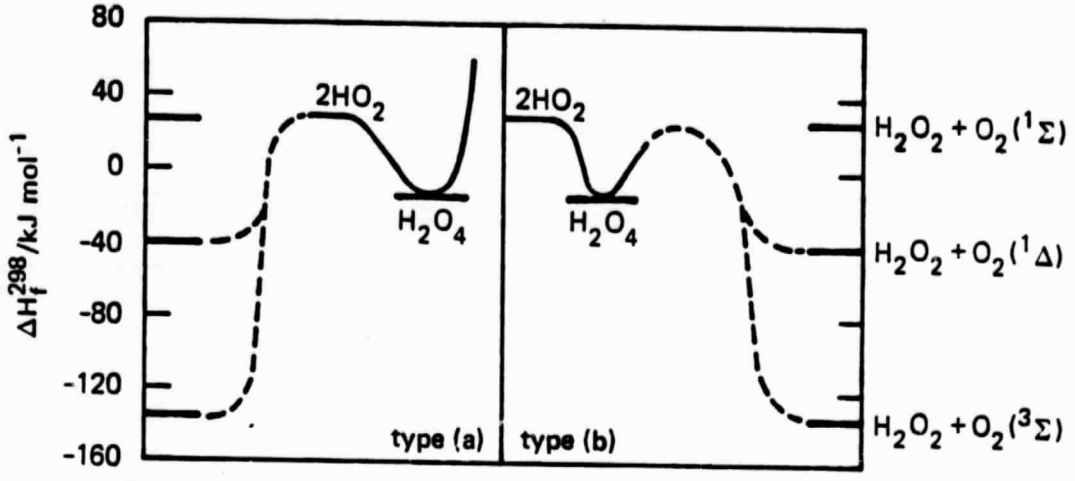
80
40
0
-40
-80
-120
-160
ΔH_f^{298}/kJ mol^{-1}
2HO$_2$
H$_2$O$_4$
type (a)
2HO$_2$
H$_2$O$_4$
type (b)
H$_2$O$_2$ + O$_2$($^1\Sigma$)
H$_2$O$_2$ + O$_2$($^1\Delta$)
H$_2$O$_2$ + O$_2$($^3\Sigma$)

SA-6534-27

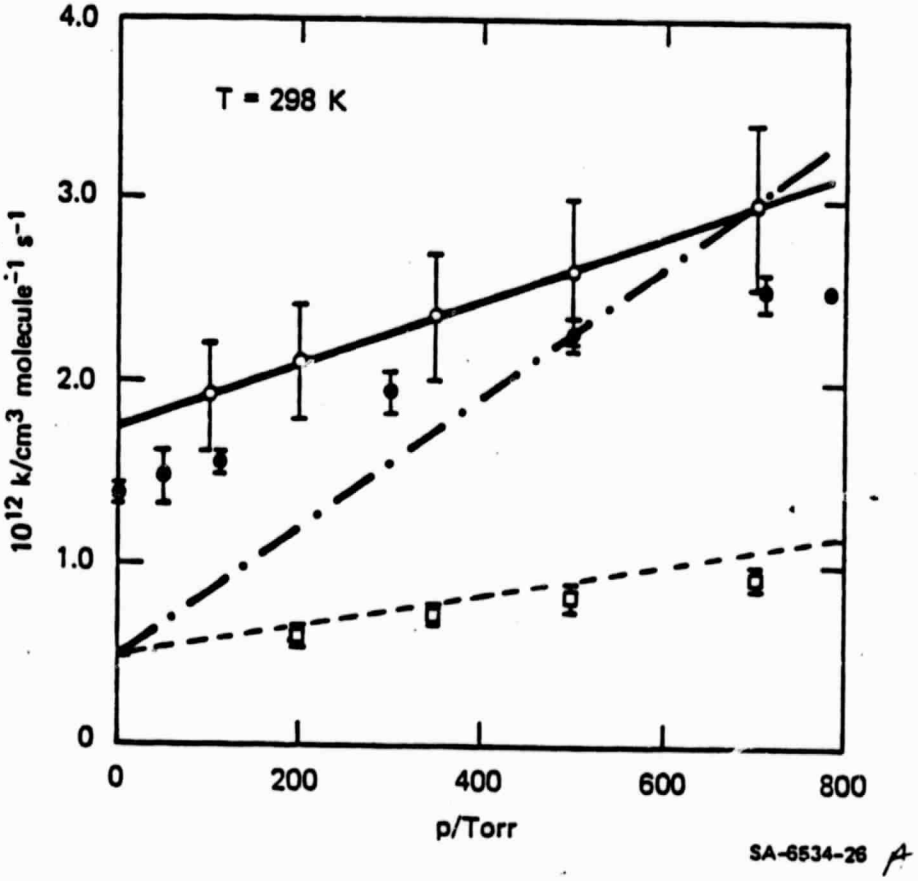
T = 298 K
4.0
3.0
2.0
1.0
0
10^{12} k/cm^3 molecule^{-1} s^{-1}
0
200
400
600
800
p/Torr
SA-6534-26

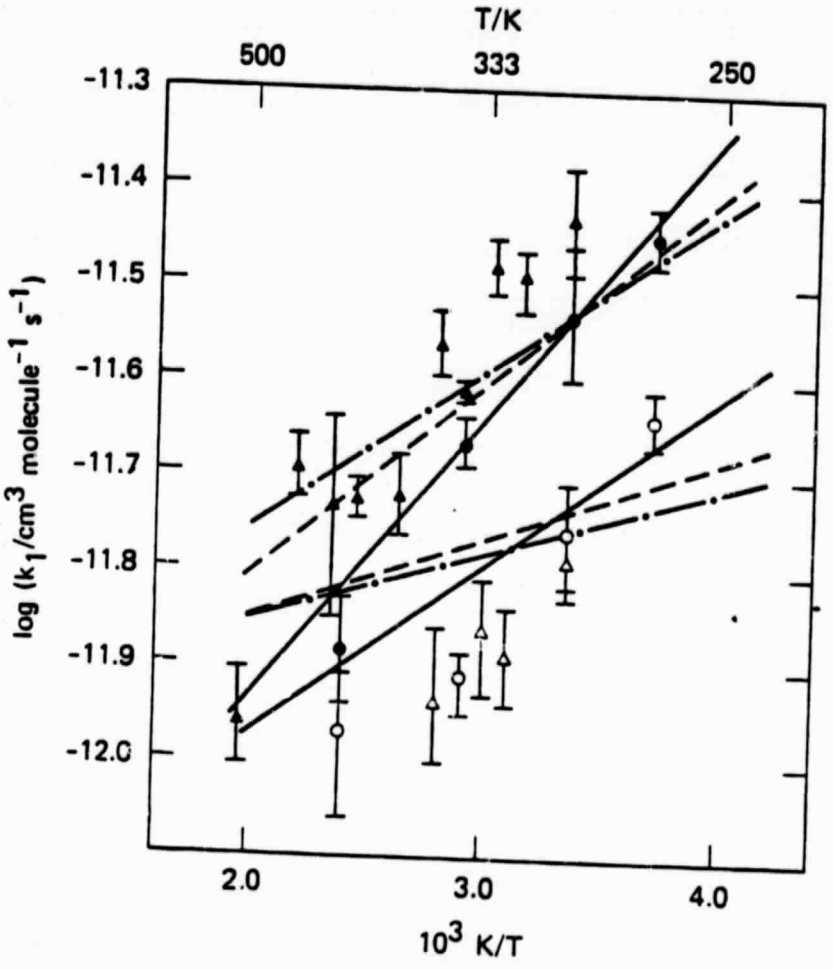
T/K
500
333
250
-11.3
-11.4
-11.5
-11.6
-11.7
-11.8
-11.9
-12.0
log (k_1/cm^3 molecule^{-1} s^{-1})
2.0
3.0
4.0
10^3 K/T
SA-6534-30

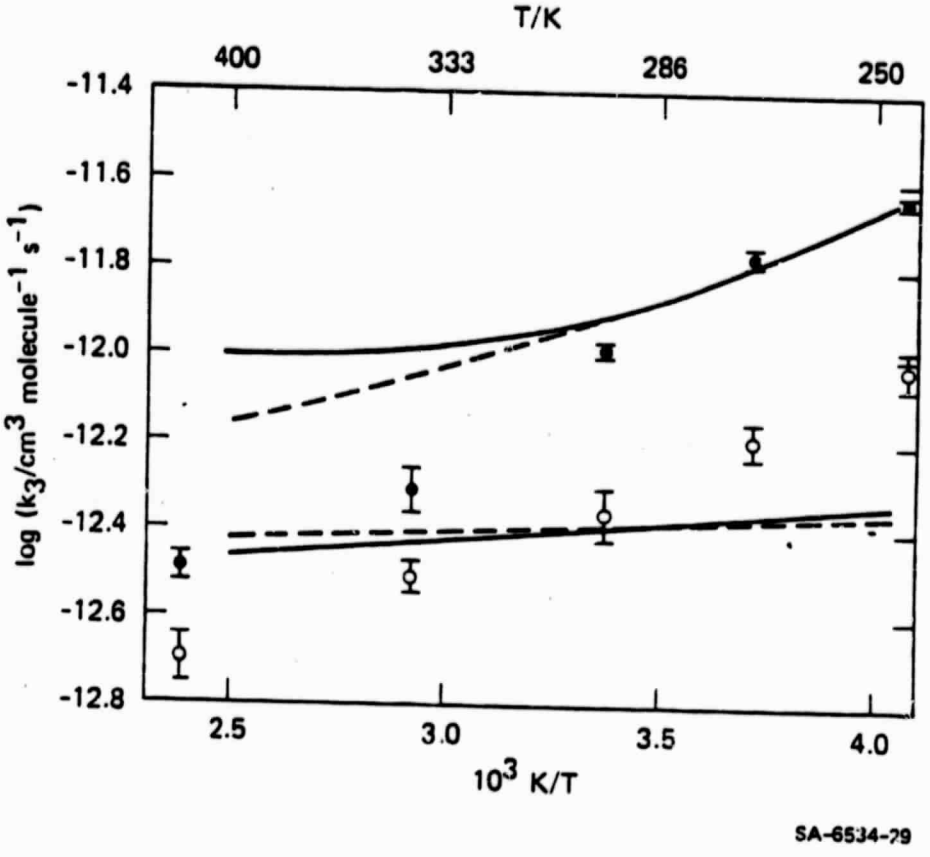
T/K
400
333
286
250
-11.4
-11.6
-11.8
-12.0
-12.2
-12.4
-12.6
-12.8
log (k_3/cm^3 molecule^{-1} s^{-1})
2.5
3.0
3.5
4.0
10^3 K/T
SA-6534-29

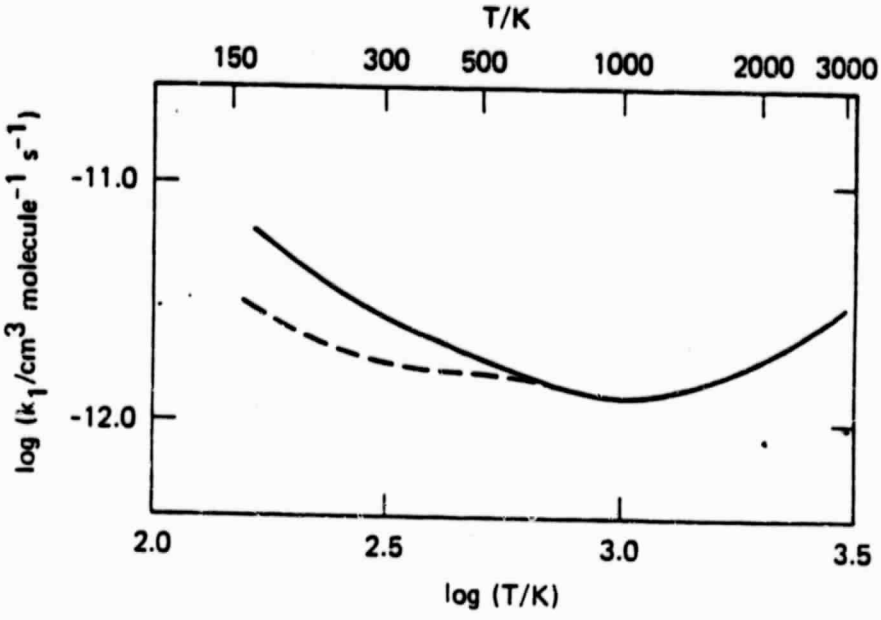
T/K
150
300
500
1000
2000
3000
-11.0
-12.0
log (k_1/cm^3 molecule^{-1} s^{-1})
2.0
2.5
3.0
3.5
log (T/K)

SA-6534-31

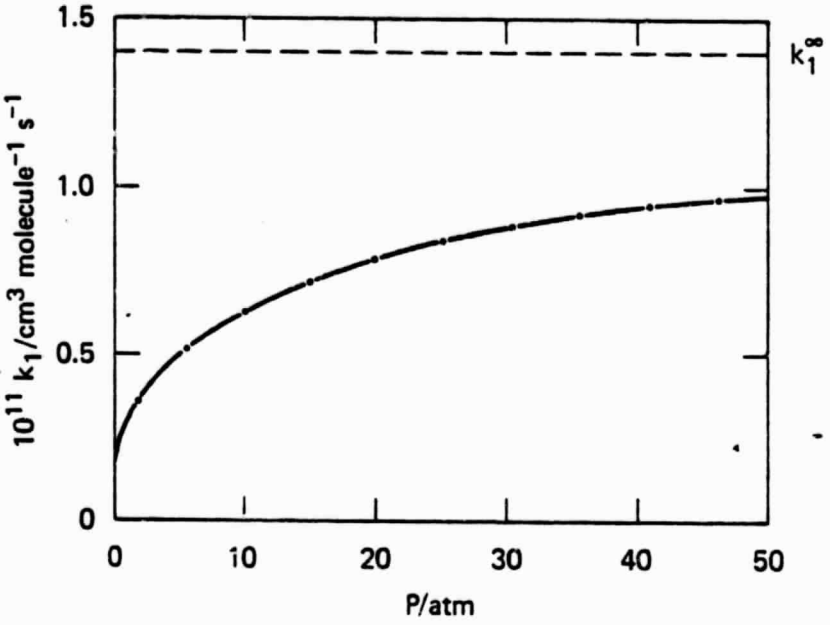

SA-7873-17A

Chapter III

MEASUREMENT AND ESTIMATION OF RATE CONSTANTS FOR MODELING REACTIVE SYSTEMS

David M. Golden

presented at Symposium on
Modeling of Chemical Reaction Systems
Heidelberg, Germany
(September 1980)

in Modeling of Chemical Reaction Systems
Springer-Verlag, Berlin, 1981, pp. 148-161
(K. H. Ebert, P. Deuflhard, and W. Jager, eds.)

MEASUREMENT AND ESTIMATION OF RATE CONSTANTS FOR MODELING REACTIVE SYSTEMS

David M. Golden
Department of Chemical Kinetics
SRI International, Menlo Park, CA U.S.A.

1. INTRODUCTION

A complex chemical system is describable in terms of discrete elementary steps. The rate constants for these steps are the input coefficients to the ensuing differential equations which may be written to describe the time-dependent change of concentrations. Solutions of the mathematical problem represented by these equations have physical meaning only to the extent that the appropriate set of steps has been taken into account (mechanism) and are quantitatively correct. Furthermore, the uncertainty in the solution depends on the combination of uncertainty and sensitivity of these rate constants.

We will discuss herein the current best framework of theory for evaluating and estimating gas-phase rate constants. We also will discuss some experimental methods by which rate constants are measured. This combination of measurement and the framework provided by theory is the basis for our very pragmatic approach to real complex chemical problems. A scenario for this approach to a given problem is as follows:

(1) Write a mechanism based on best available chemical information.

(2) Estimate rate constants and uncertainties for those steps that have not been previously studied.

(3) Calculate the desired time-dependent concentrations, their uncertainties, and the sensitivity of these to the input parameters.

(4) Measure those quantities where the combination of sensitivity and uncertainty are greater than acceptable.

(5) Continually perform experiments designed to test the limits of accepted theory.

It should be noted that rate constants for elementary steps may be functions of temperature, pressure, and the nature of other molecules present. In addition, some complex processes (such as smog) involve photochemical steps as well.

For this symposium, I will discuss the status of Items (2), (4), and (5) for gas-phase homogeneous processes.

2. THERMOCHEMICAL KINETICS

Background

The development of an empirically based framework for extrapolation and estimation is intimately tied to the available methods for measuring rate constants. These are discussed separately for organizational convenience. This framework has

been given [1] the name "Thermochemical Kinetics" by S. W. Benson. I have discussed "Thermochemical Kinetics" in the following manner with reference to tropospheric measurements, combustion problems [2], and modelling [3] recently, but I will repeat it here for completeness.

Thermochemistry

It is impossible to begin a discussion of the theoretical basis for critical evaluation and extrapolation of thermal rate data without first discussing methods for estimating thermochemical quantities, such as $\Delta H^{\circ}_{f,T}$, ΔS°_{T}, and $C^{\circ}_{p,T}$ for molecules.

Group Additivity

When a sufficient data base exists, we have found [4] the method of group additivity to best fit the need for accuracy and ease of operation. The basic concept and assumptions involved in the group additivity method are as follows:

For the disproportionation reaction

$$RNN'R + SNN'S = RNN'S + SNN'R$$

any additivity approximation assumes that $\Delta\Phi = \Delta\Phi_{\sigma}$, where Φ is any molecular property, and $\Delta\Phi_{\sigma}$ is the contribution to that property due to symmetry changes and optical isomerism. For the molecular properties of interest here, $\Delta H_T \rightarrow 0$, $\Delta C_{p,T} \rightarrow 0$, and $\Delta S_T \rightarrow S_{\sigma} = R \ln K_{\sigma}$, where $K_{\sigma} = \sigma(RRNN'R)\,\sigma(SNN'S)/\sigma(RNN'S)\,\sigma(SNN'R)$, $\sigma(X)$ being the symmetry number including both internal and external symmetry. An additional term for entropy of mixing, due to the existence of optical isomers, must also be included.

If the molecular framework NN′ is two atoms or greater, these relationships imply the additivity of group properties, which include all nearest-neighbor interactions, since a group is defined as an atom together with its ligands (e.g., in the group $C-(H)_3(C)$, the central C atom is bonded to three H atoms and one C atom). Thus the equation

$$CH_3OH + CH_3CH_2OCH_3 = CH_3CH_2OH + CH_3OCH_3$$

implies the additivity of the properties of the groups $C-(H)_3(C)$, $C-(H)_3(O)$, $O-(C)(H)$, $C-(H)_2(C)(O)$, and $O-(C)_2$, if the appropriate $\Delta\phi = \Delta\phi_{\sigma}$.

We have developed group additivity methods that permit the estimation, for many organic chemicals in the gas phase, of heats of formation to ± 1 kcal/mole, and of entropies and heat capacities to ± 1 cal/(mole-K), from which free energies of formation can be derived to better than ± 2 kcal/mole.

It should be noted that entropy and heat capacity are molecular properties that can be accurately estimated under much less stringent conditions than energy (or enthalpy). Thus the method of bond additivity seems to work quite well (± 1 cal/(mole-K)) for estimating the former properties, but not at all well (± 4 kcal/mole) for the latter.

Structural Considerations and Model Compounds

If sufficient thermochemical data is lacking for the estimation of group properties, entropy and heat capacity can often be adequately estimated from structural parameters of the molecule. (Enthalpy estimates are more difficult, requiring a better knowledge of potential functions than are usually available.) The methods of statistical thermodynamics may be used to calculate C_p° and S° directly for those molecules where a complete vibrational assignment can be made or estimated.

Also, "reasonable" structural and vibrational frequency "corrections" to the corresponding established thermodynamic properties of "reference" compounds may be made. A suitable choice of reference compound, i.e., one similar in mass size and structure to the unknown, assures that the external rotational and translational entropies and heat capacities of the reference and unknown compounds will be the same and that many of the vibrational frequencies will be similar. The basic assumption is that S° and C_p° difference can be closely estimated by considering only low-frequency motions thought to be significantly changed in the unknown. Fortunately, entropies and heat capacities are not excessively sensitive to the exact choice of these vibrational frequencies, and estimates of moderate accuracy may be made with relative ease.

Kinetics

The extension of thermochemical estimation techniques to the evaluation of kinetic data rests largely on the validity of transition state theory.

The transition state theory expression for a thermal rate constant is,

$$k = (kT/h)\exp\left[-\Delta G_T^{o\ddagger}/RT\right]$$

(the units are sec^{-1} for the first order and atm^{-1} for the second order) and,

$$\Delta G_T^{o\ddagger} = \Delta H_{300}^{\ddagger} - T\Delta S_{300}^{o\ddagger} + \langle \Delta C_p^{\ddagger} \rangle [(T-300) - T\ln(T/300)]$$

(In the ideal gas approximation we can drop the standard state notation on $\Delta H^{\ddagger}$ and $\Delta C_p^{\ddagger}$.) If the empirical temperature dependence is represented by

$$k = AT^B \exp(-C/T)$$

$$A = \left[k/h(300)^{\langle \Delta C_p^{\ddagger}/R \rangle}\right] \exp\left[(\Delta S_{300}^{\ddagger} - \langle \Delta C_p^{\ddagger} \rangle)/R\right]$$

$$B = (\langle \Delta C_p^{\ddagger} \rangle + R)/R$$

$$C = \left(\Delta H_{300}^{\ddagger} - \langle \Delta C_p^{\ddagger} \rangle (300)\right)/R$$

k = Boltzmann's constant

h = Planck's constant

$\Delta S_{300}^{\ddagger}$ = entropy of activation at 300 K, standard state of 1 atm.

$\Delta H_{300}^{\ddagger}$ = enthalpy of activation at 300 K

$\langle \Delta C_p^{\ddagger} \rangle$ = average value of the heat capacity at constant pressure of activation over the temperature range 300–T °K.

If we wish to express second-order rate constants in concentration units instead of pressure units, we must multiply by RT in the appropriate units. This has the effect of writing:

$$k = A' T^{B'} \exp(-C/T)$$

where $A' = AR$ and $B' = B + 1 = (\langle \Delta C_p^{\ddagger} \rangle + 2R)/R$

Thus, simple "Arrhenius behavior" which will be sufficient for lower tropospheric temperatures is characterized for first-order reactions by $\Delta C^{\ddagger} = -R$; ($\Delta C_p^{\ddagger} = \Delta C_v^{\ddagger} = \Delta C^{\ddagger}$), and for second-order reactions using concentration units by $\Delta C_p^{\ddagger} = -2R$ (or $\Delta C_v^{\ddagger} = -R$).

In the case of simple Arrhenius behavior:

$$k = A \exp(-B/T)$$

$$\log A = \log(ek\langle T\rangle/h) + \Delta S^{\ddagger}/R;\quad B = (\Delta H^{\ddagger} + R\langle T\rangle)/R$$

Thus, the quanties $\Delta H^{\ddagger}$, $\Delta S^{\ddagger}$, and $\Delta C_p^{\ddagger}$ are of interest. We apply similar methods to those already discussed with respect to thermochemistry to view rate data in a rational framework. These techniques are discussed in some detail by Benson[1], but certain points are worthy of re-emphasis here.

We begin by classifying reactions as unimolecular or bimolecular. (The only termolecular processes of interest to us will be energy-transfer controlled bimolecular processes.)

Unimolecular Processes

Simple Fission: $AB \rightarrow A + B$

Complex Fission: Molecule → Molecule + Molecule (or radical)

Isomerization: Intramolecular atom rearrangement

Bimolecular Processes

Direct Metathesis: $A + BX \rightarrow AX + B$

Addition: $A + \text{Molecule} \rightarrow$ Stable Adduct (reverse of complex fission)

Association: $A + B \rightarrow A - B$ (reverse of simple fission)

The first thing to notice is that of all these reactions, only direct metathesis reactions are not subject to becoming energy transfer limited at high temperatures and low pressures (i.e., in the "fall-off" region!). This means that not only does the so-called high pressure rate constant need to be estimated or known, but the extent of fall-off, as well. Methods are available for making fall-off corrections[5].

In hydrocarbon reactions in the troposphere, we may expect that most direct metathesis reactions will involve the exchange of a hydrogen atom between larger groups. A simple, semi-empirical prescription exists for estimating the value of $\Delta S^{\ddagger}$ for these types of reactions. First, one realizes that these values are limited between the "loosest" possible model (A-factor equals gas kinetic collision frequency) and the "tightest" possible model in which $R\cdots H\cdots R'$ is represented by the molecule R-R'. Experience using data in the range

$300 < T/K < 700$ has taught us that generally the $\Delta S^{\ddagger}$ value corresponds to a transition state only slightly looser than the tightest possible value.

Since the other two classes of bimolecular porcesses are the reverse of unimolecular reactions, we may consider them in that direction. (The equilibrium constant is either known or estimable.) Once again, using experimental results as our guide, we note that model transition states which correspond to the values of $\Delta S^{\ddagger}$ are generally "tight". That is, we may visualize them as minor modifications of the reactant molecule, usually involving some increase in rotational entropy due to slight enlargement of certain bonds. The dominant entropic feature is usually the stiffening of internal rotations as a result of multiple bond formation or ring formation [1].

Bond scission reactions present a particular problem, since it is particularly difficult to locate a transition state. Recent work [6] both experimental and theoretical, indicates that these reactions can be modeled with a transition state which becomes tighter as the temperature rises. Lower limits of A-factors can be estimated fairly accurately for H-atom metathesis reactions by making use of model transition states [1]. We illustrate the method for the atmospherically important reaction of OH with HNO_3 which is supposed to proceed via: $HO + HONO_2 \rightarrow H_2O + NO_3$. Reported values [7] are $k \sim 10^8$ M^{-1} s^{-1} independent of temperature. Our analysis suggests that the reported rate constant does not represent the reaction as written above.

$$HO + HONO_2 \rightarrow \left[H\overset{O}{\diagup} \cdot H \cdot \overset{O}{\diagdown} NO_2\right]^{\ddagger} \rightarrow H_2O + NO_3$$

	$\Delta S^{\circ\ddagger}_{300}$ [a]	$\Delta C^{\ddagger}_{p,300}$ [a]	$\Delta C_{p,400}$ [a]
Reference Reaction [TS = $CH_3ONO \approx HOONO_2$]	−35.4	− 1.6	1.0
Spin	1.4	—	—
Symmetry	0	—	—
External Rotation (2 x 2 x 1.5)[b]	1.7	—	—
O–O(1000 cm^{-1}) → O•H(r.c)	− 0.1	− 0.4	− 1.0
H•O(2000 cm^{-1})	0	0	0.2
O–O–N(400 cm^{-1}) → O•H•O(600 cm^{-1})	0.5	0.2	0.1
O•H•O(600 cm^{-1})	1.0	1.0	1.6
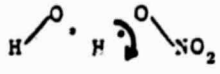 [c]	≥2.2	1.0	1.0
	> −28.7	0.2	2.9

[a] cal $mole^{-1}$ deg^{-1} (standard state, 1 atm)

[b] Estimated increase of product of inertia.

[c] 10° off linear.

$$\log[A_{300}/M^{-1}\ s^{-1}] \geq 13.2 + [-28.7 + 8.35]/4.58 \geq 8.8$$

$$\log[A_{400}/M^{-1}\ s^{-1}] \geq 13.3 + [-28.7 + 1.6\ \ln 4/3 + 8.92]/4.58 \geq 9.1$$

$$E_{300} = \Delta h^{\ddagger}_{300} + 2R(.300) = \Delta H^{\ddagger}_{300} + 1.2\ \text{kcal mole}^{-1}$$

$$E_{400} = \Delta H^{\ddagger}_{300} + 1.6(\ \ ) + 2R(.4) = \Delta H^{\ddagger}_{300} + 1.8$$

$$E_{400} - E_{300} = 0.6\ \text{kcal mole}^{-1}$$

3. MEASUREMENT TECHNIQUES

Bimolecular

Bimolecular reactions of interest are usually radical-molecule or radical-radical interactions, although occasionally a molecule-molecule reaction will be an elementary process. (Gas-phase ion-molecule reactions are of interest sometimes, and they can be included in the same general framework with the realization that attractive forces are longer ranged.) Since bimolecular rate constants can be measured only if concentrations are known, the standard "trick" is to arrange for "psuedo first-order" conditions by running the reaction in a large excess of one of the reactants. This allows the relative measurement of the other reactant to determine a first-order rate constant, k^{I}, which, when divided by the concentration of the overwhelming component, will yield k^{II}, the second-order rate constant of interest. Most experimental techniques take advantage of the psuedo-first-order trick over the ranges of T and P accessible.

Several methods exist for concentration (or relative concentration) measurements. Most prominent are mass spectroscopy and all the wavelength ranges of optical spectroscopy, both absorption and fluorescence.

The experimental environment can also vary widely: Flow tubes that monitor time as distance after an interaction region, real-time measurements that are rapid enough to determine actual concentration changes, shock tubes that create high-temperature conditions rapidly, and some recently exploited infrared laser-heating techniques (vida infra).

Unimolecular

Unimolecular reactions are measured using many of the same general techniques as for bimolecular reactions. In general, a substantial energy barrier must be surmounted in order for these processes to proceed, so that moderate-to-high temperatures are required. In addition, since unimolecular processes are dependent on the total pressure and the specific nature of other constituents of the gaseous mixture, all these properties need to be under experimental control.

Very Low-Pressure Pyrolysis (VLPP)

A particular technique that can be used is the Very Low-Pressure Pyrolysis (VLPP) technique developed at SRI International [8]. VLPP is ideally suited for the measurement of the rate of initial bond-breaking reactions in the pyrolysis of organic molecules where secondary reactions often interfere with the characterization of the initial step. The technique has been described in detail previously [8,9].

The procedure consists of allowing the reactant to flow through the inlet system at a controlled rate and switching valves in the inlet lines so that the reactant alternately flows through a Knudsen cell reactor or through the bypass directly into the mass spectrometer. Since the flow rate is held constant, the difference between the mass spectrometer signals for the reactant in the bypass position and the reactor position corresponds to the amount of reactant that is decomposed as it flows through the reactor.

The data are interpreted with the aid of various steady-state expressions derived as shown below. At low flow rates, the treatment for a simple irreversible unimolecular decomposition is appropriate, and the extraction of rate parameters is straightforward. At higher flow rates (higher reaction pressures) and smaller escape apertures, rapid bimolecular reactions can compete with unimolecular decomposition and with escape from the reactor. These interactions must be included in the analysis. The reason for using VLPP at pressure high enough for secondary reactions to occur is shown by the description given below of our recent study for the pyrolysis of 1-ethyl naphthalene and 1-ethyl anthracene [10]. Briefly, observation of competition between unimolecular bond scission and radical recombination amounts to measurement of an equilibrium constant:

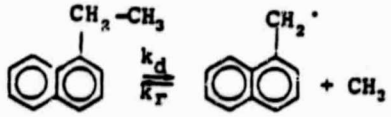

(1)

Reliable measurement of an equilibrium constant can provide very good third-law values for ΔH°, since these values are not subject to the systematic errors that can markedly affect the slope

of Arrhenius plots. Thus, by providing for measurement of an equilibrium constant that is otherwise not readily measured at higher pressures or in static systems, the VLPP system allows two largely independent measurements of bond strength and, therefore, a valuable internal consistency check.

For irreversible, unimolecular decomposition of a substance A, only three rate processes are considered:

$$\begin{aligned} \text{inlet} &\xrightarrow{R_A} \text{A} \\ \text{A} &\xrightarrow{k_d} \text{products} \\ \text{A} &\xrightarrow{k_{eA}} \text{mass spectrometer} \end{aligned} \qquad (2)$$

where R_A is the rate at which the reactant is allowed to flow into the reactor and k_{eA} is the first-order rate constant describing escape from the reactor.

Steady-state analysis provides the expression:

$$\frac{A_{escaped}}{A_{reacted}} = \frac{(A)_{ss}}{(A)_{o,ss} - (A)_{ss}} = \frac{k_{eA}}{k_d} \qquad (3)$$

where $(A)_{o,ss}$ is the steady-state concentration in the reactor when there is no decomposition.

When recombination of the radical fragments produced by unimolecular decomposition competes with escape from the reactor, the following reactions must be considered:

$$\begin{aligned} \text{inlet} &\xrightarrow{R_A} \text{A} \\ \text{A} &\underset{k_r}{\overset{k_d}{\rightleftharpoons}} \text{B}^{\cdot} + \text{C}^{\cdot} \\ \left.\begin{aligned} \text{A} &\xrightarrow{k_{eA}} \\ \text{B}^{\cdot} &\xrightarrow{k_{eB}} \\ \text{C}^{\cdot} &\xrightarrow{k_{eC}} \end{aligned}\right\} &\text{escape to mass spectrometer} \end{aligned} \qquad (4)$$

The controlled flow rate into the reactor is given by R_A, and the first-order escape rate constants for the various fragments are related by square roots of their masses so that the escape constant for the 1-naphthylmethyl radical (B$^{\cdot}$) is related to that for 1-ethylnaphthalene by

$$k_{eB} = k_{eA}\left(\frac{156}{141}\right)^{1/2} \simeq k_{eA}(1.05) \qquad (5)$$

Steady-state analysis of this sequence for 1-ethyl naphthalene provides an expression similar to equation (3):

$$\frac{A_{escaped}}{A_{reacted}} = \frac{(A)_{ss}}{(A)_{o,ss} - (A)_{ss}} = \frac{k_{eA}}{k_d} + \frac{k_r F(A)}{k_d (3.39)} \qquad (6)$$

Equation (6) indicates that decomposition and competitive recombination will provide a straight line of slope k_r/k_d and intercept k_{eA}/k_d. In the limiting case where recombination is unimportant, equation (6) reduces to equation (3).

Photolytic Radical Production

We have recently [11] combined the phenomenon of infrared multiphoton dissociation of organic molecules with the VLPP technique to produce a method for determining the rate constant for radical-molecule reactions at temperatures determined by reactor wall temperatures and completely independent of any need to heat the radical precursor. (Current powerful dye lasers will allow this technique to be useful for UV-vis photochemical radical production as well.) The current application has been to reactions of CF_3 radicals from CF_3I, but extension to aliphatic and aromatic systems requires only time and funds.

In this experiment, as previously, the effusive molecular beam was mechanically chopped in the second (differentially pumped) chamber before it reached the ionizer of the quadrupole mass filter (Finnigan 400). The signal was demodulated by a lock-in amplifier (PAR 128A) whose output was now stored in a signal averager (PAR 4202), which also served to trigger the laser. The two-aperture Knudsen cell was fitted with KCl windows and had an optical pathlength of 20.5 cm and a volume of approximately 105 cm^3. The cell was coated with Teflon by rinsing with a finely dispersed Teflon slurry in a water/aromatic solvent mixture (Fenton Fluorocarbon, Inc.) and curing at 360 C.

The Lumonics TEA-laser (Model K-103) was operated at the R(16) line of the 9.6μ transition at a pulse repetition frequency of .25 Hz, slow enough to permit $>$ 99% of the reaction products to escape from the cell before the next laser shot. The multimode output of the laser consisted of a pulse of

approximately 5.0 J, directed through the photolysis cell after being weakly focused by a concave mirror (fl = 10 m), which gave a beam cross section of 2.67 cm^2 at the KCl-entrance window of the cell.

The typical experiment consisted of averaging the time-dependent mass spectroscopic signal intensity of the products for a number of laser shots (10-100) as a function of the flow rate of the reactant gases at constant CF_3I flow rate and constant energy per pulse. Although experiments could be performed on a single-shot basis, the signal/noise ratio was improved by averaging the results of a number of laser shots.

The total yield of product formed in the reaction of interest was then determined by integration of the accumulated time-dependent signal of the signal averager on a strip-chart recorder fitted with an electronic integrator (Linear Instruments, Inc.).

Using the apparatus described above, reaction products could be observed as well as the transient depletion of CF_3I. An advantage of the low-pressure technique is that the effects of secondary reactions are minimized, although they must be considered in the data analysis.

The following chemical reaction mechanism is appropriate for studying the reaction $CF_3 + Br_2 \rightarrow CF_3Br + Br$:

$$CF_3I + nh\nu \rightarrow CF_3 + I$$

$$CF_3 + Br_2 \overset{1}{\rightarrow} CF_3Br + Br$$

$$CF_3 \overset{k_w}{\rightarrow} \text{(wall loss } \underline{\text{not}} \text{ yielding } CF_3Br)$$

No heterogeneous first-order reaction of CF_3 to produce CF_3Br is included, since the data interpretation does not suggest it. As in the usual data treatment for VLPP studies, each molecular and radical specie escapes from the reactor with a characteristic first-order escape rate constant; for CF_3I, Br_2, CF_3, and CF_3Br, the escape rate constants are k_2, k_3, k_4, and k_5.

Analysis of the reaction mechanism and solution of the appropriate differential equations give an expression for the time-dependent mass spectrometer signal due to CF_3Br. The total yield of CF_3Br, (Y), is related to the rate constants as follows:

$$Y^{-1} = \left(\alpha\beta V\left[CF_3I\right]_o\right)^{-1}\left[1 + \frac{k_4 + k_w}{k_1\left[Br_2\right]}\right]$$

where pseudo-first-order conditions are assumed to hold. In this expression, α is a mass spectrometric sensitivity factor, β is the fraction of the initial CF_3I that is dissociated by the laser pulse, and V is the volume of the cell. The initial $[CF_3I]_o = F_{CF_3I}/(V \cdot k_2)$, where F_{CF_3I} is the flow rate of CF_3I into the reactor, and V is the reactor volume; similarly, $[Br_2] = F_{Br_2}/(V \cdot k_3)$. For each F_{Br_2}, two escape apertures can be used, giving two different values for the escape rate constants, corresponding to the "big" and "small" apertures. Plots of Y^{-1} versus $F_{Br_2}^{-1}$ give two straight lines with intercepts c_s and c_b (small and big apertures) given by i = s or b):

$$c_i = \frac{k_{2i}}{\alpha\beta V F_{CF_3I}}$$

The slopes of the straight lines are given by

$$m_i = \frac{c_i V(k_{4i} + k_w)k_{3i}}{k_1}$$

Laser-Powered Homogeneous Pyrolysis (LPHP)

In VLPP experiments aimed at obtaining unimolecular rate information, we rely on the walls of the VLPP reactor to be the source of heat through gas-wall collisions, while at the same time being non-catalytic for the destruction of the substrate. Sometimes this latter condition is not met. Therefore, we may, in addition to VLPP, use the technique of laser-powered homogeneous pyrolysis [12]. This technique is a valuable complement

to the VLPP procedure, since it essentially provides a "wall-less" reactor. The total pressure in the reactor is on the order of 100 torr, consisting mostly of bath gas and SF_6. An IR laser is used to heat the strongly absorbing sensitizer (SF_6), using a wavelength at which the substrate does not absorb. The SF_6 transfers its thermal energy by collision to the substrate molecules, and decomposition takes place. As described by Shaub and Bauer [12], the technique worked well for compounds of relatively high vapor pressure, using a static reactor system and a CW laser; we are currently adapting the technique for application to poly-nitro aromatics and other low-vapor-pressure substrates, using a pulsed CO_2 laser and a flow system with GC detection. The reasons for these modifications are: (1) When operation is with a pulsed laser, reaction times are short because of rapid cooling by contact with the off-axis cell contents, and secondary reactions are either unimportant or can be minimized by suitable choice of a scavenger, and (2) when low-vapor-pressure substrates are being studied, quantitative recovery and measurement of products and unreacted starting material is simpler with a flow system.

We have preliminary evidence from this technique [13] which indicates that nitrotoluenes decompose by NO_2-aromatic bond scission. This seems to be true of those with ortho-methyl substitution as well, in contrast to earlier reports.

4. DISCUSSION

There are various limitations on the usefulness of thermochemical kinetics. These range from quantitative to qualitative uncertainties. We need to test some of the preceding ideas with experiments conceived for just that purpose. Since the ideas are based on the transition state theory formalism, it is important to address the question of limits of validity of transition state theory. In general, these testing reactions should be measured under conditions where isolated reactions can be observed, as the extraction of individual rate constants from complex reacting systems is fraught with difficulty.

There are many examples of reactions for which rate constants have been studied, but product studies are lacking. Thus,

in reactions of OH with olefins current smog and combustion models must arbitrarily decide on branching ratios. This is equally true in aromatic systems.

In all of the above discussion of estimation of rate data, the importance of thermochemical values for all species has been emphasized. It is particularly important to have a good set of values for the entropy and heat of formation of organic free radicals.

Very few spectroscopic assignments exist for modest-to-large size organic free radicals. Entropies (and heat capacities) have generally been estimated by methods discussed earlier. Uncertainties arise from changes in hindered rotation barriers and changes in skeletal bending frequencies.

Many bimolecular reactions are not direct, rather involving bound complex as an intermediate. These give rise to what seem to be unusual parameters for bimolecular processes [14].

A simple treatment for the pressure dependence of unimolecular processes, which would lend itself to easy use in large models, is seemingly close at hand, but care must be exercised.

In summary, we have a framework for the codification and extrapolation of rate data, but much testing and modification will be necessary.

REFERENCES

1. Benson, S. W., Thermochemical Kinetics, 2nd Ed., John Wiley and Sons, Inc., New York, 1976.

2(a) Golden, D. M., in Chemical Kinetics Data Needs for Modeling the Lower Troposphere, Proceedings of a Workshop at Reston, VA, May 1978. NBS Special Publication 557, US Government Printing Office, Washington, DC, August 1979.

(b) Golden, D. M., "Estimation of Rate Constants of Elementary Processes--A Review of the State of the Art," Fourteenth Symposium (International) on Combustion, The Combustion Institute, Pittsburgh, PA, 1973.

(•) Golden, D. M., in Summary Report on the Workshop on High Temperature Chemical Kinetics, NBS Special Publication 531, US Government Printing Office, Washington, DC, December 1977.

(¢) Golden, D. M., "Pyrolysis and Oxidation of Aromatic Compounds" in Progress in Astronautics and Aeronautics, Vol. 62, 233 (1978), Chapt. III, Craig T. Bowman and Jorgen Birkeland, Ed., Proceedings of Project SQUID Workshop on Alternative Hydrocarbon Fuels: Combustion and Chemical Kinetics, September 1977, Columbia, MD.

3. Golden, D. M. "Measurement and Estimation of Rate Constants" in Dynamics and Modelling of Reactive Systems, W. E. Stewart, W. Harmon Ray, Charles C. Conley, Eds., Academic Press, New York, 1980.

4. Benson, S. W., F. R. Cruickshank, D. M. Golden, G. R. Haugen, H. E. O'Neal, A. S. Rodgers, R. Shaw, R. Walsh, Chem. Rev., 69, 279 (1969).

5. (a) Golden, D. M., Richard K. Solly, and Sidney W. Benson, J. Phys. Chem., 75, 1333 (1971).
   (b) Troe, J., J. Phys. Chem., 83, 114 (1979).

6. (a) Golden, D. M., A. C. Baldwin, and K. E. Lewis, Int. J. Chem. Kinetics, 11, 529 (1979).
   (b) Quack, M., and J. Troe, Ber. Bunsenges, Phys. Chem., 81, 329 (1977).

7. (a) Smith, I.W.M., and R. Zellner, Int. J. Chem. Kinetics, Symp. No. 1, 341 (1975).
   (b) Margitan, J. J., F. Kaufman, and J. G. Anderson, Int. J. Chem. Kinetics, Symp. No. 1, 281 (1975).

8. Golden, D. M., S. W. Benson, and G. N. Spokes, Angew. Chem. (International Edition), 12, 534 (1973).

9. Golden, D. M., M. Rossi, and K. D. King, J. Amer. Chem. Soc., 101, 1223 (1979).

10. McMillen, D. F., P. Trevor, and D. M. Golden, J. Amer. Chem. Soc., 102, 000 (1980).

11. Rossi, M., J. R. Barker, and D. M. Golden, J. Chem. Phys. 71, 3722 (1979); Chem. Phys. Lett., 65, 523 (1979).

12. Shaub, W. M., and S. H. Bauer, Int. J. Chem. Kinetics, 7, 509 (1975); Shaub, W. M., Ph.D. Thesis, Cornell Univ., 1975.

13. Lewis, K. E., D. F. McMillen, and D. M. Golden, J. Phys. Chem., 84, 226 (1980).

14. Golden, D. M., J. Phys. Chem., 83, 108 (1979).

Chapter IV

KINETICS AND THERMODYNAMICS FOR ION-MOLECULE ASSOCIATION REACTIONS

J. S. Chang and D. M. Golden

(J. Am. Chem. Soc., 1981, 103, 496-500)

Reprinted from the Journal of the American Chemical Society, 1981, *103*, 496.

Kinetics and Thermodynamics for Ion-Molecule Association Reactions

J. S. Chang[‡] and D. M. Golden*

Department of Chemical Kinetics, SRI International, Menlo Park, California 94025.
Received June 30, 1980

Abstract: Rate constants for ion-molecule association reactions have been calculated according to a simple model. The model, which mimics RRKM results, is constrained to reach limiting values corresponding to ADO (or Langevin) collision frequencies at the high-pressure limit and the strong-collison energy-transfer rate constant at the low-pressure limit. For those reactions at the low-pressure limit, the required information is the density of states (entropy) of the association complex. Low-pressure-limit rate constants and those in the "fall-off" regime are compared with data.

Introduction

Ion–molecule clustering or association reactions are of interest in physical, organic, and atmospheric chemistry. The overall process, typically written

$$A^+ + B + M \underset{k_r}{\overset{k_f}{\rightleftharpoons}} AB^+ + M \qquad (1)$$

can more descriptively be illustrated as

$$A^+ + B \underset{k_b}{\overset{k_c}{\rightleftharpoons}} (AB^+)^* \xrightarrow{k_s[M]} AB^+ \qquad (2)$$

The collision rate constants, k_c and k_s, are given by Langevin[1] and ADO theory[2-4] as appropriate.

It has already been pointed out[5,6] that this type of reaction is totally analogous to neutral radical-combination reactions. Thus, since it is really the microscopic reverse of a unimolecular bond-scission process, all the considerations associated with the

[‡] Postdoctoral research associate.

(1) G. Gioumousis and D. P. Stevenson, *J. Chem. Phys.*, **29**, 294 (1959).
(2) T. Su and M. T. Bowers, *J. Chem. Phys.*, **58**, 3027 (1973).
(3) T. Su and M. T. Bowers, *Int. J. Mass Spectrom. Ion Phys.*, **12**, 347 (1973).
(4) L. Bass, T. Su, W. J. Chesnavich, and M. T. Bowers, *Chem. Phys. Lett.*, **34**, 119 (1975).
(5) W. N. Olmstead, M. Lev-On, D. M. Golden, and J. I. Brauman, *J. Am. Chem. Soc.*, **99**, 992 (1977).
(6) (a) J. M. Jasinski, R. N. Rosenfeld, D. M. Golden, and J. I. Brauman, *J. Am. Chem. Soc.*, **101**, 2259 (1979); (b) D. R. Bates, *Proc. R. Soc. London, Ser. A*, **360**, 1 (1978); (c) E. Herbst, *J. Chem. Phys.*, **70**, 2201 (1979); (d) D. R. Bates, *ibid.*, **71**, 2318 (1979).

Table I. Low-Pressure-Limit Rate Constants[a]

	reaction	k/cm^6 molecule^{-2} s^{-1} calcd	k/cm^6 molecule^{-2} s^{-1} exptl	ref
(1)	$H_3O^+ + H_2O + Ar \rightarrow H_3O{\cdot}H_2O^+ + Ar$	5 (−28)[b]	6 (−28)	18
			2 (−28)	19
	$H_3O^+ + H_2O + He \rightarrow H_3O{\cdot}H_2O^+ + He$	4 (−28)	6.7 (−28)	11
			7.2 (−28)	20
			1.2 (−27)	12
(2)	$NO^+ + CO_2 + N_2 \rightarrow NO^+{\cdot}CO_2 + N_2$	2 (−29)[c]	2.5 (−29)[c]	21
(3)	$O_2^+ + N_2O + N_2O \rightarrow O_2^+{\cdot}N_2O + N_2O$	3 (−29)[c]	5.2 (−29)[c]	22
(4)	$O_2^+ + O_2 + O_2 \rightarrow O_4^+ + O_2$	1.9 (−30)	2.5 (−30)	23a
			2.8 (−30)	23b
			2.4 (−30)	23c
(5)	$O_2^+ + N_2 + He \rightarrow O_2^+{\cdot}N_2 + He$	1.5 (−29)[d]	1.9 (−29)[d]	22
		7 (−31)	8 (−31)	15
(6)	$O_2^+ + H_2O + O_2 \rightarrow O_2^+{\cdot}H_2^2O + O_2$	1 (−28)	1 (−28)	24
			2.3 (−28)	25

[a] Calculations and experiments at 300 K unless otherwise cited. [b] Number in parentheses is the power of ten. [c] 200 K. [d] 80 K.

origin and nature of pressure dependence, as well as temperature dependence, arise when quantitatively discussing the rates of such processes. Ion-molecule association reactions are therefore treated by RRKM theory[5,6a] in order to codify and extrapolate the data to various conditions of temperature and pressure.

RRKM treatments involve complicated computer codes and detailed molecular information, and Troe and co-workers[7,8] have presented a model that allows a simpler calculation. We have adapted Troe's model to ion-molecule reactions, by taking into account the differences in the collision process.

Background

The model for the calculation of the association rate constant can be treated in three parts: high-pressure limit (second order), low-pressure limit (third order), and intermediate-pressure regime (fall-off region).

High-Pressure Limit. For the high-pressure-limit rate constant, we use Langevin and ADO theory to calculate k_c, the collision frequency between A^+ and B.

Low-Pressure Limit. We first calculate $(k_r)_0$, the low-pressure-limit rate constant in the unimolecular direction, for the decomposition of AB^+ (see eq 1). We then calculate the low-pressure-limit rate constant of interest from the overall equilibrium constant ($K = k_f/k_r$).

In complete analogy with Troe[7] we calculate the collision frequency between AB^+ and M by using ADO theory and a simple harmonic oscillator model followed by a few correction factors which account for (1) anharmonicity, (2) energy dependence of the density of states, (3) overall rotation, and (4) internal rotation, i.e.

$$k_r = \beta Z_{ADO} \frac{\rho_{vib,h}(E_0)kT}{Q_{vib}} \exp(-E_0/kT) F_{anh} F_E F_{rot} F_{int\,rot} \quad (3)$$

where β = collision efficiency (vida infra), Z_{ADO} = ADO collision frequency, $\rho_{vib,h}$ = harmonic oscillator density of states, Q_{vib} = vibrational partition function, and E_0 = critical energy (bond dissociation energy at 0/K). (Explicit formulas[7] for the various factors used in this calculation are listed in Appendix I.) Since one of the oscillators is represented by an R^{-4} potential, there may be a difference in anharmonicity correction factors between ion-molecule and neutral-molecule reactions, but the difference due to this one oscillator should be small, especially when the associated molecular ion has many atoms. β is assumed to be unity.[5] Equation 3 arises from[7]

$$\frac{(k_r)_0}{k_s[M]} = \frac{[AB^{+*}]}{[AB^+]} = \frac{Q_{AB^{+*}}}{Q_{AB^+}} = \frac{\int_{E_0}^{\infty} \rho(E) e^{-E/kT}\, dE}{Q_{AB^+}} = \frac{(k_r)_0}{\beta Z_{ADO}} \quad (4)$$

(7) J. Troe, *J. Chem. Phys.*, **66**, 4758 (1977).
(8) K. Luther and J. Troe, "Proceedings of the 17th International Symposium on Combustion", Leeds, England, 1978, p 535.

Table II. Collision Efficiences–Small Complex
$O_2^+ + H_2O + M \rightarrow (O_2{\cdot}H_2O)^+ + M$

M	k_{exptl}[a]	ref
He	8.7×10^{-29}	24
	9×10^{-29}	25
Ar	1.7×10^{-28}	24
	2.0×10^{-28}	25
O_2	2.3×10^{-28}	24
	1×10^{-28}	25
N_2	2.5×10^{-28}	24
	2.8×10^{-28}	25

[a] cm^6 molecule^{-2} s^{-1}; 300 K. $k_{calcd} = 1 \times 10^{-28}$ cm^6 molecule^{-2} s^{-1} for all cases.

Note that this is independent of transition-state or RRKM theory.

This low-pressure-limit decompsition rate constant is then multiplied by the equilibrium constant to calculate the low-pressure-limit association rate constant. Unfortunately, thermochemical data are not always available. In these cases, we estimate some of the thermochemical data from geometry and vibrational frequencies to calculate the equilibrium constant.

Fall-Off Region. After we have obtained both the high-pressure-limit rate constant and the low-pressure-limit rate constant, the intermediate-pressure rate constant is obtained from a formula,[8] empirically designed to mimic RRKM curves, which has been successfully used[9,10] in neutral molecule association reactions. For each temperature, this formula is

$$k \simeq \frac{k_0[M]}{1 + k_0[M]/k_\infty} F_c^{[1+\{\log(k_0[M]/k_\infty)\}^2]^{-1}} \quad (5)$$

where k_0 and k_∞ represent low-pressure-limit and high-pressure-limit rate constants, respectively.

F_c is a constant that can be evaluated[8] for different conditions. We find that for our limited purposes, a value of $F_c = 0.6$ is sufficient to reproduce values computed with a full RRKM calculation to within a factor of less than 2. (More accurate reproduction of RRKM can be obtained by using the more detailed formulas in ref 8.)

Results and Discussion

(A) Low-Pressure-Limit Association Rate Constants. The results of low-pressure-limit rate constant calculations for six association reactions are listed in Table I. The molecular parameters and thermochemical data used in the calculations are listed in Table IV. As shown in Table I, the agreement between the experimental data and the calculated rate constants is excellent. (This is also true for reactions shown in Tables II and III.) This not only means that this model works extremely well in relating the thermochemical and the kinetic data but also allows us to

(9) R. Zellner, *Ber. Bunsenges. Phys. Chem.*, **82**, 1172 (1978).
(10) D. M. Golden, J. S. Chang, and A. C. Baldwin, NASA Workshop on Stratospheric Chemistry. JPL Publication No. 79-27, Evaluation No. 2, April 15, 1979.

Table III. Collision Efficiencies–Large Complex
$C_6H_6^+ + C_6H_6 + M \rightarrow (C_6H_6)_2^+ + M$

M	$10^{28}k_{calcd}$[a]	k_{exptl}[a]	ref
He	3.8	4×10^{-27}	26
Ne	1.2	$\gtrsim 5 \times 10^{-28}$	26
Ar	1.3	7×10^{-27}	26
Kr	1	1.1×10^{-26}	28
Xe	1	1.6×10^{-26}	26
C_6H_6	2	1.2×10^{-25}	26

[a] cm^6 $molecule^{-2}$ s^{-1}; 300 K.

understand and predict many gas-phase ion-molecule association rate constants.

Of particular note is the inference that for some reactions that are difficult to study, we may predict rate constants if we have the requisite thermochemical data. In fact, we argue[6e] that pursuit of the thermochemical information would be the more useful endeavor.

(B) Fall-Off Phenomena. Ion-molecule association rate constants will change from third order in the low-pressure regime to second order at the high-pressure limit. At the medium pressures where the transition takes place, "fall-off" phenomena are expected to be observed. RRKM treatments of this are adequate, as previously demonstrated.[5,6e] In this paper, we use eq 5 to predict the fall off. The result of this prediction is very close to an RRKM calculation which employs the same values of k_0 and k_∞.

A few experimental techniques have been widely used in studying the kinetics of ion-molecule association reactions. Most of them employ relatively low-pressure conditions such as the

Table IV. Vibrational Frequencies and Thermochemical Data

complex[a]	freq	ΔH,[b] ΔS[c]	ref	complex[a]	freq	ΔH,[b] ΔS[c]	ref
(I-1) $H_3O^+ \cdot H_2O$	3100 (4)[d]	$\Delta H = -31.6$,	6a		1485 (2)		
	1800 (1)	$\Delta S = -24.6$			1326 (1)		
	1600 (2)				1310 (1)		
	500 (4)				1178 (2)		
410 (1)	410 (1)				1146 (1)		
	142 (2)				1089 (10)		
	50 (1)				1037 (2)		
(I-2) $NO^+ \cdot CO_2$	1343	$\Delta H = -11.3$,	21		1010 (1)		
	667	$\Delta S = -25.0$			992 (1)		
	2349				985 (1)		
	2377				970 (2)		
	1600				847 (3)		
	500				800 (2)		
	100				703 (1)		
	100				600 (1)		
	500				400 (7)		
(I-3) $O_2^+ \cdot N_2O$	1580	$\Delta H = -12.9$,	22		300 (2)		
	1275	$\Delta S = -29.0$	estimated		70 (5)		
	589 (2)				50 (1)		
	2225			(F) $CH_3NH_3^+ \cdot CH_3NH_2$	3300 (4)	$\Delta H = -21.7$,	5
	1275				2970 (6)	$\Delta S = -23.6$	
	400				1600 (1)		
	100				1450 (6)		
	100				1175 (4)		
(I-4) O_4^+	1110	$\Delta H = -9.6$,	27, 23b		1000 (3)		
	1043	$\Delta S = -20.6$	27, 23b		900 (2)		
	800				820 (2)		
	400				740 (2)		
	400				600 (1)		
	100				400 (1)		
(I-5) $O_2^+ \cdot N_2$	1100	$\Delta H = -7$,	22, 27		300 (2)		
	1100	$\Delta S = -20$			200 (2)		
	1200				175 (2)		
	400				100 (1)		
	400			(T) $C_2H_5ClCH_3^+$	3002	$\Delta H = -30.7$,	16
	75				580	$\Delta S = -30.7$	
(I-6, II) $O_2^+ \cdot H_2O$	1100	$\Delta H = -16$,	24, 25		3184 (2)		
	1043	$\Delta S = -17.9$			1383 (2)		
	3600				1020 (2)		
	3600				1460 (1)		
	400				1020 (2)		
	1000				1000 (1)		
	1000				1350 (1)		
	1400				3000 (5)		
	100				1150 (2)		
(III) $(C_6H_6)_2^+$	3082 (6)	$\Delta H = -15.1$,	6a		400 (1)		
	3080 (2)	$\Delta S = -23.2$			125 (2)		
	3062 (1)				100		
	3060 (1)				100		
	3047 (2)				550 (5)		
	1597 (6)						
	1596 (2)						

[a] I-1 through I-6 refer to Table I; II refers to Table II; III refers to Table III; F refers to the figure; T refers to the text. [b] ΔH for the reaction: $A^+ + B \rightarrow AB^+$ in kcal mol^{-1} (300 K). [c] ΔS for the reaction: $A^+ + B \rightarrow AB^+$ in cal mol^{-1} K^{-1} (300 K).

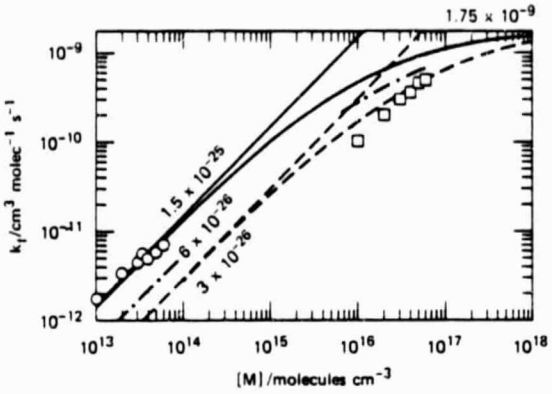

Figure 1. Pressure dependence of k_f at 300 K for the reaction $CH_3NH_2 + CH_3NH_3^+ + M \rightleftharpoons CH_3NH_2{-}H^+NH_2CH_3 + M$ (○, ref 13; □, ref 14): (—) a priori best estimates from methods outlined herein; (---) reduction of k_0 by a factor of 5 to accommodate data of ref 14; (···) compromise value to best accommodate high- and low-pressure data.

flowing-afterglow technique[11,12] and ion-cyclotron resonance spectroscopy at mili torr pressures, leading in general to near low-pressure-limit rate constants. However, some of the reactions may still show deviation from the low-pressure limit, particularly when mass spectrometric techniques in the torr range are employed. Extrapolation out of the experimental pressure range will be unreasonable[13] unless this is taken into account.

Prediction is compared to experiments using, as an example, the reaction

$$CH_3NH_3^+ + CH_3NH_2 + M \rightarrow CH_3NH_3^+CH_3NH_2 + M$$

Two groups have studied this reaction by two different techniques. Neilson et al.[13] studied this reaction over the pressure range of 1×10^{-4} to 3×10^{-3} torr of CH_3NH_2 by using the ion-cyclotron resonance mass spectroscopic technique and concluded that the low-pressure-limit and high-pressure-limit rate constants were 1.8×10^{-25} cm^6 molecule^{-2} and 2.1×10^{-11} cm^3 molecule^{-1} s^{-1}, respectively.

Meot-Ner and Field[14] used a pulsed high-pressure mass spectrometer to study this reaction over the pressure range of 0.5–2 torr isobutane and concluded that the low-pressure-limit and high-pressure-limit rate constants were 2.5×10^{-26} cm^6 molecule^{-2} s^{-1} and 4.0×10^{-10} cm^3 molecule^{-1} s^{-1}.

The disagreement between these two reports results, in part, from systematic differences in the experiments and, in part, from an incorrect extrapolation of the data.[15] Figure 1 is illustrative. The higher pressure data[14] can be fit by assuming that $k_\infty = k_{ADO} = 1.75 \times 10^{-9}$ cm^3 molecule^{-1} s^{-1} and $k_0 = 3 \times 10^{-26}$ cm^6 molecule^{-2} s^{-1}. We compute a value of $k_0 = 1.1 \times 10^{-25}$ cm^6 molecule^{-2} s^{-1} (in isobutane) by using the methods outlined herein. This is not out of the bounds of possible error. However, the lower pressure data[13] fit well the computed value (in methylamine) of $k_0 = 1.5 \times 10^{-25}$ cm^6 molecule^{-2} s^{-1}. Taking this latter at face value suggests that the higher pressure data are in error by a factor of ca. 2. Of course, a value of $k_0 = 6 \times 10^{-26}$ cm^6 molecule^{-2} s^{-1} splits the difference accommodating reasonable opposing errors in the two data sets, as well as an acceptable deviation from the calculation. (This latter line gives values within a factor of 2 of the RRKM calculations of Olmstead et al.,[5] who had only the high-pressure results at their disposal.)

Another example of the usefulness of this approach is illustrated for the reaction

$$C_2H_5^+ + CH_3Cl + CH_4 \rightarrow (C_2H_5ClCH_3)^+ + CH_4$$

The rate constant for this process has been measured[16] at ~4 torr. The authors, having supposed the process to be in the low-pressure limit, interpreted the data to yield $k = 1.7 \times 10^{-26}$ cm^6 molecule^{-2} s^{-1} at 300 K. However, this rate constant multiplied by the pressure (i.e., 1.7×10^{-26} cm^6 molecule^{-2} s$^{-1} \times 1.3 \times 10^{17}$ molecule cm^{-3}) yields $k_f = 2.2 \times 10^{-9}$ cm^3 molecule^{-1} s^{-1}. The limiting values (k_0(cm^6 molecule^{-2} s^{-1}) = 3.5×10^{-25}, calculated by methods of ref 7; k_∞(cm^3 molecule^{-1} s^{-1}) = 2.02×10^{-9}, calculated from ADO theory along with eq 4) predict a value of k(cm^3 molecule^{-1} s^{-1}) = 1.8×10^{-9}, well within all the error limits. Notice that rather than following the author's supposition, at this pressure the process is very close to the high-pressure limit. This is to be expected for this large complex which is strongly bound (30.7 kcal mol^{-1}).

(C) M Effect (Nature of the Bath Gas). The assumption that β is unity (the strong collision assumption) has been discussed previously.[5] There is no reason to expect that the efficiency for the rare gases in not somewhat less than unity. We report here that for small ion-molecule complexes $(AB^+)^*$, $\beta = 1$ (this assumption is good within experimental scatter), but that for large $(AB^+)^*$ (see Table III), the efficiency of small bath gases seems to be low. These effects can be demonstrated with the following two reactions.

For small AB^+ molecules, the reaction

$$O_2^+ + H_2O + M \rightarrow O_2^+{\cdot}H_2O + M$$

is used as an example. The M effect in the calculations resulted from the difference in Langevin collision frequencies which is proportional to $(\alpha_{M_1}\mu_{M_2}/\alpha_{M_2}\mu_{M_1})^{1/2}$ for different M, where α is polarizability and μ is the reduced mass of AB^+ and M. Usually, the calculated values of the rate constant for different M's are fairly close. The calculated and the experimental results are shown in Table II. All the experimental rate constants for different M's are within a factor of 3 compared with the calculated values, which lends credence to the notion that all bath gases are "good" third bodies.

For large AB^+ molecules, the reaction

$$C_6H_6^+ + C_6H_6 + M \rightarrow (C_6H_6)_2^+ + M$$

is used as an example. Table III shows all the experimental and calculated results. These results suggest that all rare gases are inefficient energy receivers or carriers, while C_6H_6 itself works well. This suggestion of inefficient energy transfer from a large ion-molecule complex to "small" bath-gas molecule warrants further investigation.

(D) Other Considerations. The temperature dependence of the rate constant can also be calculated according to this model. The results are similar to the results from RRKM calculations, which have also been shown to yield good agreement with some experiments.[5,6]

The uncertainties of around a factor of 2 or 3 in the low-pressure rate constant calculation are mainly due to current insufficient knowledge of the thermochemical data and of the geometry (structure) of the associated ion-molecule complex. For these association reactions, the influence on the rate constant from uncertainties in enthalpies is not as significant as those from entropies. This has been discussed previously with respect to both neutral and charged reactants.[6a,17] Therefore, it seems clear that any studies designed to yield entropic information on the ion-molecule complexes created by association reactions such as those dealt with herein will enhance the ability to predict rate constants for these processes.

(11) V. M. Bierbaum, M. F. Golde, and F. Kaufman, *J. Chem. Phys.*, **65**, 2715 (1976).
(12) C. J. Howard, V. M. Bierbaum, H. W. Rundle, and F. Kaufman, *J. Chem. Phys.*, **57**, 2491 (1972).
(13) P. V. Neilson, M. T. Bowers, M. Chau, W. R. Davidson, and D. H. Aue, *J. Am. Chem. Soc.*, **100**, 3649 (1978).
(14) M. Meot-Ner and F. H. Field, *J. Am. Chem. Soc.*, **97**, 5339 (1975).
(15) L. Bass, W. J. Chesnavich, and M. T. Bowers, *J. Am. Chem. Soc.*, **79**, 1501 (1979).
(16) D. K. Sharma and P. Kebarle, *J. Am. Chem. Soc.*, **100**, 5826 (1978).
(17) J. S. Chang, A. C. Baldwin, and D. M. Golden, *J. Chem. Phys.*, **71**, 2021 (1979).
(18) C. E. Young, D. Edelson, and W. F. Falconer, *J. Chem. Phys.*, **53**, 4295 (1970).
(19) U. A. Arifov, S. L. Pozharov, and I. G. Chemov, *Khim. Vys. Energ.*, **5**, 3 (1971); *Izv. Akad. Nauk. Uzb. SSR, Ser. Fiz.-Mat. Nauk.*, **15**, 49 (1971).

Conclusion

Thermal ion-molecule association reactions may be treated via RRKM theory[5,6,15] and thus also by the simplified computational schemes of Troe and co-workers[7,8] if neutral-neutral collision frequencies are replaced by ion-neutral frequencies (Langevin and ADO). Crucial inputs are the thermodynamic parameters of the association complex, especially the entropy.

Acknowledgment. This work was supported by Contract NAS7-100 (JPL Subcontract 954815) with the National Aeronautics and Space Administration.

Appendix I. List of Formulas

(a) ADO collision frequencies

$$Z_{ADO} = \frac{2\pi q}{\mu^{1/2}}\left[\alpha^{1/2} + C\mu_0\left(\frac{2}{\pi kT}\right)^{1/2}\right] \qquad (A1)$$

where q is the charge of the ion, μ is reduced mass between colliders, α is polarizability of the molecule, μ_0 is the dipole moment of the molecule, C is the correction factor as derived in ref 2, and k is the Boltzmann constant.

(b) Harmonic oscillator density of states

$$\rho_{vib,h} = [E + a(E)E_Z]^{s-1}/(s-1)!\prod_{i=1}^{s}(h\nu_i) \qquad (A2)$$

where E is the energy, E_Z is $^1/_2\sum_{i=1}{}^s h\nu_i$, s is number of oscillators, $a(E)$ is the empirical Whitten–Rabinovitch corrector, and ν_i are the vibrational frequencies.

(c) Anharmonicity correction factor

$$F_{anh} = \left(\frac{s-1}{s-{}^1/_2}\right)^m \qquad (A3)$$

where m is the number of oscillators that disappear during the dissociation reaction.

(d) Energy dependence of the density of states corrector is given as

$$F_E \simeq \sum_{\nu=0}^{r-1}\frac{(s-1)!}{(s-1-\nu)!}\left(\frac{kT}{E_0 + a(E_0)E_Z}\right)^{\nu} \qquad (A4)$$

(e) Rotational contribution

$$F_{rot} \simeq [(s-1)!/(s+{}^1/_2)!][E_0 + a(E_0)E_Z/kT]^{3/2} \times \left\{\frac{2.15(E_0/kT)}{2.15(E_0/kT)^{1/3} - 1 + [E_0 + a(E_0)E_Z/(s+{}^1/_2)kT]}\right\} \qquad (A5)$$

(f) Internal rotation factor

$$F_{int\ rot} = \frac{(s-1)!}{(s-{}^1/_2)!}\left(\frac{E_0 + aE_Z}{kT}\right)^{1/2}\left[1 - \exp\left(\frac{-E_0}{sV_0}\right)\right]\left\{\left[1 - \exp\left(\frac{-kT}{V_0}\right)\right]^{1.2} + \frac{\exp(-1.2kT/V_0)}{\sqrt{2\pi I_m kT/\hbar^2}[1 - \exp(-\sqrt{\pi^2\hbar^2 V_0/2I_m(kT)^2})]}\right\}^{-1} \qquad (A6)$$

(20) R. C. Bolden and N. D. Twiddy, *Discuss. Faraday Soc.*, **53**, 192 (1972).
(21) D. B. Dunkin, F. C. Fehsenfeld, A. L. Schmeltekopf, and E. E. Ferguson, *J. Chem. Phys.*, **54**, 3817 (1971).
(22) N. G. Adams, D. K. Bohme, D. B. Dunkin, F. C. Fehsenfeld, and E. E. Ferguson, *J. Chem. Phys.*, **52**, 3133 (1970).
(23) (a) J. D. Poyzant, A. J. Cunningham, and P. Kebarle, *J. Chem. Phys.*, **59**, 5615 (1973); (b) D. A. Durden, P. Kebarle, and A. Good, *ibid.*, **50**, 805 (1969); (c) A. Good, D. A. Durden, and P. Kebarle, *ibid.*, **52**, 222 (1970).
(24) C. J. Howard, V. M. Bierbaum, H. W. Rundle, and F. Kaufman, *J. Chem. Phys.*, **57**, 57, 3491 (1972).
(25) F. C. Fehsenfeld, M. Moseman, and E. E. Ferguson, *J. Chem. Phys.*, **55**, 2115 (1971).
(26) V. G. Anicich and M. T. Bowers, *J. Am. Chem. Soc.*, **96**, 1279 (1974).
(27) G. S. Janik and D. C. Conway, *J. Phys. Chem.*, **71**, 823 (1967).

Chapter V

ENTROPY BARRIERS IN ION-MOLECULE REACTIONS

James A. Dodd, David M. Golden, and John I. Brauman

(Accepted for publication in the Journal of Chemical Physics)

Entropy Barriers In Ion-Molecule Reactions

James A. Dodd, David M. Golden,[+] and John I. Brauman

Department of Chemistry

Stanford University

Stanford, California 94305

Abstract: The significance of entropic barriers to dissociation and recombination in the prototype ionic system $CH_3 + CH_3^+$ has been investigated. Ion-molecule systems are shown to react through an entirely different dynamics than neutral systems, due to intrinsic differences in the shapes of the relevant potential surfaces. Consequences with regard to the interpretation of experimental rate parameters in the ion-molecule area are discussed.

[+]Department of Chemical Kinetics, SRI International

Introduction

To a first approximation, ion-molecule dissociation and recombination reactions might appear to be analogous to the corresponding neutral processes of unimolecular dissociation and the reverse association. In this paper, however, we show that while much of the analogy is valid, ion-molecule systems react through an entirely different dynamics than neutral systems. Specifically, ion-molecule reactions proceed through "orbiting" transition states, even though radical-radical processes occur via "tight" transition states representative of an entropic barrier.

Unimolecular reaction rates of many neutral reactions have been shown to be well modeled through the use of variational transition state theory (VTST).[1-5] Problems arise in the application of traditional transition state theory for reactions in which there is no potential energy maximum between reactants and products, such as simple bond homolysis; an example is the methyl radical/ethane system, whose potential is outlined in Figure 1. Depicted are curves for $J = 0$ and some average $J = \langle J \rangle$; the latter shows the centrifugal barrier (greatly exaggerated) that results from angular momentum conservation requirements. Neglecting minor centrifugal additions onto the carbon-carbon (CC) bond stretch reaction coordinate, a potential maximum occurs only at infinite methyl radical separation. One is faced with the problem of where to place the transition state. In his analysis of this same system, Hase located the transition state at the site of minimum number of

bound quantum states,[5a-c] which of necessity lies on the side of a potential "hill". In doing so he was successful at modeling the rate parameters both of the dissociation of ethane and the recombination of two methyl radicals.

In terms of a statistical theory of unimolecular reactions, the above treatment takes on the following form: The microcanonical rate constant for dissociation is written[6]

$$k(E) = \frac{G^{\dagger}(E^{\dagger})}{hN(E)}$$

where $G^{\dagger}(E^{\dagger}) = G^{\dagger}(E - E_c)$ is the number of states in the transition state with non-fixed energy $E - E_c = E^{\dagger}$. E_c is the "critical energy" or barrier height, and N(E) is the density of states in the decomposing molecule at total energy E. The purpose of the VTST algorithm (often stated in terms of flux through phase space[7]) is to minimize k(E) in the course of minimizing the number of states $G^{\dagger}(E^{\dagger})$. For a canonical ensemble this sum of states minimization is equivalent to locating the point of highest <u>free</u> energy along the reaction coordinate; thus the procedure accounts for possible entropic as well as enthalpic barriers in the course of a reaction.[8a,b] This free energy criterion is arguably[9] superior to the more traditional potential energy criterion for transition state placement. In any event, numerous investigators have found this extended definition valuable for rate parameter modeling in the neutral domain.[1-5]

In contrast to neutrals, ion-molecule association processes have been modeled with an orbiting transition state located at the

maximum of the centrifugal potential (see Figure 1; the actual potential will look slightly different owing to the long-range r^{-4} ion-induced dipole interaction as opposed to the r^{-6} attractive potential in the neutral case). A sum of states "bottleneck" on the side of a potential hill, however, could possibly control the rate parameters of such association processes.[7] Indeed, the significance of the minimum quantum sum transition state in ionic systems finds support in a number of recent reports. For instance, entropic barriers have been invoked by Chesnavich et al. to explain the rate parameters of $C_4H_8^+$ decomposition,[10] and by Kebarle to model the temperature dependence of rates of hydride transfer between alkanes and alkyl carbonium ions.[11]

Nevertheless, in general this model fails to explain the behavior of experimentally determined rates of ion-molecule reactions. We note two important facts:

1) Many ion-molecule reactions proceed at the Langevin (or encounter) limit;[12]

2) If a transition state of the kind described by Hase[5] were always operative, ion-molecule reactions would never proceed at the Langevin limit.

We conclude that the reaction coordinate leading directly to covalent bond formation is not the operative reaction coordinate for ion-molecule association. Ion-molecule reactions differ from radical-radical combinations due to the strength of the long-range interactions. These ion-dipole and ion-induced dipole interactions lead to reactive intermediates formed via the orbiting transition

state; these relatively long-lived complexes can either decompose to products or break apart to regenerate reactants. Consequently ion-molecule association processes with no potential energy barrier are encounter controlled. Those reactions that proceed more slowly than the encounter limit, do so as the result of potential energy barriers rather than as a result of the entropic barrier introduced by minimizing $G^{\dagger}(E^{\dagger})$.

Calculations

For our computations we have chosen the reaction

$$CH_3^+ + CH_3 \longrightarrow CH_3CH_3^+$$

i.e. the association reaction of a methyl radical with a methyl cation to yield ethane radical cation. This system is the ionic analogue of the well-studied neutral reaction[5a-c]

$$CH_3 + CH_3 \longrightarrow CH_3CH_3$$

In each of the above reactions there is no potential maximum along the (incipient covalent) carbon-carbon bond distance reaction coordinate (see Figure 1). In fact, our calculations show (see below) that the variation of numbers of states along the reaction coordinate is remarkably similar for both the neutral and ionic systems.

In order to compute numbers of states, one needs to specify three quantities that vary with the reaction coordinate r: the

non-fixed energy E(r), the vibrational frequencies $\nu_i(r)$, where the index i runs over the 3N - 7 internal degrees of freedom (the CC stretch is not included since it is the reaction coordinate), and the shape of the potential curve V(r) along the reaction coordinate. The non-fixed energy is approximated as

$$E(r) = \langle E \rangle - V_{eff}(r)$$

The average energy $\langle E \rangle$ is estimated through the Boltzmann-weighted sum of states expression[6]

$$\langle E \rangle = \frac{\Sigma (E - E_0) G(E - E_0) \exp[-(E - E_0)/kT]}{\Sigma\, G(E - E_0) \exp[-(E - E_0)/kT]}$$

where $G(E - E_0)$ is the sum of molecular quantum states between energies E_0 and E, E_0 is taken to be the potential energy at infinite fragment separation, and the summations are taken over a suitably fine grain of energies E. The expression is evaluated at the orbiting configuration (located at the Langevin[13] fragment separation of 4.95 Å), and $\langle E \rangle$ is assumed to be a constant independent of fragment separation. For T = 300 °K and 600 °K one finds $\langle E \rangle$ = 2.30 kcal/mole and 5.85 kcal/mole, respectively.

An approximate effective potential function $V_{eff}(r)$ is constructed by summing the two components $V_{4\text{-}6\text{-}12}(r)$ and $V_{rot}(r)$. $V_{4\text{-}6\text{-}12}(r)$ is the common form for an ion-molecule interaction[14]

$$V_{4\text{-}6\text{-}12} = \tfrac{1}{2} D_e \left[(1 + \gamma) \left(\frac{r_e}{r}\right)^{12} - 4\gamma \left(\frac{r_e}{r}\right)^{6} - 3(1 - \gamma) \left(\frac{r_e}{r}\right)^{4} \right] \qquad (1)$$

where D_e is the dissociation energy, r_e is the equilibrium bond

length, and $0 < \gamma < 1$ is a parameter that measures the relative importance of the r^{-4} ion-induced dipole interaction term compared to the r^{-6} term typical of neutral-neutral interactions. The r^{-12} term corresponds to a repulsive core. γ is determined given D_e, r_e, and the polarizability α of the neutral fragment via

$$\gamma = 1 - \frac{e^2\alpha}{3 D_e r_e^4}$$

where e is the charge on a proton.

The dissociation energy of $CH_3CH_3^+$ is estimated to be 78.3 kcal/mole, given the known heats of formation of CH_3,[15] CH_3^+,[16] and CH_3CH_3,[15] and the adiabatic ionization potential of ethane.[17] In their theoretical study of the radical cation,[16] Pople and co-workers have determined the equilibrium CC bond distance to be 2.0 Å, where the ionizing electron has been removed from the CC sigma bond. With $\alpha(CH_3) = 2.2$ Å^3 one can thus solve for $\gamma = 0.82$ (indicating some r^{-4} character in the potential) and generate the 4-6-12 potential function (1).

In addition, one must account for conservation of the orbiting angular momentum of the two fragments about their common center of mass. This is done by adding onto the potential $V_{4\text{-}6\text{-}12}(r)$ the term

$$V_{rot}(r) = \frac{\langle J(J+1)\rangle h^2}{8\pi^2\mu r^2} \qquad (2)$$

where J is the quantum number for rotation, and μ is the reduced

mass.[18] The average value $\langle J \rangle$ is estimated to be about 30 at room temperature. $V_{rot}(r)$ constitutes a minor correction to $V_{4\text{-}6\text{-}12}(r)$ at reasonably low temperatures and $\langle J \rangle$ values. The resultant curve $V_{eff}(r)$ is plotted in Figure 2.

Loosening in the critical configuration along this curve was accomplished by lowering the frequencies in the four rocking motions of the cation (analogous to the two doubly degenerate frequencies ν_9 and ν_{12} of neutral ethane[19]) according to a decaying exponential in r,[5a] i.e.

$$\nu_9 = 822 \exp[-0.73(r - 1.54\ \text{Å})]\ \text{cm}^{-1}$$

$$\nu_{12} = 1190 \exp[-0.73(r - 1.54\ \text{Å})]\ \text{cm}^{-1}$$

The choice of the factor 0.73 will be explained below. 1.54 Å is the equilibrium bond length of neutral ethane; thus note that this bending mode loosening gives lower frequencies in the radical cation equilibrium configuration, in accord with theoretical predictions.[17] The other degrees of freedom in the critical configuration are taken to be the remaining normal vibrations of ethane,[19] except that the CC stretching mode becomes the reaction coordinate, and the methyl groups are allowed to rotate freely.[5a] Sums of states were calculated by a direct count of vibrational states and a semi-classical count of rotational states.[20]

For comparison we also calculated the sum of states at the orbiting transition state. In our computations we treated the system as two wholly disengaged D_{3h} fragments, with geometries and

vibrational frequencies corresponding to those reported for the methyl radical,[21] and with free tumbling of the fragments.[22] This model for the orbiting transition state has been referred to as the Gorin model[23] for neutral molecule decompositions. The factor of 0.73 used above in the exponentials describing bending mode loosening was chosen such that both models--the loosened vibrational and the fragmented--yield the same number of states at the orbiting CC separation of 4.95 Å.

See Table 1 for the input parameters for all of the sums of states computations.

Results and Discussion

Results of CH_3/CH_3^+ Model Calculations

Using the above parameters for the CH_3/CH_3^+ system, we find the sums of states minimum to occur at a CC separation of 4.3 Å, where the potential attraction is of the order of 1-2 kcal/mole. In Figure 3, we plot the potential and the sums of states against the reaction coordinate. According to statistical unimolecular reaction rate theory,[6] the microscopic reaction rate constant k(E) is proportional to the sum of quantum states $G^\dagger(E^\dagger)$ available to the transition state, where E and $E^\dagger$ are the non-fixed energies of the reactant and transition state, respectively. Thus the effect of the minimum is such that if the unimolecular dissociation of ethane cation were to occur along this reaction coordinate (bond stretch), the thermal rate constant for dissociation at 300 °K would be about half of that predicted if the orbiting complex were

taken to be the transition state. The rate of CH_3/CH_3^+ association would be likewise depressed.

Note that one can interpret the minimum sum transition state in terms of a "locking" of the external rotations of the fragments as they recombine. The locking process converts rotations into vibrations, thus lowering the number of states; the play between this locking, and an increased amount of non-fixed energy as the recombination reaction proceeds, determines the location of the transition state. Thus we shall henceforth refer to the minimum sum transition state as the "locked-rotor" transition state.

In Figure 4 we plot the variation of sums of states with temperature for each of the models outlined above. The positions of both the locked-rotor and orbiting transition states along the reaction coordinate are relatively weakly dependent on non-fixed energy, and are here assumed to be independent of temperature.

Hase was able to parameterize loosening in the ethane homolysis process so as to locate the locked-rotor transition state and fit experimental rate parameters.[5a] Since analogous data for ethane radical cation dissociation do not exist, the placement of the locked-rotor transition state on the ion-induced dipole attractive coordinate is admittedly somewhat arbitrary. Nevertheless, we feel that despite the quantitative uncertainties of our model, several important observations can be drawn concerning the CH_3/CH_3^+ system, and, we suggest, for unimolecular ionic dissociation and association reactions in general:

First, the locked-rotor transition state exists for ionic as well as for neutral reactions. Second, the locked-rotor transition state is located "inside" the orbiting complex, that is, at a smaller fragment separation on the coordinate leading to CC covalent bond formation. This makes good physical sense: the free rotors can lock up only after they have passed the orbiting complex in the recombination process. Third, the locked-rotor configuration is located in a potential regime where only a few kilocalories of non-fixed energy are available to it. Fourth, the locked-rotor transition state becomes more important relative to the orbiting complex as the temperature is raised. Finally, the low number of quantum states associated with the locked-rotor transition state must result in significantly decreased microscopic rate constants for association and dissociation reactions relative to those expected with an orbiting transition state. Many incoming reactive configurations would reflect off such a barrier.

Proposed Mechanism for Ion-Molecule Reactions

We propose that ionic systems take advantage of their inherent ion-dipole and ion-induced dipole attractions, which can allow quite substantial energies (10-15 kcal/mole[24]) of <u>unstructured</u> association between charged and neutral fragments.[25] In Figure 5 we employ an energy contour description of the CH_3/CH_3^+ system dynamics. One of the methyl fragments is fixed at the origin, and the other is allowed to approach it. The radial coordinate r ($0 \leq r < \infty$) corresponds to intercarbon separation. The angular

coordinate $\theta(-\pi/2 < \theta < +\pi/2)$ corresponds to the acute angle between the line joining the carbon atoms, and the normal to the plane described by the atoms of the non-fixed fragment:

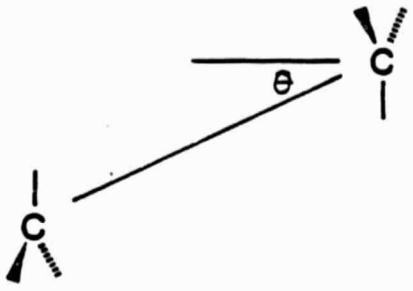

The approximate potential energy contours were generated by using the construction

$$V(r,\theta) = V_{dir}(r)\cos^2\theta + V_{ind}(r)\sin^2\theta$$

where $V_{dir}(r)$ is the effective potential function $V_{eff}(r)$ for direct CC bond formation, developed in the calculations section. $V_{ind}(r)$ is the appropriate 4-6-12 function for the formation of a loose association complex, and is generated in the following way: The binding energy of the association complex can be estimated as 5 kcal/mole, given the polarizability of methyl radical. If we model the CH_3 fragments as spheres with radii of 1.5 Å--CH bond length plus the radius of H--then r_e = 3.0 Å. From these parameters a reasonable potential curve is constructed using equation (1). Note that $V(r,\theta)$ reduces to $V_{dir}(r)$ for $\theta = 0$, and to $V_{ind}(r)$ for $\theta = +\pi/2, -\pi/2$.

The outer circle at zero energy corresponds to the orbiting transition state at a CC separation of 5 Å; its location is independent of relative orientation. The molecular cation equilibrium CC separation at r = 2.0 Å shows up as a very deep well (V(2.0 Å, θ = 0) = -78 kcal/mole), while the potential minimum along a coordinate of constant θ decreases in magnitude as θ varies toward $+\pi/2$ or $-\pi/2$. At $\theta = +\pi/2, -\pi/2$ the minimum of -5 kcal/mole arises solely through ion-induced dipole attraction, with no covalent component to the potential.

The dashed line corresponds to the approximate location of the set of locked-rotor transition states on the two-dimensional surface. The inclusion of this line is based on the assumption that the two methyl groups lock up only if (1) the approaching fragment is aligned to within a specified angle θ (θ is estimated as $\pi/4$ in the Figure), and (2) the fragment separation is within the distance r = 4.3 Å, which is the location of the locked-rotor transition state on the CC covalent bond potential profile (θ = 0) that we determined above. This assumption is in accord with the arguments presented above, namely, that the formation of a loose association complex does not lock up the free rotations of the fragments. The entropic barrier lies inside a large portion of the surface that is stabilized by ion-induced dipole interactions to the extent of 5-10 kcal/mole.

So long as the methyl fragments do not lock up, and are able to freely tumble about each other, one can make the reasonable assumption that the frequencies and moments of inertia of the

fragments remain constant as r is varied, i.e. these parameters can be considered to be independent of fragment separation in the process of forming a loose association complex. Thus the number of states for a loose complex increases monotonically, and drastically, with decreasing CC separation, as the system gains non-fixed energy. The fragments can lock easily, with a negligible sum of states bottleneck, if the locking occurs in a region of the potential surface where many kcal of non-fixed energy are available to the system.

The trajectory in Figure 5 near the $\theta = 0$ coordinate corresponds to direct CC bond formation. It crosses the entropic barrier early in the bonding process. On the other hand, the second trajectory provides an example of indirect association, in which the formation of an unstructured complex precedes covalent bonding. This trajectory crosses the barrier later (in the sense that the system is at lower potential energy) in the bonding process.

Thus we believe that the ion-neutral system is able to access a well that does not exist in the neutral system; an ion and molecule can avoid the locking up of the free rotors that characterizes the entropic barrier to association. The neutral and ionic fragments approach each other and the system passes through the orbiting transition state (which is the operative transition state for the process). At this point, however, the system "feels" the entropic barrier that would be brought on by the formation of a chemical bond and concomitant locking of the free rotors, and

avoids that locking by channeling away from the locked-rotor into a well representing an unstructured intermediate. This well does not exist in the case of neutral-neutral interactions, and the locked-rotor transition state cannot be circumvented in the same manner. Of course, the ion-neutral system must still undergo a locking up of the rotors at some point, regardless of reaction path; however, because the formation of an unstructured complex has released some 5 kcal/mole of non-fixed energy into the system, the ion-neutral intermediate can pass with ease into the well representing the structured molecule. This process corresponds to a trajectory crossing the dashed line in Figure 5. The locking process that occurs upon forming a chemical bond is kinetically unimportant in a potential regime so far below the energy of the separated fragments. Moreover, we have treated a rather conservative system in the CH_3/CH_3^+ case: most loose ion-molecule complexes have association energies significantly greater than 5 kcal/mole, since larger neutrals are more polarizable than CH_3.

Thus the locked-rotor transition state has a chance of being rate-determining only if the system channels through it relatively early in the recombination process, away from any deep potential wells. If the system can somehow avoid locking until later in the process, then the locked-rotor state is unimportant. Ion-molecule systems can channel away from an early confrontation with the locked-rotor entropy barrier through the dynamical mechanism described above; neutral systems do not have that same choice, but must channel through the locked-rotor state relatively early in a

recombination reaction, where the entropic barrier could be significant.

One can also consider this notion in terms of an ensemble of incoming reactive systems, constituting a distribution of molecular orientations and impact parameters. An ion and molecule are mutually attracted long before they are close enough to discern how they are oriented with respect to each other; they will form an unstructured complex regardless of orientation. If properly oriented, they can do the reaction directly, but the probability of this is so low and the rate of the process so small that this pathway is unimportant.

Note that this model implies certain unusual characteristics in the dynamics of the ethane radical cation dissociation/recombination system. The incoming fragments, given appropriate trajectories to form a chemical bond upon close approach, actually "prefer" to avoid forming that bond, and instead tumble about each other in a loose association complex prior to chemical structuring. By microscopic reversibility, the ethane cation dissociates not through simple CC bond stretching, but through some kind of bending and subsequent collapse to the same unstructured intermediate. This process would be followed by diffusion of the fragments away from each other, with the Langevin orbiting complex serving as the transition state.[13,18]

Actually, for the CH_3/CH_3^+ system the locked-rotor configuration does not constitute a severe entropic barrier; in general, the barrier may be large, depending on the particular system treated.

Both Hase's and our modeling suggest that severe bottlenecks (as evidenced by a sharp minimum in the sums of states) occur in the regime of a few kcal of non-fixed energy, since more energy than that will increase the sum of states greatly.

Consequences with Regard to Interpretation of Experiments

The results of this work have important implications in interpreting some experiments in the ion-molecule area. Chesnavich et al., in their analysis of $C_4H_8^+$ decompositions, have pointed out that apparent inconsistencies exist between PIPECO (photoion-photoelectron coincidence spectroscopy) results that imply barriers, and the often observed orbiting transition state rate constant for thermal ion-molecule reactions.[10] In addition, the product translational energy distribution appears to be statistical, even in cases where the decomposition reactions are slow. They suggest that a locked-rotor transition state can account for the above results.

As we have shown above, the locked-rotor cannot be playing an important role in any of the dynamics. Thus, an alternative explanation is required. In spite of the statement of Chesnavich et al. that no model has been postulated which accounts for the literature results, any double well potential surface will suffice. The double well potential has been suggested to account for slow ion-molecule reactions,[26] and it has been noted that its effects will be increasingly important at higher temperatures or energies. There is good reason to believe that many reactions which are encounter controlled at room temperature will be slow at higher

temperature owing to barriers, and in at least some cases there is experimental verification of this.[27] Any potential surface of this type will produce statistical translation in the products, because the loose complex following the barrier can equipartition its energy. The locked-rotor transition state will, of course, also produce statistical translation, even if no other barriers are present.

The central barrier (or barriers) will, in general, be chemical in nature. For example, rearrangements in the $C_4H_8^+$ system surely involve activation energy (as in solution). It is very unlikely that fragmentations which involve such extensive rearrangements could occur on a monotonically increasing surface. An analysis of the details of the surface is not in order here, although there may well be a common intermediate or intermediates present. In any case, the system resembles many others whose dynamics have been interpreted in terms of this general model; there is nothing about its characteristics which are at variance with the simple double well potential picture.

Conclusion

In summary, we have shown that the locked-rotor transition state occurs late, and has negligible kinetic importance in ion-molecule reactions, in contrast to neutral systems where it can play a crucial role in the dynamics. Quantitative differences between ion-neutral and neutral-neutral interactions produce a qualitative change in the chemical mechanism: namely, the

> 5 kcal/mole energy stabilization of unstructured ion-molecule intermediates always allows the circumvention of early entropic barriers. Potential surfaces incorporating true chemical barriers can explain the reaction patterns of ions; in particular, the previously suggested double well potential accounts for the seemingly anomalous rates of decomposition and product ratios of energized ions. In reactions such as dissociation in which there is no major potential barrier, centrifugal additions onto the zero-angular momentum reaction coordinate determine the distance of the (orbiting) transition state.

Acknowledgment The Stanford University authors are grateful to the donors of the Petroleum Research Fund and to the National Science Foundation for support of this research. J.A.D. acknowledges the National Science Foundation for a graduate fellowship (1981-1984). D.M.G. acknowledges support from NASA through contract NAS7-100 with JPL, as well as support through an SRI Fellowship. We thank C. R. Moylan for advice and stimulating discussions, and Professor W. L. Hase for comments on the manuscript.

References

[1]See references 1-22 in D. G. Truhlar, N. J. Kilpatrick, and B.C. Garrett, J. Chem. Phys., 78, 2438 (1983) for a number of accounts detailing the historical development of variational transition state theory and its relation to the minimum sum of states criterion. Apparently Wigner was the first to introduce the notion with regard to chemical transition states (E. Wigner, J. Chem. Phys., 5, 720 (1937)).

[2]P. Pechukas, Ann. Rev. Phys. Chem., 32, 159 (1981).

[3]For a general discussion of the various unimolecular reaction rate theories and the relationships between them see M. Quack and J. Troe, in Gas Kinetics and Energy Transfer, edited by P. G. Ashmore and R. J. Donovan (Specialist Periodical Reports, The Chemical Society, Burlington House, London, 1977), Vol. 2, p. 175.

[4]D. L. Bunker and M. Pattengill, J. Chem. Phys., 48, 772 (1968).

[5](a) W. L. Hase, J. Chem. Phys., 57, 730 (1972); (b) W. L. Hase, in Potential Energy Surfaces and Dynamics Calculations, edited by D. G. Truhlar (Plenum Press, New York, 1981), p. 1; (c) W. L. Hase, in Dynamics of Molecular Collisions, edited by W. H. Miller (Plenum Press, New York, 1976), Part B, p. 121.

[6]P. J. Robinson and K. A. Holbrook, Unimolecular Reactions (Wiley-Interscience, New York, 1972); W. Forst, Theory of Unimolecular Reactions (Academic Press, New York, 1973). The notation is that used by Forst.

[7]B. C. Garrett, D. G. Truhlar, and R. S. Grev in Potential Energy Surfaces and Dynamics Calculations, edited by D. G. Truhlar (Plenum Press, New York, 1981), p. 587.

[8](a) W. H. Wong and R. A. Marcus, J. Chem. Phys., 55, 5625 (1971); (b) D. G. Truhlar and B. C. Garrett, Acc. Chem. Res., 13, 440 (1980).

[9]K. J. Laidler, Theories of Chemical Reaction Rates (McGraw-Hill, New York, 1969), pp. 76-79.

[10]W. J. Chesnavich, L. Bass, T. Su, and M. T. Bowers, J. Chem. Phys., 74, 2228 (1981).

[11]T. F. Magnera and P. Kebarle, presented at the NATO Advanced Study Institute on Chemistry of Ions in the Gas Phase, Vimeiro, Portugal, September 1982.

[12]V. L. Talrose, P. S. Vinogradov, and I. K. Larin, in Gas Phase Ion Chemistry, edited by M. T. Bowers (Academic Press, New York, 1979), Vol. 1, p. 305.

[13]T. Su and M. T. Bowers, in Gas Phase Ion Chemistry, edited by M. T. Bowers (Academic Press, New York, 1979), Vol. 1, p. 83.

[14]L. A. Viehland, E. A. Mason, W. F. Morrison, and M. R. Flannery, At. Data Nucl. Data Tables, 16, 495 (1975).

[15]S. W. Benson, Thermochemical Kinetics (Wiley-Interscience, New York, 1976).

[16] Ionization Potentials, Appearance Potentials, and Heats of Formation of Gaseous Positive Ions, edited by J. L. Franklin, J. G. Dillard, H. M. Rosenstock, J. T. Herron, K. Draxl, and F. H. Field (NSRDS-NBS 26, 1969), p. 29.

[17] W. A. Lathan, L. A. Curtiss, and J. A. Pople, Molecular Phys., 22, 1081 (1971).

[18] E. V. Waage and B. S. Rabinovitch, Chem. Rev., 70, 377 (1970).

[19] T. Shimanouchi, Tables of Molecular Vibrational Frequencies (NSRDS-NBS, 1967), Part 1, p. 42.

[20] W. L. Hase and D. L. Bunker, Quantum Chemistry Program Exchange No. 234, Indiana University. State counting subroutines were lifted from this RRKM algorithm.

[21] A. Snelson, J. Chem. Phys., 74, 537 (1970).

[22] W. N. Olmstead, M. Lev-On, D. M. Golden, and J. I. Brauman, J. Amer. Chem. Soc., 99, 992 (1977).

[23] E. Gorin, W. Kauzmann, J. Walter, and H. Eyring, J. Chem. Phys., 7, 633 (1939).

[24] R. Yamdagni and P. Kebarle, J. Amer. Chem. Soc., 94, 2940 (1972).

[25] The stability of unstructured ion-molecule complexes is not mirrored by unstructured neutral-neutral complexes, because neutral systems must rely on relatively weak van der Waals interactions for any stabilization over the separated fragments. Work with molecular beams has shown neutral-neutral association energies to be very weak.

[26]W. N. Olmstead and J. I. Brauman, J. Amer. Chem. Soc., 99, 4219 (1977).

[27]M. Meot-ner (Mautner), in Gas Phase Ion Chemistry, edited by M. T. Bowers (Academic Press, New York, 1979), Vol. 1, p. 198.

Table 1. Parameters Used in the Calculation of Sums of States.[a]

	Orbiting transition state	Locked-rotor transition State
ν_i	3162 (4)	2975 (4)
	3044 (2)	2915 (2)
	1396 (4)	1472 (2)
	617 (2)	1460 (2)
		1388 (2)
		160[b] (2)
		111[b] (2)
I_i, s_i	1.23, 2 (2)	3.56, 3 (1)
	1.23, 1 (2)	
	3.56, 3 (1)	

[a] Degeneracies are in parentheses. Frequencies are in cm^{-1}, moments of inertia in amu $Å^2$. s_i is the symmetry number for rotation.

[b] Values that minimize the number of states; see text.

Figure Captions

Figure 1. Potential energy functions for CH_3CH_3 homolysis, plotted against CC bond distance coordinate. Note that accounting for nonzero angular momentum raises the potential at all values of r, and creates a maximum in $V_{eff}(r)$ at $r = r_L$. In the case of ions r_L is the orbiting (or Langevin) radius. D_e is the dissociation energy for $J = 0$.

Figure 2. Potential energy function $V_{eff}(r) = V_{4\text{-}6\text{-}12}(r) + V_{rot}(r)$ for $CH_3CH_3^+$ dissociation, plotted against CC bond distance coordinate. The potential energy zero (here and in Figure 3) is taken as that of infinite fragment separation.

Figure 3. Potential energy function $V_{eff}(r)$ as shown more fully in Figure 2, along with the sums of states function $G^\dagger(r)$, both plotted against CC bond distance coordinate.

Figure 4. Variation of the sums of states function $G^\dagger$ with temperature, shown for the orbiting configuration (r = 4.95 Å, upper curve) and for the locked-rotor configuration (r = 4.3 Å, lower curve).

Figure 5. Energy contour plot showing the dynamics of the $CH_3CH_3^+$ system. See text for discussion.

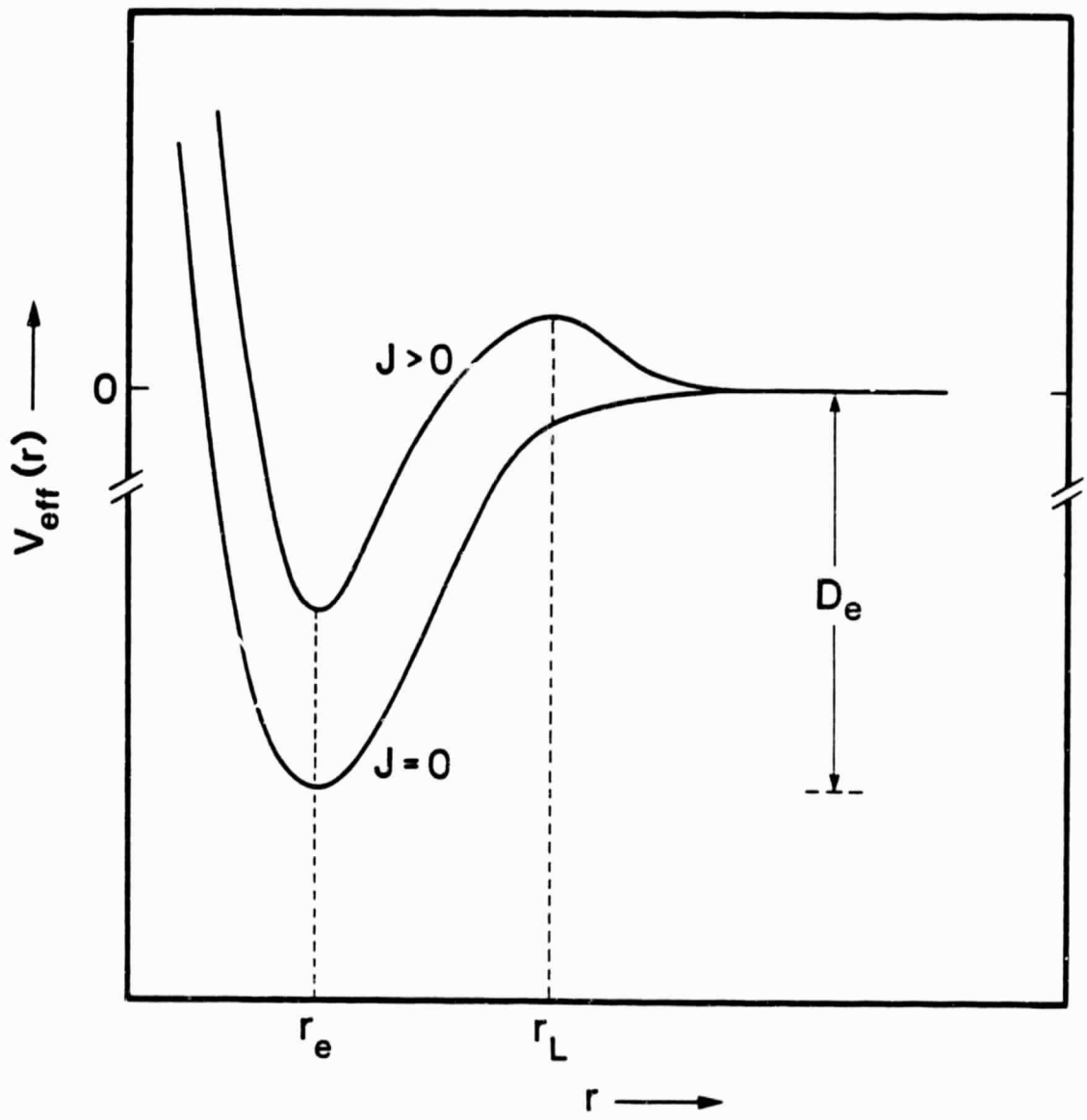
$V_{eff}(r)$
0
J>0
J=0
D_e
r_e
r_L
r

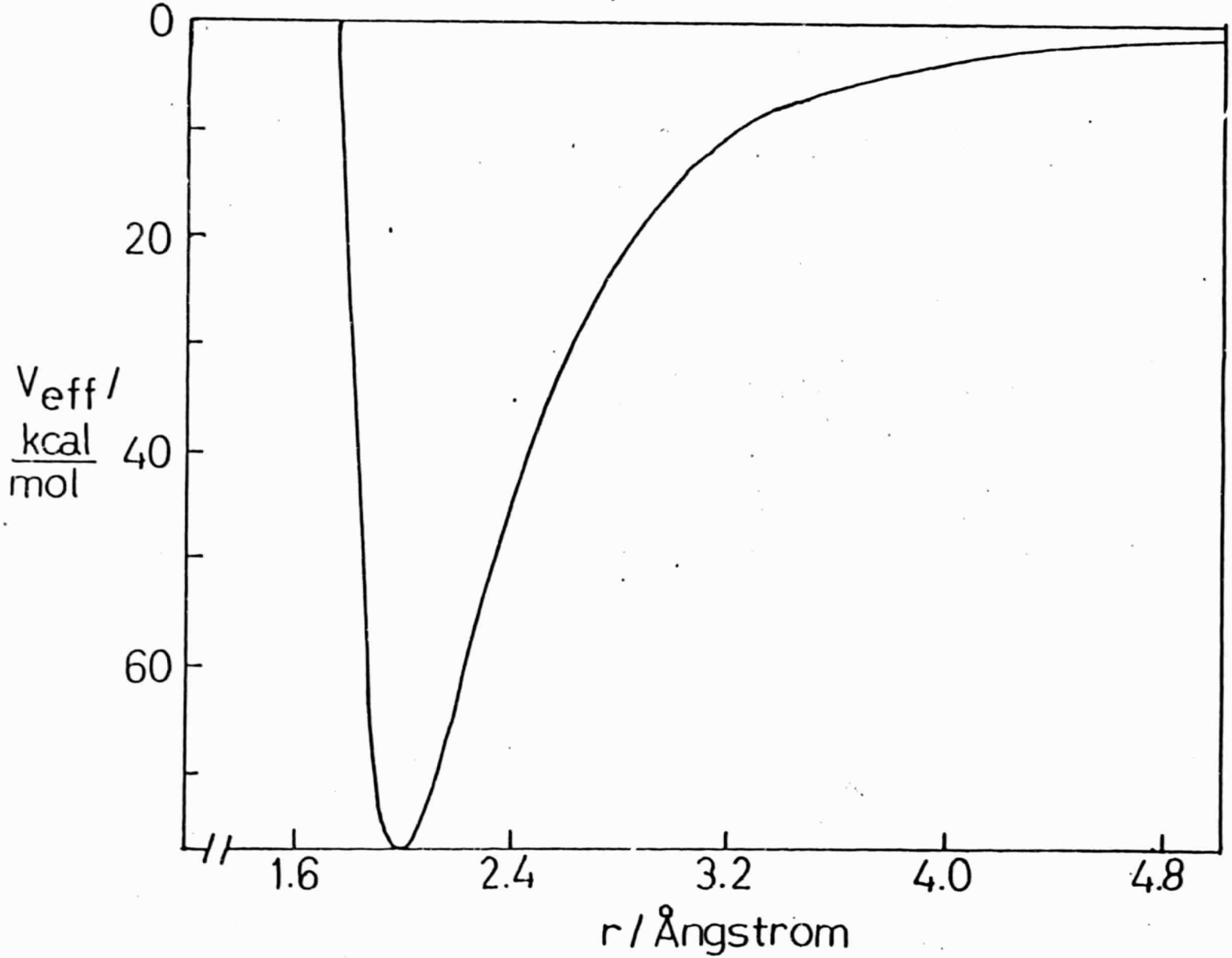
0
20
40
60
V_{eff} / kcal / mol
1.6
2.4
3.2
4.0
4.8
r / Ångstrom

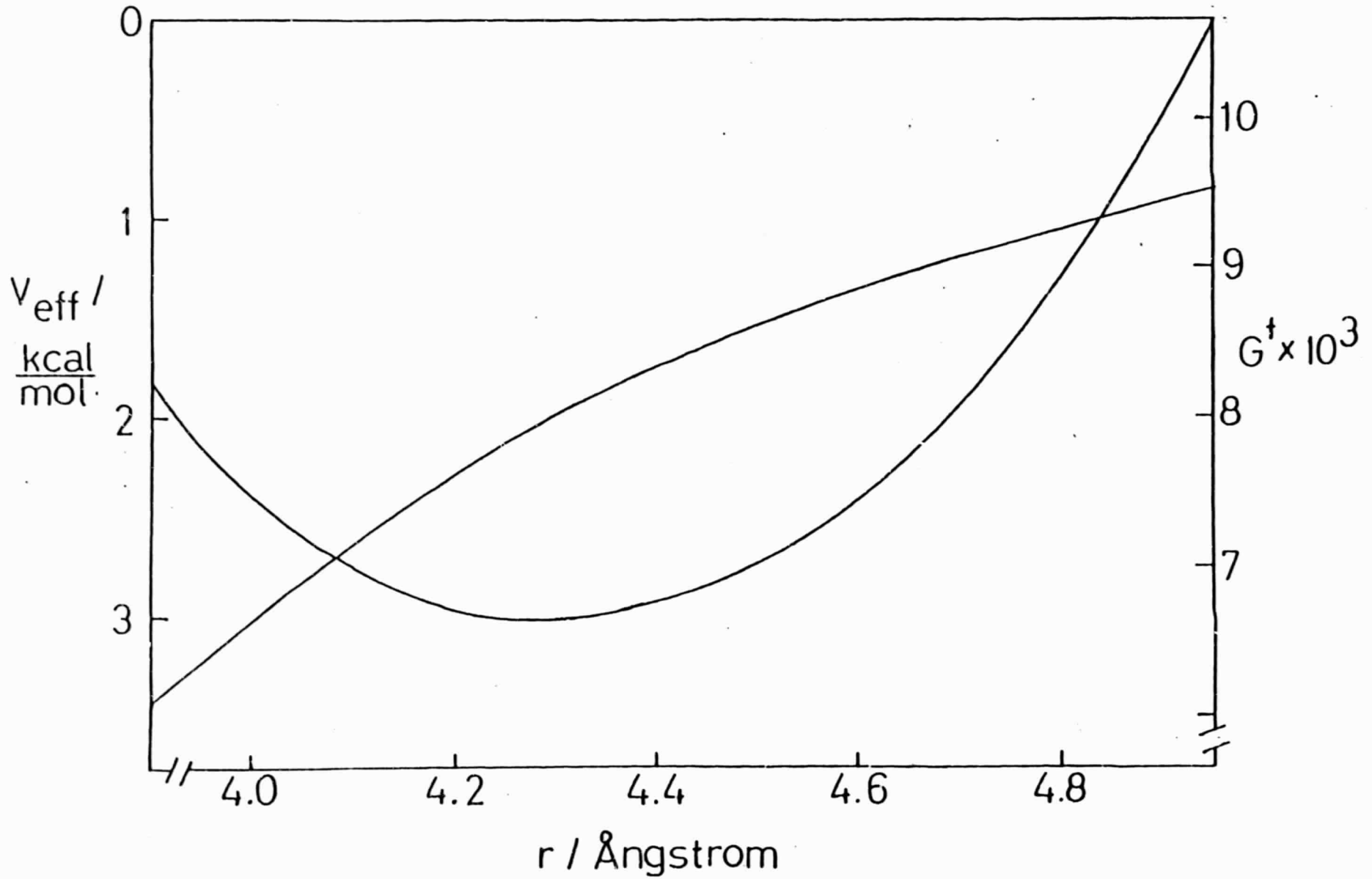
0
1
2
3
V_{eff} / kcal/mol
10
9
8
7
$G^t \times 10^3$
4.0
4.2
4.4
4.6
4.8
r / Ångstrom

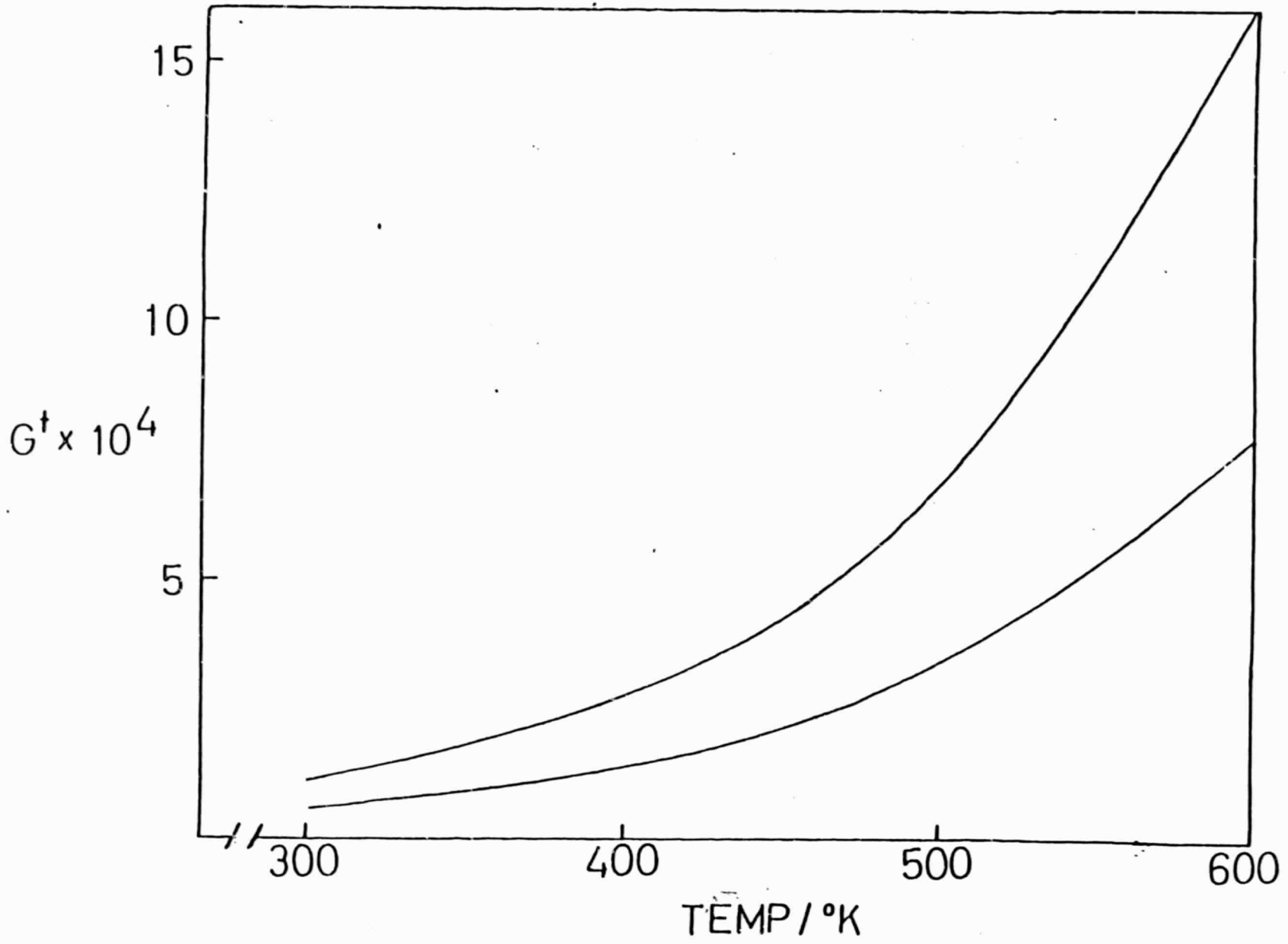
15
10
5
$G^t \times 10^4$
300
400
500
600
TEMP / °K

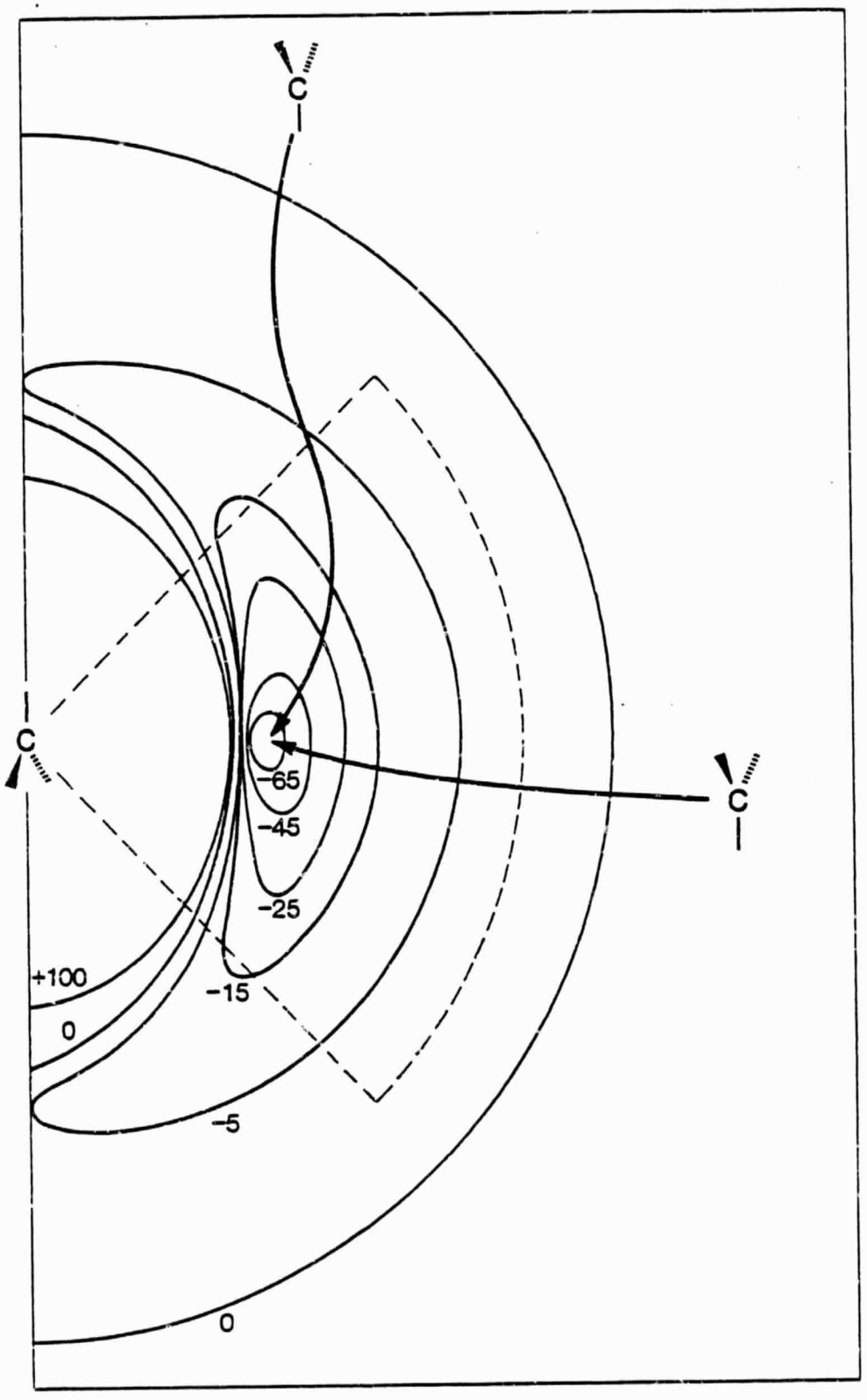
C
C
C
-65
-45
-25
-15
+100
0
-5
0

Chapter VI

REACTION RATE CONSTANTS FOR OH + $HOONO_2$ → PRODUCTS OVER THE TEMPERATURE RANGE 246 to 324 K

Paula L. Trevor, Graham Black, and John R. Barker

(J. Phys. Chem., 1982, 86, 1661-1669)

Reprinted from The Journal of Physical Chemistry, 1982, 86, 1661.

Reaction Rate Constant for OH + $HOONO_2$ → Products over the Temperature Range 246 to 324 K

Paula L. Trevor, Graham Black, and John R. Barker*

Physical Sciences Division, SRI International, Menlo Park, California 94025 *(Received: February 12, 1981; In Final Form: November 23, 1981)*

Absolute bimolecular reaction rate constants for the title reaction have been determined for temperatures ranging from 246 to 324 K. The laser flash-photolysis resonance-fluorescence (LFPRF) technique was used to generate $O(^1D)$ which reacted with H_2 and/or H_2O to produce OH radicals. The bimolecular rate constants for the title reaction showed no dependence on total (He) pressure over the range ~3 to 15 torr, and they did not depend upon initial [OH] or upon its mode of formation. The H_2O_2 impurity was explicitly measured in all experiments, and the rate constants were corrected for its contribution. A weighted least-squares analysis of the data obtained at nine temperatures (226 data points) gave the Arrhenius expression ($k \pm 1\sigma$) = $(8.05 \pm 5.69) \times 10^{-12} \exp(-193 \pm 194/T)$ $cm^3\ s^{-1}$ with covariance 1.098×10^{-9}. A simple weighted average (temperature independent) fits the data just as well, and when the effects of systematic errors are taken into account, our *recommended* rate constant is ($k \pm 2\sigma$) = $(4.0 \pm 1.6) \times 10^{-12}$ $cm^3\ s^{-1}$.

Introduction

Both HO_2 and NO_2 play crucial roles in the chemistry of the upper atmosphere. For several years, these two species were thought to react via a radical disproportionation reaction, although it was suggested[1] that a longer-lived complex could be formed according to reaction 1.

$$HO_2 + NO_2 + M \rightleftharpoons HOONO_2 + M \qquad (1)$$

The importance of reaction 1 has been verified by direct observation of HO_2NO_2 using Fourier transform infrared spectroscopy.[2] Moreover, the rate of reaction 1 has been measured,[3,5] and its reverse reaction (−1) has been studied.[4]

(1) R. Simonaitis and J. Heicklen, *J. Phys. Chem.*, 80, 1 (1976).

(2) H. Niki, P. D. Maker, C. M. Savage, and L. P. Breitenbach, *Chem. Phys. Lett.*, 45, 564 (1977).

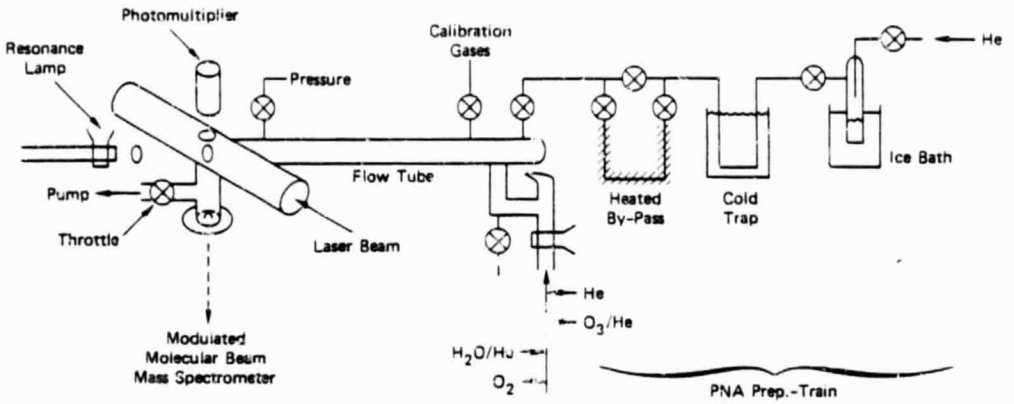

Figure 1. Schematic diagram of laser flash photolysis resonance-fluorescence experimental apparatus. For experiment series B, a KrF excimer laser (248 nm) was used, and for experiment series C and D, the quadrupled output (266 nm) of a Nd:YAG laser was used.

Also, RRKM theory has been applied to these data for reaction −1 so that its rate can be reliably estimated as a function of both temperature and pressure.[5] In another publication, the effect of HO_2NO_2 on tropospheric photochemical smog chemistry[6] was discussed.

A concerted effort is underway to investigate peroxynitric acid (PNA) and determine the rates of various loss mechanisms that affect its residence time in the stratosphere. In addition to the experimental studies reported on its thermal decomposition rate, results of investigations on optical absorption cross sections have been reported,[7-9] permitting calculation of the photolysis rates appropriate for the atmosphere.

In our laboratory, reactions of PNA with several atmospheric species have been studied to determine bimolecular rate constants for the destruction of PNA, including reactions with O atoms,[10] H atoms,[11] and O_3.[12] Each of these three reactions is too slow to be important for atmospheric chemistry.

Of the atmospheric species, the OH radical is probably the most reactive, and its reaction with PNA can have a profound effect on the chemistry of the stratosphere. The reaction products are not known, but several sets are thermochemically possible.

$$\mathrm{OH + HOONO_2} \rightarrow \mathrm{H_2O + O_2NO_2} \quad \text{(2a)}$$
$$\downarrow$$
$$\mathrm{O_2 + NO_2}$$
$$\rightarrow \mathrm{H_2O_2 + NO_3} \quad \text{(2b)}$$
$$\rightarrow \mathrm{HO_2 + HNO_3} \quad \text{(2c)}$$

If the reaction products are given by eq 2a, model calculations[13] show that the net result of reactions 1 and 2 is the NO_2-catalyzed disproportionation of OH and HO_2 radicals. The effect of this reaction is to reduce the calculated depletion of the stratospheric ozone column by about a factor of 2.[13] Because of the sensitivity of stratospheric chemistry calculations to the rate and products of reaction 2, we have made a great effort to obtain a reliable experimental measurement of the reaction rate constant.[14] Unfortunately, we are not yet able to identify the reaction products.

Although the primary reason for studying PNA reactions is their potential importance in the atmosphere, PNA also is an interesting chemical that is part of the fabric of HNO species. In this sense, it is a member of the homologous series of nitrogen acids (e.g., HONO, $HONO_2$, $HOONO_2$), as well as being the first member of a series of pernitrates (e.g., $HOONO_2$, CH_3OONO_2, $CH_3(CO)ONO_2$; in addition, it is a hydroperoxide (e.g., HOOH, HOOR, $HOONO_2$). All these species are important for various reasons, and data are needed on their reactions. Such data can then be used as a basis for predicting reaction rate constants for species that have not, as yet, been studied experimentally.

Experimental Section

The experiments were performed in four series, each differing from the other in various ways, mostly due to improvements in technique. Series A was performed using a flow-tube apparatus and was unsuccessful, but series B, C, and D were performed using variations on the flash-photolysis resonance-fluorescence (FPRF) technique coupled with mass spectrometric measurement of [PNA], and they were fully successful. Although the flow-tube experiments were unsuccessful, much of the apparatus is common to the other series and the flow tube itself was used as a mixing mainfold in the other series, justifying a brief description of the apparatus.

Series A: Flow-Tube Apparatus.[14] The apparatus[15] consists of two main parts, the flow system and the mass spectrometric detection system. The flow system consists of a flow tube, a gas-metering system, a mass spectrometric-sampling device, and a high-capacity pump. As shown in Figure 1, the main flow tube is a Pyrex tube, 1 m long and 2.5 cm i.d., equipped with a manifold to prepare the

(3) C. J. Howard, *J. Chem. Phys.*, 67, 5258 (1977).
(4) R. A. Graham, A. M. Winer, and J. N. Pitts, Jr., *Chem. Phys. Lett.*, 51, 215 (1977); *J. Chem. Phys.*, 68, 4505 (1978).
(5) A. C. Baldwin and D. M. Golden, *J. Phys. Chem.*, 82, 644 (1978).
(6) A. C. Baldwin, J. R. Barker, D. M. Golden, and D. G. Hendry, *J. Phys. Chem.*, 81, 2483 (1977).
(7) R. A. Graham, A. M. Winer, and J. N. Pitts, *Geophys. Res. Lett.*, 5, 909 (1978).
(8) R. A. Cox and K. Patrick, *Int. J. Chem. Kinet.*, 11, 635 (1979).
(9) L. T. Molina and M. J. Molina, 14th Informal Conference on Photochemistry, Mar 30–Apr 3, 1980, Paper C2; M. J. Molina, Report No. FAA-EE-80-07, U.S. Department of Transportation, Federal Aviation Administration, 1980.
(10) J. S. Chang, P. L. Trevor, and J. R. Barker, *Int. J. Chem. Kinet.*, 13, 1151 (1981).
(11) P. L. Trevor and J. R. Barker, *Int. J. Chem. Kinet.*, 13, 1163 (1981).
(12) P. L. Trevor and J. E. Davenport, private communication.
(13) (a) R. Cicerone and S. Walters, 14th Informal Conference on Photochemistry, Mar 30–Apr 3, 1980, Paper C6; (b) W. H. Duewer and D. J. Wuebbles, *ibid.*, Paper J6; (c) J. Steed, private communication; (d) S. C. Liu, private communication.
(14) Preliminary results for the flow-tube data were presented earlier: P. Trevor, J. S. Chang, and J. R. Barker, 14th Informal Conference on Photochemistry, Mar 30–Apr 3, 1980, Paper C3.
(15) J. S. Chang and J. R. Barker, *J. Phys. Chem.*, 83, 3059 (1979).

main flow mixture before it is introduced into the flow tube. Typically, a small amount of hydrogen mixed with helium constitutes the main flow which is then passed through a microwave discharge (2450 MHz) before being introduced into the flow tube. A Wood's horn is used to prevent light generated by the microwave discharge from entering the main flow tube. The He flow is controlled with a needle valve and is measured by a Fisher-Porter rotameter; reactant flows are measured by the pressure changes in a calibrated volume fitted with a Validyne pressure transducer (±0.1 psi).

Sampling of the reactants and the products from the flow tube to the mass spectrometer is accomplished by a Teflon cap that is located at the downstream end of the flow tube. In the center of the Teflon cap, a 0.010 in. diameter pinhole, situated close to the center of the flow tube, serves as a molecular beam source; the beam is modulated by a mechanical chopper and detected by the mass spectrometer. The pressure in the first pumping chamber after the pinhole is typically $\sim 1-3 \times 10^{-5}$ torr, while the pressure in the second chamber (containing the Finnigan quadrupole) is $\sim 10^{-6}$ torr. The same modulated molecular-beam mass spectrometer (MMBMS) has been used for detection in various other studies, such as very low-pressure pyrolysis and very low-pressure photolysis, and a description can be found elsewhere.[16]

Series B: 248-nm Flash-Photolysis Resonance-Fluorescence (FPRF). The apparatus used in experiment series B, C, and D is shown schematically in Figure 1. For this setup, the flow tube described above was coupled to a resonance-fluorescence cell as shown in the figure. The cell is not the same one used for series A and is 70 cm on the long axis to reduce scattered light from the CaF_2 windows that transmit the laser beam. The top and side windows are quartz to transmit the OH radical resonance-fluorescence light centered near 3100 Å. Light from the OH resonance lamp (2450 MHz; 9 torr He passed over H_2O) is collimated or weakly focussed with a quartz lens and directed through the side window of the cell. The flow tube is coupled to the cell directly opposite the side window. Since the long axis of the cell is oriented at ~35° from the axis of the flow tube, the light from the resonance lamp does not pass down the length of the tube but is stopped by the bend of the coupling tubulation. This arrangement acts as a crude Wood's horn to reduce scattered light from the lamp.

The photomultiplier tube (EMI Model 6255B) was wired for single photon counting and viewed the OH fluorescence through the top window of the cell. The 3100-Å interference filter was used to reduce scattered light. Output from the photomultiplier was amplified and an amplifier/discriminator was used to detect single-photon pulses. The output of the discriminator was stored in a multichannel analyzer (Nuclear Data, Model ND100) that was operated in the multichannel scaling mode, where each channel corresponds to a time increment. After several thousand laser shots, the memory contents were recorded on an $x-y$ chart recorder and were then analyzed to determine the fluorescence decay rate.

The gas flow entered the cell at the port opposite the side window and then turned 90° downward through the exit tube that is opposite the top window. About 8 cm from the optical center, the gas stream was sampled through a Teflon cap, perforated with a hole ~0.008 in. in diameter that acted as the originating orifice of the modulated molecular-beam mass spectrometer described above. The gas flow pattern in the fluorescence cell is somewhat complex (see Figure 1) but probably consists of a rapid, turbulent flow in the optical viewing region, but nearly stagnant behavior in the long side arms. The mass spectrometer sampling orifice is only about 8 cm directly downstream from the optical center and appeared to give a reliable measure of gas composition at that center, as demonstrated with test reactions. At the exit port of the cell (see Figure 1), a 10-mm glass or Teflon-bore stopcock fitted with Viton O-rings was used as throttle valve to control gas flow velocity and total pressure. From this valve, the gas flow was conducted directly to the main flow-tube pump.

Temperature control of the cell was maintained by circulating fluid from a constant-temperture bath (Neslab LT-50) through coils of tubing wrapped around the cell. A sheet of closed-cell foam insulation covered the coils and five chromel–constantan thermocouples attached at various points around the cell body showed the temperature to be constant and uniform within ±2 °C during the experiments.

In these experiments, the flow tube was used primarily as a gas-mixing manifold; linear flow velocities were usually of the order of 0.5–3 m/s, but faster velocities were used occasionally. Concentration calibrations for NO_2, H_2, and HNO_3 were performed by measuring the rate of pressure increase in calibrated volumes, as described previously.[17] Dry HNO_3 was prepared by mixing $NaNO_3$ with concentrated H_2SO_4 in an evacuated bulb. Ozone concentration calibrations were performed daily by measuring the attenuation[18] of light from a Hg 2537-Å penlight source viewed through an interference filter by a RCA 1P28 photomultiplier down the long axis of the photolysis cell.

Ozone was prepared in a separate vacuum line by an electric discharge in O_2 and was trapped and stored in a silica gel-packed trap maintained at −78 °C. The ozone concentration was controlled by sweeping it out of the trap with a stream of helium diverted from the main flow. Mass spectrometric analysis showed that H_2O vapor was released from the trap along with O_2 and O_3.

Pulses of OH radicals were generated according to the following scheme

$$O_3 + h\nu(248\ \text{nm}) \rightarrow O(^1D) + O_2 \quad (3)$$

$$O(^1D) + H_2 \rightarrow OH + H \quad (4)$$

$$O(^1D) + \text{PNA} \xrightarrow{?} OH + O_2 + NO_2 \quad (5)$$

$$H + O_3 \rightarrow OH(\text{vib}) + O_2 \quad (6)$$

The 248-nm light was generated by a Lambda-Physik excimer laser (Model EMG 101) operated with a mixture of krypton, fluorine, and helium. Output energies were measured with a Scientech calorimeter-type power meter (Model 360203) and averaged ~80 mJ/pulse, of which energy about 25% actually entered the cell after collimation. Typically, pulse repetition frequencies used were ~5–10 Hz. Since gas residence times in the cell body were $\sim^1/_2$ s, the O_3 was significantly depleted by the laser beam, but the PNA concentration showed less than ~5% depletion, demonstrating the validity of pseudo-first-order conditions. It was found by experimentation that the observed OH fluorescence decay rates were independent of O_3 pressures (at this laser pulse energy) as long as they were less than ~1 mtorr, corresponding to an initial OH

(16) J. S. Chang, J. R. Barker, J. E. Davenport, and D. M. Golden, *Chem. Phys. Lett.*, **60**, 385 (1979).

(17) R. L. Kenley, P. L. Trevor, and B. Y. Lan, *J. Am. Chem. Soc.*, **103**, 2203 (1981).

(18) M. Griggs, *J. Chem. Phys.*, **49**, 857 (1968).

concentration of $\lesssim 2 \times 10^{13}$ radicals/cm^3. Hydrogen concentrations were high enough (2×10^{15} molecules/cm^3) so that all of the O(^{1}D) reacted by reaction 4 within ~ 10 μs after the laser pulse.[19]

The troublesome possibility existed that vibrationally excited OH was present initially, and an observed spectrum showed our resonance lamp could excite OH($v = 1$), if present. Thus, the fluorescence data for times shorter than 2.5 ms after the laser pulse were ignored to allow some time for vibrational relaxation of OH(vib). Several spikes due to electronic pickup from the laser appeared on each decay curve, providing a convenient time marker for the 2.5-ms delay.

In this series of experiments, it was found that PNA decomposition on the Pyrex surface could be somewhat inhibited by application of a thin coating of halocarbon wax (the preparation and absolute concentration measurements of PNA are discussed below). This treatment permitted the incorporation of a cold trap in the PNA preparation train that helped to reduce unwanted H_2O_2. Moreover, higher total pressures were obtainable without excessive decomposition of the PNA. The primary high-pressure limitation, however, was the residual gas pressure tolerable for the mass spectrometer.

Series C: 266-nm FPRF.[20] This series of experiments was performed in a manner similar to series B, with a few differences. The light source for this series was a Quanta Ray Nd:YAG laser whose output was quadrupled in frequency to give 266-nm light (~ 20 mJ/pulse, 90% of which entered the cell). The source of OH was

$$O_3 + h\nu(266\ \text{nm}) \rightarrow O(^1D) + O_2 \qquad (3)$$

$$O(^1D) + H_2O \rightarrow 2OH \qquad (7)$$

This source of OH was "cleaner" than in series B, because the initial vibrational excitation in OH produced by reaction 7 is quite low,[21] and there is no subsequent reaction of H + O_3 to produce highly vibrationally excited radicals. Due to the absence of vibrationally excited radicals, the data analysis could be carried out for all data from $t = 0$. The initial OH concentration is estimated to be $\lesssim 2 \times 10^{13}$ radicals/cm^3 for 1 mtorr O_3.

A new quadrupole mass spectrometer (Balzers Models 311, 140) was substituted for the Finnigan instrument and a new series of relative mass spectrometer sensitivity measurements was performed.

One additional change was made in the data analysis procedure. The trigger sequence was arranged so that background fluorescence was recorded for several tenths of a millisecond before the laser was pulsed, enabling us to digitally subtract the background light intensity. After subtraction of background, the memory contents of the MCA were passed through a logarithmic amplifier prior to the x-y recorder. These steps considerably reduced the time consumed in the data analysis process.

Series D: 266-nm FPRF. This series of experiments was performed in just the same way as series C, except that the lens elements of the mass spectrometer were cleaned and the electron multiplier was rejuvenated (because of an accidental vacuum failure), necessitating a new series of relative sensitivity measurements.

PNA Preparation, Purity, and Concentration Determination. The preparation, purity, and concentration determination of PNA require a separate section because this aspect of the experiments is the single largest source of error and uncertainty.

Our experience is that PNA tends to decompose relatively rapidly (seconds) on Pyrex and metal surfaces. Halocarbon wax and Teflon tend to be more inert, but some decomposition still takes place. Due to this behavior by PNA, we did not use static mixtures of PNA in storage bulbs, but generated the PNA batchwise and mixed it with the gas stream in the flow tube. Small preparative batches of PNA are advised because, during this study (CAUTION!!) two minor explosions took place, one of which destroyed a heated glass tube, even though the partial pressure of PNA was probably less than 5 torr and the total pressure was less than 20 torr.

As described elsewhere, PNA was prepared[17] by cautiously and slowly adding 0.6 g of NO_2BF_4 (Alfa-Ventron) to 90% H_2O_2 maintained at 0 °C and rapidly stirred. This preparative solution was kept at 0 °C until the small vessel (~ 25 cm^3) was O-ring sealed to the preparative train and pumped down to the flow tube pressure. PNA was carried out of the preparative vessel by a stream of helium (diverted from the main flow) that was passed over the liquid surface. Bubbling the carrier gas through the solution did not significantly improve the PNA yield. The flow-tube PNA concentration was controlled by varying the helium flow rate and by varying the bath temperature of the PNA preparative solution up to ~ 15 °C; it was deemed too dangerous to allow the temperature to go higher.

In experimental series B, C, and D, a U-trap followed the preparation vessel, and when held at a temperature of ~ -15 °C, it seemed to reduce the relative amount of impurity H_2O_2 that was released.

Potential impurities, such as NO_2, H_2O_2, and HNO_3, were specifically sought using the mass spectrometer, and it was found that HNO_3 either was not present or its level was <5% of the PNA (see below). Hydrogen peroxide appeared as a highly variable impurity, ranging from undetectable levels ($m/e = 34$) up to concentrations several times as large as the PNA concentration. NO_2 was often present as an impurity, but its level was usually ≲10%, and never more than ~50% of the PNA concentration. As discussed later, the reaction rate of OH with NO_2 at the total pressures of He used here are slow, and thus the effect of NO_2 is small. H_2O and O_2 were also impurities, but they were not monitored.

The basic idea behind the relative mass spectral sensitivity measurements for PNA and NO_2 is that the thermal decomposition of PNA quantitatively yields NO_2

$$HOONO_2 \xrightarrow{\text{heat}} HOO + NO_2 \qquad (8)$$

$$2HO_2 \rightarrow H_2O_2 + O_2 \qquad (9)$$

$$H_2O + {}^1/_2O_2$$

The experimental procedure was as follows. For a constant flow of PNA: (1) Measure the mass spectral intensity at $m/e = 46$: I_1 (millivolts). (2) Using the flow-tube microwave discharge, add O atoms and titrate away any NO_2 impurity using the NO_2^* afterglow technique; measure the mass spectral intensity: I_2. (3) With the O atom concentration from step 2, divert the PNA flow through the heated bypass [a $^1/_4$-in. × 50 cm stainless steel (because of explosion hazard) U-tube maintained at 300 °C], and measure the mass spectral intensity: I_3. (4) Add more O atoms to titrate the NO_2 produced by the thermal decomposition of PNA, and measure the mass spectral intensity: I_4. (Titration of NO_2 by O atoms is an effective technique, because the rate constant O + NO_2 is about

(19) J. A. Davidson, H. I. Schiff, G. E. Streit, J. R. McAfee, A. L. Schmeltekopf, and C. J. Howard, *J. Chem. Phys.*, 67, 5021 (1977).

(20) Preliminary results obtained in experiment Series C were reported earlier: J. R. Barker, G. Black, and P. L. Trevor, 1980 American Geophysical Union Fall Meeting, San Francisco, CA, 8-12 December 1980.

(21) K. H. Gericke and F. J. Comes, *Chem. Phys. Lett.*, 74, 63 (1980).

TABLE I: Relative Mass Spectrometer Sensitivities for PNA and NO_2

exptl series	$S \pm 1\sigma$	data points	mass spectrometer
B	7.48 ± 1.05	21	Finnigan
C	4.44 ± 0.74	9	Balzers
D	5.07 ± 0.34	14	Balzers

three orders of magnitude faster than that of the reaction O + PNA. As long as a modicum of care is taken, PNA is not depleted by reaction with O atoms under these conditions).

The difference $(I_3 - I_4)$ is proportional to the amount of NO_2 produced by the thermal decomposition of PNA. The difference $(I_2 - I_4)$ is proportional to the amount of PNA decomposed. The ratio of these quantities is the ratio of the mass spectrometer sensitivities for the two compounds

$$(I_3 - I_4)/(I_2 - I_4) = S^{-1} \tag{10}$$

and $[PNA] = S^{-1}\alpha_{NO_2}I_2$, where α_{NO_2} is the calibrated NO_2 sensitivity (molecules cm^{-3} mV^{-1}). Since a small fraction of the PNA can survive the heated tube, I_4 is usually not identically zero; the portion of PNA that survived depended upon flow conditions and ranged from nearly zero up to ~20%.

To determine whether HNO_3 is an impurity originally present in the PNA or is produced in its thermal decomposition and contributes to the observed mass spectral intensity of $m/e = 46$, the PNA is diverted through the heated bypass *and* a great excess of O atoms (i.e., $>10^{14}$ atom/cm^3) is added to remove the NO_2 and the PNA that survived the heated tube. Under these conditions (reaction time ~1 s), it is observed that virtually all of the intensity at $m/e = 46$ disappears, indicating the absence of HNO_3 since HNO_3 does not thermally decompose under these conditions, and it reacts only very slowly with O atoms. On the other hand, PNA both thermally decomposes and reacts with O atoms at a moderate rate ($k \sim 10^{-15}$ cm^3 s^{-1} at 300 K).[10] All experiments of this type that were performed showed negligible amounts of HNO_3.

It was concluded that the thermal decomposition of PNA under our conditions quantitatively gives NO_2 for the following reasons. (1) HNO_3 was shown not to be a significant product. (2) The ratio of intensities at $m/e = 46$ and at $m/e = 30$ were consistent with product NO_2, although the experimental scatter was large due to PNA interference and due to taking the differences of relatively noisy values. (3) Experiments in which mixtures of NO_2 and H_2O_2 were passed through the heated bypass showed that the NO_2 was unaffected by the treatment. (4) In the highly oxidizing environment containing $HOONO_2$ and H_2O_2, it seems unlikely that the PNA decomposition product would be HONO or other reduced forms of nitrogen.

The results obtained for the relative sensitivities of NO_2 and PNA in experiment series B, C, and D, are presented in Table I. The uncertainties quoted include effects from all sources.

Results and Discussion

The conventional flow-tube resonance fluorescence experiments (series A) were performed under conditions where pseudo-first-order conditions obtain. In the course of the experiments, it was found that an inordinate amount of time was necessary for the signal to stabilize after moving the probe position. Moreover, there was a large amount of scatter in the data, perhaps symptomatic of wall reactions involving OH, PNA, or both species.

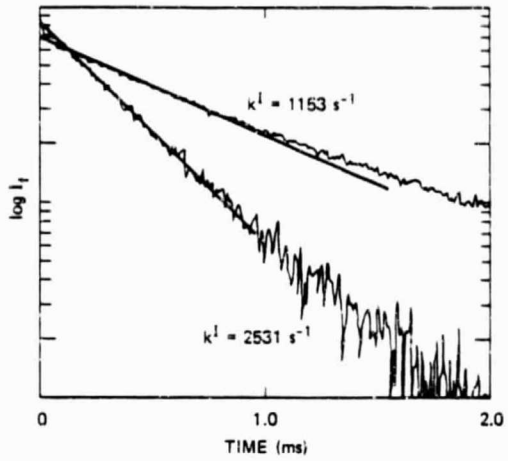

Figure 2. First-order plot of log I_f vs. time. Rate data giving $k' = 1155$ s^{-1} are for $[PNA] = 1.06 \times 10^{14}$ molecules/cm^3 and $[H_2O_2] = 1.05$ millivolts. Data giving $k' = 2531$ s^{-1} are for $[PNA] = 1.51 \times 10^{14}$ molecules/cm^3 and $[H_2O_2] = 21.9$ millivolts (too high for use in second-order analysis). Both sets of data are from experiment series C, $T = 324$ K.

After many efforts to eliminate the anomalous scatter in the data, we have concluded that this behavior may be due to a wall reaction of OH and PNA that is dependent on the PNA concentration and/or H_2O_2 concentration and the history of the flow tube. Halocarbon wax is among the least likely substances to cause adsorption of PNA and thus is one of the best for inhibiting wall reactions. Since it has turned out that this coating is not effective, we concluded that further experiments using the flow-tube technique on this reaction would not be fruitful, and we turned to the FPRF approach.

For the FPRF technique, the OH concentration change with time is conventionally written[22]

$$d[OH]/dt = -(k_2[PNA] + k_p)[OH] \tag{11}$$

and the inverse decay lifetime of the fluorescence intensity I_f is

$$\tau^{-1} = k_2[PNA] + k_p \tag{12}$$

where k_2 is the bimolecular reaction rate constant and k_p is a parameter that describes the effective "rate constant" for loss of OH due to physical processes. At high pressures, k_p may be identified with the first-order diffusion process alone. For the particular conditions in the present experiments, the physical processes include the translational motion of gas parcels as they pass into and out of the intersection of the detector field of view and the region illuminated by the resonance lamp. Such motions are due to the gas-stream velocity as it is pumped through the cell and to mass diffusion of [OH]. Neither of these processes is exactly represented by the first-order "rate constant" k_p since the pumping velocity is clearly independent of the OH concentration, and spherical diffusion subsequent to excitation in a cylindrical profile coupled with crossed-optical-beam detection is not expected to be so simple. These effects are exhibited in that k_p appeared to be time dependent, resulting in OH fluorescence decay plots that deviate slightly from exponential decay (Figure 2). Nevertheless, eq 12 is a good, pragmatic representation as long as the expression is employed for the local slope at the same *average* elapsed time followed the laser pulse and the time dependence of k_p is not too pronounced.

(22) For example, see ref 24b.

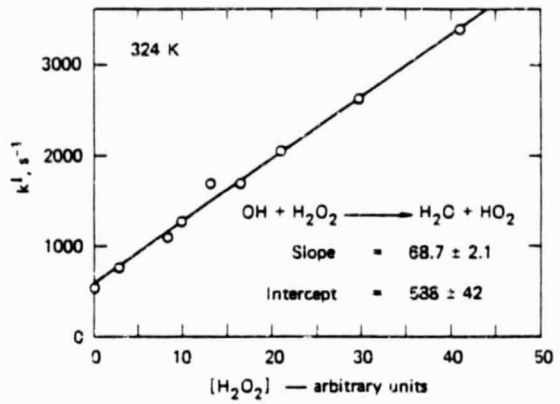

Figure 3. Second-order plot of k^I vs. $[H_2O_2]$ from experiment series C, 324 K (uncertainties shown are 1σ).

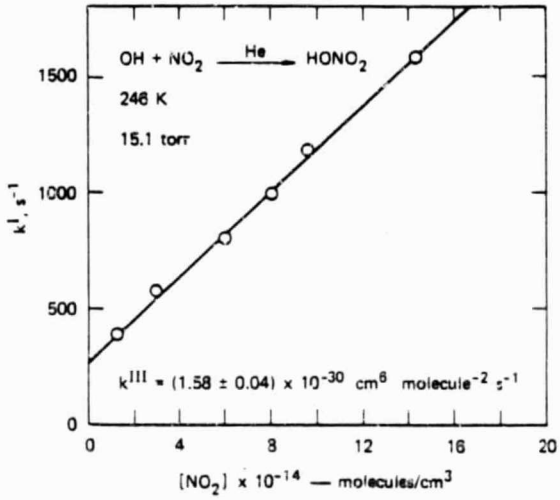

Figure 4. Second-order plot of k^I vs. $[NO_2]$. The effective bimolecular rate constant is $k^{II} = (9.23 \pm 0.22) \times 10^{-13}$ cm^3 s^{-1} (uncertainties shown are 1σ).

Under pseudo-first-order conditions, a plot of log I_f vs. time will give a nearly straight line, if k_p is only slightly dependent on time. Two such plots are shown in Figure 2 for experiment series C. For series C and D, the protocol was established that the initial slopes on first-order plots be taken; this protocol is supported because second-order plots of τ^{-1} vs. reactant concentrations give good straight lines. Two such examples are presented in Figures 3 and 4 for the reaction

$$OH + H_2O_2 \rightarrow H_2O + HO_2 \qquad (13)$$

and for

$$OH + NO_2 + He \rightarrow HONO_2 + He \qquad (14)$$

Both second-order plots show very good straight-line behavior. The absolute rate constant for reaction 13 was not determined because the mass spectrometer could not easily be calibrated for sensitivity to H_2O_2. (This is due to the unknown extent of H_2O_2 decomposition in the inlet lines. In subsequent analysis, we have assumed that the mass spectrometer signal at $m/e = 34$ is linearly proportional to the unknown H_2O_2 concentration. This assumption is consistent with our experience using mass spectrometers for detection.) The absolute rate constant for reaction 14, determined from the data in Figure 5, is 1.6×10^{-30} cm^6 molecule^{-2} s^{-1}, in excellent agreement with literature data.[23]

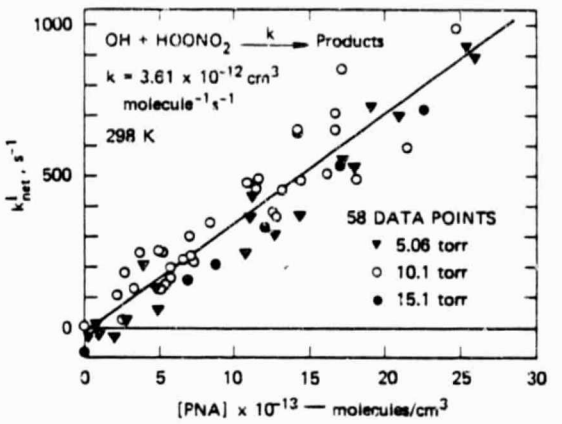

Figure 5. Second-order plot of k^I_{net} vs. [PNA] for experiment series C, $T = 298$ K.

TABLE II: Test Reactions and Results of Present Study

reaction	T, K	P, torr	k^{II}_{obsd}, cm^3 s^{-1}
$OH + iC_4H_{10}$	298	9.2	3.6×10^{-12}
	324	10.1	$(3.62 \pm 0.40) \times 10^{-12}$
	267	10.1	$(2.70 \pm 0.20) \times 10^{-12}$
$OH + NO_2 + He$	246	15.1	$(9.23 \pm 0.22) \times 10^{-13}$

Similar tests were performed using isobutane as reactant, also leading to rate constants in excellent agreement with literature values.[24] The test reaction rates determined are summarized in Table II. These results show that concentrations monitored 8 cm downstream from the optical center are accurate.

For experiment series B, the protocol for data treatment was somewhat different for two reasons. First, because it was felt that OH(vib) could cause problems, the first 2.5 ms of data from each run were ignored, and the first-order plots were constructed from data beginning at 2.5 ms after the laser pulse. The second reason for this procedure was that two or three "spikes" due to electronic pickup from the excimer laser appeared in each run, causing some interference. The last spike occurred at 2.5 ms after the laser pulse, providing a convenient time marker.

Because the data for series B correspond to lower OH concentrations (due to decay after the pulse), the fluorescence data were significantly noisier than those of series C and D, but they, again, gave good straight second-order plots and absolute rate constants in good agreement with the literature. The excellent linearity exhibited in Figures 3 and 4 and the excellent results presented in Table II support the use of the approximately accurate eq 12 for the second-order plots.

In all these series—B, C, D— the intercept of the second-order plots can be identified with k_p. It was observed that k_p is larger at lower pressures, as expected for diffusive loss, and it seemed to depend upon day-to-day variation in optical alignment and linear flow velocity through the optical intersection region, as expected. Quantitative estimates of linear flow velocity through the ~1 cm optical center are difficult due to the geometry of the cell, but they are probably about the same as in the flow tube (50–300 cm/s). At the low pressures of the present experiments, OH diffusive loss rates are probably of the order of 50–300

(23) (a) For a summary, see R. F. Hampson, Jr., and D. Garvin, *NBS Spec. Publ. (U.S.)*, No. 513 (1977); (b) P. H. Wine, N. M. Kreutter, and A. R. Ravishankara, *J. Phys. Chem.*, **83**, 3191 (1979).

(24) (a) N. R. Greiner, *J. Chem. Phys.*, **53**, 1070 (1970); (b) K. R. Darnall, R. Atkinson, and J. N. Pitts, Jr., *J. Phys. Chem.*, **82**, 1581 (1978), and references cited therein.

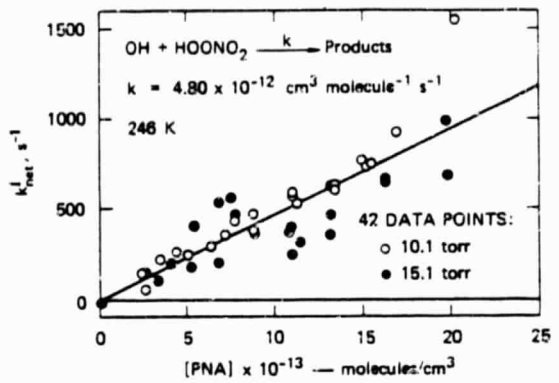

Figure 6. Second-order plot of k^I_{net} vs. [PNA] for experiment series C, T = 246 K.

s^{-1}. These values are consistent with the observed values for k_p.

When H_2O_2 and NO_2 are present as impurities, eq 12 must be generalized to

$$\tau^{-1} = k_2[PNA] + k_{14}[He][NO_2] + k_{13}[H_2O_2] + k_p \quad (15)$$

As mentioned earlier, the NO_2 impurity is relatively small, and at the pressures and temperatures of the present study, its effect on the observed τ is also small and can be neglected (see below). Since k_p varies on a day-to-day basis, the best way of combining all of the data for a given temperature and pressure is to consider only the net first-order rate constant resulting from the following expression

$$k^I_{net} = k_2[PNA] = \tau^{-1} - k_{13}[H_2O_2] - k_p \quad (16)$$

For experimental runs performed using just H_2O_2, we have

$$k^I_{H_2O_2} = k_{13}[H_2O_2] + k_p \quad (17)$$

For each set of conditions runs were carried out using only H_2O_2 as reactant, and a linear least-squares analysis gave values for k_{13} and k_p. Since H_2O_2 concentration was measured by the MMBMS as peak height (millivolts) at m/e = 34, k_{13} has units of $(mV)^{-1}\ s^{-1}$; k_p is obtained in units of s^{-1}. Once k_p and k_{13} are known, H_2O_2 and PNA concentrations are monitored mass spectrometrically and recorded along with τ^{-1}. From these quantities, k^I_{net} is determined, and second-order plots of k^I_{net} vs. [PNA] can be constructed as shown in Figure 5.

The data for 298 K presented in Figure 5 were obtained on several different days for three different total pressures and several different linear flow velocities. Clearly, the data are quite consistent with one another, showing no significant dependence on total pressure. For the purpose of illustration, the data for 246 K are presented in Figure 6, and again, there is no significant dependence on total pressure.

From the O_3 concentration, laser energy, and ozone absorption coefficient,[18] we can estimate that the initial OH concentration does not exceed $\sim 2 \times 10^{13}$ radicals/cm^3. Several tests were performed to determine whether the observed fluorescence decay rates depended upon either the source of OH radicals or on their initial concentration. In experiment series B, the O_3 partial pressure was varied from 0.23 to 0.8 mtorr with no perceptable variation in either decay rate or in the shape of the fluorescence decay curve, although the absolute fluorescence intensity varied. When the O_3 partial pressure was raised to 3 mtorr, a faster decay rate occurred at early times, but by the 2.5 ms time marker, there was little effect.

TABLE III: Rate Constants for OH + PNA → Products

T, K	data points[a]	$10^{12}k$, cm^3/s	$10^{12}\cdot\sigma_{FPRF}$	$10^{12}\cdot\sigma_{NO_2/PNA}$	$10^{12}\cdot\sigma_{net}$
		Series B: 248-nm FPRF			
251	11	3.84	0.28	0.54	0.61
273	17	4.60	0.41	0.65	0.77
298	23	6.05	0.52	0.84	0.99
316	12	4.95	0.31	0.69	0.76
		Series C: 266-nm FPRF			
246	42	4.80	0.46	0.80	0.92
267	22	4.83	0.21	0.81	0.84
298	58	3.61	0.16	0.60	0.62
324	20	3.79	0.21	0.63	0.66
		Series D: 266-nm FPRF			
254	21	3.24	0.30	0.22	0.37

[a] Total = 226 data points.

In experiments series C, more extensive tests were performed. With 30 mtorr H_2O, the O_3 partial pressure was varied from 0.4 to 4.0 mtorr, resulting in a variation of ~10% in the OH + H_2O_2 bimolecular rate constant. The 4 mtorr O_3 data for OH + PNA may have been ~15% lower than the usual, but this variation is not significant and the data were included in the overall data set.

In another series of test runs in series C, H_2 was substituted for H_2O, to reproduce the conditions of experiment series B. Subsitution of 85 mtorr H_2 for the usual H_2O gave no significant difference in observed rate constant. Indeed, runs with *no* H_2 or H_2O added to the gas stream also agreed with the rest of the data. This result can be understood, since reaction of $O(^1D)$ with PNA may give OH and since H_2O was observed evolving both from the PNA preparation train and from the O_3 trap. Thus, it appears that H_2O was always present in significant quantities. Since $H_2O + O(^1D)$ gives relatively "cool" OH, and because H_2O is an efficient quencher for vibrationally excited OH, it appears that if any residual vibrational excitation remained, it played no significant role in the observed rate constants.

In addition to varying the O_3, H_2O, and H_2 partial pressures, the laser power was also varied in experiment series C. When the laser pulse energy was reduced by about a factor of 10 from the usual 20 mJ/pulse, there was a reduction in fluorescence intensity, but no significant variation in observed rate constant. Thus, we may conclude that (1) secondary reactions of OH and reaction products are not significant, (2) depletion of PNA concentration is not significant, and (3) OH disproportionation is not significant. Thus, the system appears to be kinetically well behaved.

The measured bimolecular rate constants for each temperature are summarized in Table III and Figure 7, along with least-squares and propagation of errors estimates of the associated experimental uncertainties. The first uncertainty σ_{FPRF} listed for each rate constant is just the statistical uncertainty associated with the second-order plot of k^I_{net} vs. [PNA]. The second uncertainty listed is that associated with the PNA/NO_2 relative mass spectrometric sensitivity. The third uncertainty listed is the propagation of errors combination of these two sources of error.

A major contributor to σ_{FPRF} is the uncertainty associated with the quantity $(k_{13}[H_2O_2] + k_p)$ in eq 16. For small values of $[H_2O_2]$, this uncertainty is quite small, but for a few runs, $k_{13}[H_2O_2]$ was very large, possibly resulting in large uncertainties in k^I_{net}. To avoid this problem, the few runs giving $k^I_{net} < 0.5k_{13}[H_2O_2]$ were neglected, although they would not have affected the final bimolecular rate constant. It should be pointed out that pseudo-first-order

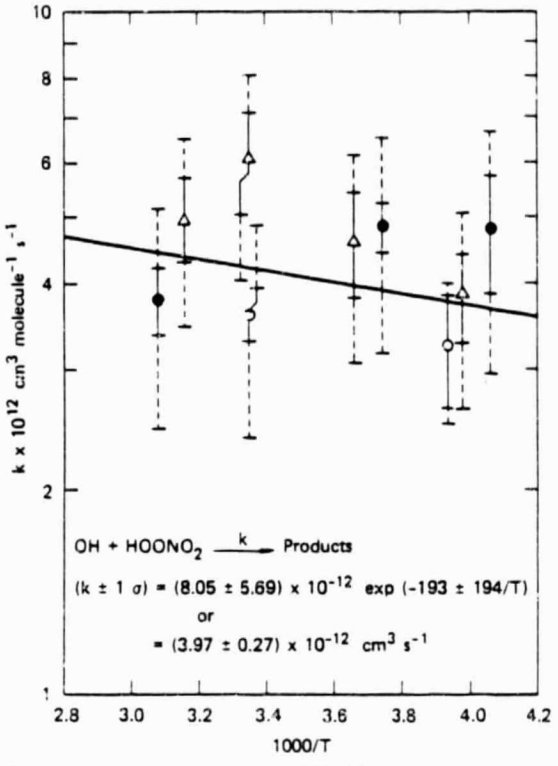

Figure 7. Arrhenius plot of log k vs. $1000/T$: (△) experiment series B; (●) experiment series C; (○) experiment series D. The solid error bars are the 2σ statistical uncertainties not including calibration errors; the dashed error bars are the total 2σ statistical uncertainties from all sources.

conditions were assumed in the analysis, but some runs may have had a [PNA]/[OH] ratio of less than 5, introducing some error into the analysis. Because the determination of k_{13} and k_9 introduce correlation into the runs performed on a given day, it is possible that slight errors are introduced into the rate constants derived from the least-squares analysis. We feel that these errors must be very small, however, since rate constants derived from experiments performed on different days usually show good consistency. A potential source of systematic error in the derived rate constants is the behavior of the "static" gas in the long side arms of the cell. The magnitude of error from this source is not known, but we feel it to be small, since variation of linear flow velocity and pressure did not significantly affect the derived bimolecular rate constants.

The effect of any NO_2 impurity can be shown to be small. In the *worst case*, for our lowest temperature (246 K) and highest pressure (15.1 torr), the effective bimolecular rate constant for reaction of NO_2 with OH is $k_{14}[He] = (9.23 \pm 0.22) \times 10^{-13}$ cm^3 s^{-1} (Figure 3). If, for our *worst case* estimate, the NO_2 impurity is 50% of the PNA concentration, the relative contribution of NO_2 to the observed rate constant is less than 10%. Since this *worst case* scenario is intended to be pessimistic and the effect is smaller than the other sources of error, effects due to the small NO_2 impurity have been neglected.

The data from Table III show very little variation with temperature, but a weighted least-squares calculation[25] of the Arrhenius parameters was performed, giving $(k \pm 1\sigma) = (8.05 \pm 5.69) \times 10^{-12} \exp(-193 \pm 194/T)$ cm^3 s^{-1}, covariance $= 1.098 \times 10^{-9}$; at the center of our temperature range, these parameters give a one standard deviation uncertainty of about 8%.

Because the temperature dependence of the rate constant is so small, a simple weighted average of the nine rate constants in Table III is of equal usefulness. Such an average gives $(k \pm 1\sigma) = (3.97 \pm 0.27) \times 10^{-12}$ cm^3 s^{-1}. Since the uncertainties quoted refer only to statistical fluctuation and do not include systematic errors, our *recommended* rate constant and 95% limit uncertainty is $(k \pm 2\sigma) = (4.0 \pm 1.6) \times 10^{-12}$ cm^3 s^{-1}, where the uncertainty is assigned by a subjective estimate of systematic error.

Our recommended value of $(4.0 \pm 1.6) \times 10^{-12}$ can be compared to the "upper limit" rate constant of $\sim 3 \times 10^{-12}$ estimated by Graham, Winer, and Pitts[4] on the basis of a competitive rate measurement in a smog chamber. More recently, an excellent molecular-modulation spectroscopy study was reported by Littlejohn and Johnston[26] that gave a rate constant $k_2 = (2^{+2}_{-1}) \times 10^{-12}$. This last result is noteworthy since it depends upon the accuracy and completeness of a reaction mechanism consisting of more than a dozen reactions, and yet the result is in good agreement with the present study. Moreover, the PNA in that study was prepared by an entirely different technique and the reaction mixture was analyzed spectroscopically, rather than by mass spectrometry. Thus, the agreement of these two very different studies is quite satisfactory. Further experiments using the molecular modulation technique may give information on the reaction products as well.

In Table IV the present results are compared to rate constants measured for H_2O_2, HONO, and $HONO_2$. The most perplexing of these rate constants is the recent result[27] for OH + HNO_3, since it exhibits a "negative activation energy." (The Arrhenius form of data expression is probably not appropriate for such reaction rate constants, but it is convenient in the present context.) Although the reaction products are not beyond question, indications are that it is a simple abstraction reaction[28] making interpretation of the reaction dynamics even more obscure (a displacement reaction could be explained on the basis of long-range chemical attraction). The OH +

TABLE IV: Rate Constant Comparisons

reaction	rate constant, cm^3 s^{-1}	ref
OH + H_2O_2	$(2.51 \pm 0.6) \times 10^{-12} \cdot \exp(-126 \pm 76/T)$	29
	$(2.96 \pm 0.50) \times 10^{-12} \cdot \exp(-164 \pm 52/T)$	30
OH + $HOONO_2$	$\lesssim 3 \times 10^{-13}$	4
	$(4.0 \pm 1.6) \times 10^{-12}$, independent of T	present work
	$(2^{+2}_{-1}) \times 10^{-12}$	26
	4×10^{-13}	31
OH + $HONO_2$	$(1.52 \pm 0.38) \times 10^{-14} \cdot \exp(649 \pm 69/T)$	27
OH + HONO	7×10^{-12}	32

In Table IV the present results are compared to rate constants measured for H_2O_2, HONO, and $HONO_2$. The most perplexing of these rate constants is the recent result[27] for OH + HNO_3, since it exhibits a "negative activation energy." (The Arrhenius form of data expression is probably not appropriate for such reaction rate constants, but it is convenient in the present context.) Although the reaction products are not beyond question, indications are that it is a simple abstraction reaction[28] making interpretation of the reaction dynamics even more obscure (a displacement reaction could be explained on the basis of long-range chemical attraction). The OH +

(25) R. J. Cvetanovic, R. P. Overend, and G. Parasakevopoulous, *Int. J. Chem. Kinet.* 1, 249 (1975); R. J. Cvetanovic, D. L. Singleton, and G. Parasakevopoulos, *J. Phys. Chem.*, 83, 50 (1979).

(26) D. Littlejohn and H. S. Johnston, 1980 American Geophysical Union Fall Meeting, San Francisco, CA, Dec 8–12, 1980.

(27) P. H. Wine, A. R. Ravishankara, N. M. Kreutter, R. C. Shah, J. M. Nicovich, R. L. Thompson, and D. J. Wuebbles, *J. Geophys. Res.*, in press.

(28) W. J. Marinelli, H. H. Nelson, and H. S. Johnston, 1980 American Geophysical Union Fall Meeting, San Francisco, CA, Dec 8–12, 1980.

(29) L. F. Keyser, *J. Phys. Chem.*, 84, 1659 (1980).

(30) U. C. Sridharan, B. Reisnann, and F. Kaufman, *J. Chem. Phys.*, 73, 1286 (1980).

(31) F. Zabel, private communication, 1981.

(32) R. A. Cox, R. G. Derwent, and P. M. Holt, *J. Chem. Soc., Faraday Trans. 1*, 72, 2031 (1976).

PNA reaction rate constant seems to be unexceptional in this group, since no clear trends are apparent. The A factor is appropriate either for abstraction or for displacement or complex formation. Further work should be done on this series of reactions to elucidate the dynamical pathways involved.

Acknowledgment. We gratefully acknowledge conversations with our colleagues here at SRI. We are also appreciative of the loan of photon-counting equipment from PAR Corporation. The Nd:YAG laser was rented from the San Francisco Laser Center,[33] and this work was funded primarily by the Federal Aviation Administration/Department of Transportation under Contract DOT-FA78WA-4228. Supplemental funding was provided by the National Aeronautics and Space Administration under Contract 954815/NAS7-100.

(33) This material is based upon work supported by the National Science Foundation under Grant No. CHE79-16250 awarded to the University of California at Berkeley in collaboration with Stanford University. Any opinions, finding, and conclusions or recommendations expressed in this publication are those of the author(s) and do not necessarily reflect the views of the National Science Foundation, University of California at Berkeley, or Stanford University.

Chapter VII

VERY LOW-PRESSURE PHOTOLYSIS OF tert-BUTYL NITRITE AT 248 nm

Paula L. Trevor and David M. Golden

(Short Communication: J. Photochem., 1983, 23, 277-281)

Journal of Photochemistry, 23 (1983) 277 - 281

Short Communication

Very low pressure photolysis of *tert*-butyl nitrite at 248 nm

PAULA L. TREVOR† and DAVID M. GOLDEN

Department of Chemical Kinetics, SRI International, Menlo Park, CA 94025 (U.S.A.)

(Received June 22, 1983)

Low pressure photolysis of *tert*-butyl nitrite at 248 nm with an excimer laser includes secondary photolysis of products under conditions where these same products do not photolyze. The addition of HI to the photolyzing mixture suppresses secondary product formation.

1. Introduction

An experimental apparatus designed to investigate photolysis pathways has been built in our laboratory. A schematic diagram is shown in Fig. 1. The very low pressure photolysis (VLPΦ) technique [1] employed allows gas molecules to flow through a Knudsen cell at low pressures (10^{15} cm^{-3} or less) where the average residence time is controlled by the rate of escape through an aperture [2]. The modulated molecular beam mass spectrometer analyzes the composition of the effluent gas; the Knudsen cell (or reactor) is fitted with high quality Suprasil windows to permit laser irradiation of the sample gas. The high sensitivity of the machine (*e.g.* the detection limit at unit mass resolution is about 5×10^{10} cm^{-3}) enables good product detection. A Lambda Physics excimer laser was used to study the photolysis of *tert*-butyl nitrite at 248 nm where the photon energy is about 120 mJ pulse^{-1}.

2. Results and discussion

tert-butyl nitrite (TBN) was chosen as a trial molecule to test the system because of its large cross section [3] at 248 nm and the relative stability of its photolysis products:

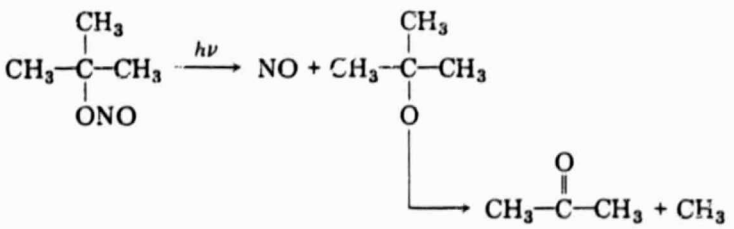

† Present address: Bell Laboratories, Murray Hill, NJ 07974, U.S.A.

0047-2670/83/$3.00

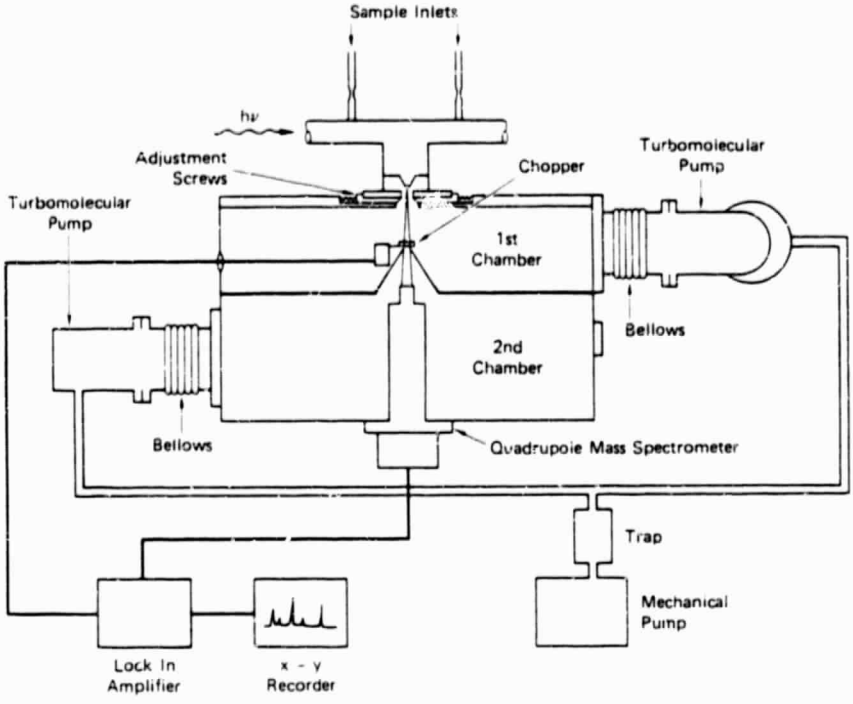

Fig. 1. Schematic diagram of VLPΦ apparatus.

The cell that was used has been characterized and described in the literature [1]. Prior to use, it was thoroughly cleaned and coated with Teflon (DuPont PTFE 852-200) according to specifications. The TBN (ICN Chemicals) was introduced into the cell at a concentration of about 2×10^{13} cm^{-3} with an average residence time of 0.75 s. The sample was irradiated at 248 nm (120 mJ $pulse^{-1}$; 50 pulses s^{-1}). A mass spectrum was recorded before and during photolysis; an example is given in Fig. 2. Care was taken to avoid hitting any surfaces other than the windows with the laser beam and to perform a blank photolysis run on the empty cell each day. TBN did not have a parent peak (m/e = 103), so the cracking peak at m/e = 88 served to monitor the concentration of unreacted TBN. Because an integrated mass spectrum was recorded, the 50 pulse s^{-1} laser repetition frequency was used to maintain a steady state concentration of photolysis products in the cell. Our experimentally measured absorption cross section for TBN compared favorably with the literature value [3] under these conditions. Mass balances were performed, and in the absence of any gas other than TBN the acetone yield (m/e = 58) was 60% - 80% of the photodissociated TBN. Unfortunately, the mass spectrometer was equally sensitive to m/e = 30 from the NO parent and the TBN cracking peak; thus no product information was ascertained at this mass.

A product peak at m/e = 28 appeared, and if it was interpreted as CO formation its yield was 10% - 20% of the dissociated TBN. Some peak inten-

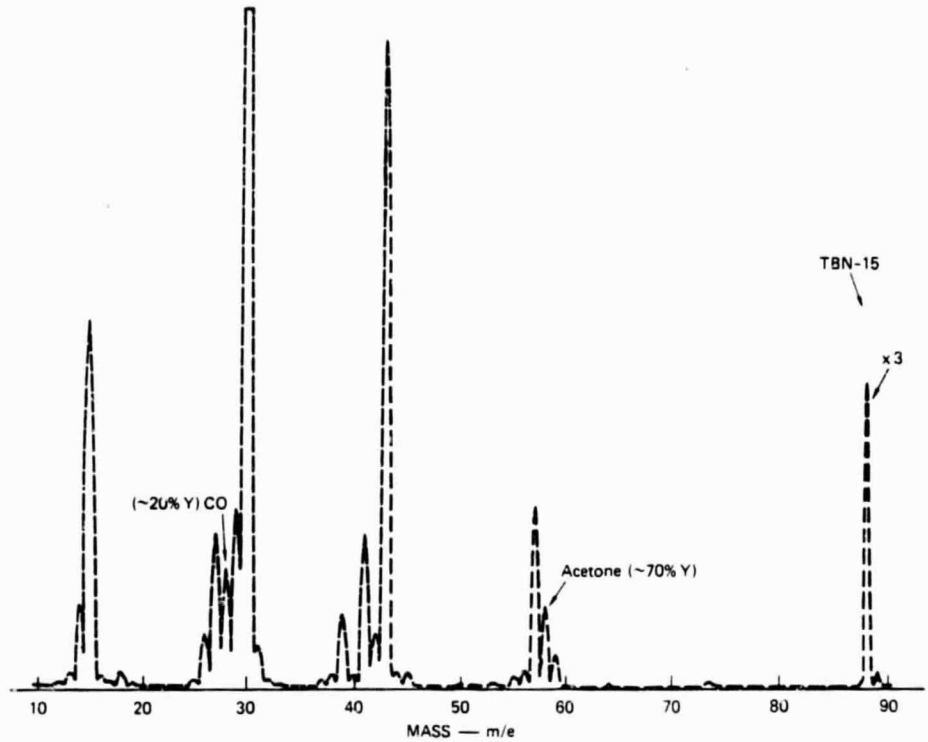

Fig. 2. Mass spectrum of TBN: ——, unphotolyzed TBN; — — —, TBN undergoing photolysis.

sity at $m/e = 15$ was assigned to CH_3 although no CH_4 ($m/e = 16$) was observed. At higher concentrations of TBN (10^{14} cm^{-3} or more) the percentage photodissociated TBN decreased as a result of recombination competing with acetone formation from the *tert*-butoxy radical [4]. Also, *tert*-butanol ($m/e = 58$) was formed as a product (about 10% yield) at the higher TBN pressures which was consistent with secondary reactions becoming important relative to acetone formation and/or secondary photolysis. However, the acetone yield was not improved over that from the lower pressure runs and no CH_4 was measured.

In order to quantify the production of CH_3, HI was added to the cell in varying amounts and the concentration of CH_4 was monitored. Several effects occurred during the photolysis of TBN in the presence of HI (2×10^{14} - 2×10^{15} cm^{-3}): (1) the acetone yield increased to about 100%, within experimental error, although the amount of photodissociated TBN did not change; (2) the peak at $m/e = 28$ (CO) was no longer observed as a product; (3) the CH_4 yield varied between 50% and 100%, giving about 100% yield only at high concentrations of HI (10^{15} cm^{-3} or more). Many runs were performed to verify the reproducibility of these observations. Lower concentrations of HI that should have been more than adequate to trap CH_3 [5] resulted in neither CH_4 production nor increased acetone yield. Only at those

concentrations where gas–gas collisions became equal to or greater than gas–wall collisions were the above effects important. This suggested that perhaps the HI was acting primarily as a quencher rather than as a titrant. Under our conditions, the *tert*-butoxy radical could have an excess energy of as much as 60 kcal mol^{-1} which may have been sufficient to access the first excited electronic state of the radical. Two different experiments were performed, one in which O_2 was substituted for HI and the other in which CH_4 was used instead of HI; in both cases the acetone yield resembled that of the pure TBN experiments although the m/e = 28 (CO) production was not significant. These data may indicate that an excited electronic state is not involved as the addition of relatively efficient electronic quenchers such as O_2 and CH_4 should have increased the acetone yield. Perhaps HI is a much more efficient quencher.

To check for complications from absorption of products by the Teflon-coated surface (which could have been reduced by monolayers of HI), the Teflon was completely removed and the photolysis of TBN was repeated in the Pyrex cell. The acetone yield still remained at about 70%. Although this test did not absolutely rule out product loss on the walls, it is rather unlikely to have been a significant process and remain unchanged by the absence of the Teflon surface.

Reaction of the methyl radical with the excited *tert*-butoxy radical seemed inconsistent with the facts that no CH_4 was observed except with HI addition and that several lower TBN pressure runs (about 10^{12} cm^{-3}) did not increase the acetone yield. Secondary photolysis could certainly have been a complicating process in this study, given that the m/e = 28 peak, if interpreted as CO, nearly compensated for the incomplete acetone yield and that this peak disappeared when the acetone yield increased to about 100% with HI present. Several runs were made in which acetone was introduced into the Teflon-coated cell (about 10^{13} cm^{-3}) and was photolyzed under the same conditions as TBN; there were no changes in the mass spectra nor was there any apparent dissociation (m/e = 58). The laser repetition frequency was reduced to 10 Hz and the TBN spectra were again recorded. Clearly a single-shot experiment with real-time product analysis would have been the ideal test for secondary photolysis, but the above experiment permitted the same steady state product analysis with a reduced photon flux in the same experimental configuration. The negative results do not rule out the importance of secondary photolysis since several laser shots may have been adequate to produce our observations. It does seem unusual that HI addition [6] should have reduced this process, especially in view of the many wall collisions that occurred in the pure TBN experiments. However, the conclusion that secondary photolysis took place is consistent with much of the experimental data.

This work was supported in part by the National Aeronautics and Space Administration under Contract NAS-7-100/JPL-954815.

1 M. J. Rossi, J. R. Barker and D. M. Golden, *J. Chem. Phys.*, *9* (1979) 3722.
2 D. M. Golden, G. N. Spokes and S. W. Benson, *Angew. Chem., Int. Edn. Engl.*, *12* (1973) 534.
3 J. G. Calvert and J. N. Pitts, *Photochemistry*, Wiley, New York, 1966, p. 455.
4 K. Y. Choo and S. W. Benson, *Int. J. Chem. Kinet.*, *13* (1981) 833.
5 M. C. Flowers and S. W. Benson, *J. Chem. Phys.*, *38* (1963) 882.
6 C. W. Larson and H. E. O'Neal, *J. Phys. Chem.*, *70* (1966) 2475.

Chapter VIII

SUMMARY OF PRELIMINARY DATA FOR THE PHOTOLYSIS OF $ClONO_2$ AND N_2O_5 AT 285 nm

P. L. Trevor, M. J. Rossi, and D. M. Golden

SUMMARY OF PRELIMINARY DATA FOR THE PHOTOLYSIS OF $ClONO_2$ AND N_2O_5 AT 285 nm

P. L. Trevor, M. J. Rossi, and D. M. Golden, Department of Chemical Kinetics, SRI International, Menlo Park, CA 94025

A series of preliminary experiments were conducted to determine the primary photolysis pathways of N_2O_5 and $ClONO_2$ at 285 nm. The study was performed under low-pressure conditions, using the SRI Quantel laser system and an apparatus (see Figure 1) specifically built for such studies.

The low-pressure photolysis (VLPΦ) technique[1] has been described previously. Basically, the sample gas flowed through the Knudsen cell (equipped with white cell optics ~ 50 passes) at low pressures ($\leq 10^{14}$ cm^{-3}) where the average residence time was controlled by the rate of escape out of an aperture.[2] The composition of the effluent gas was analyzed by the modulated molecular beam mass spectrometer. The high sensitivity of the machine (e.g., detection limit at unit mass resolution: 5×10^9 cm^{-3} for $ClONO_2$ at m/e = 46) enabled good product detection.

The Knudsen cell, as shown in Figure 2, can be characterized by the following: $k_{e\ small\ aperture} = 8.83 \times 10^{-2}\ (T/M)^{1/2}$, vol = 800 cm^3, $length_{mirror-mirror}$ = 29 cm. The stopcock attached directly to the cell metered in varying concentrations of $O(^3P)$ from a steady-state microwave source (2450 MHz). The cell was also appropriately equipped for resonance fluorescence detection[3] of both $O(^3P)$ and $Cl(^2P_{3/2})$ on a real-time, single-laser-shot basis. The CaF_2 windows in front of the resonance lamp and photomultiplier tube (EMR 542G-08-18) conveniently discriminated against Lyman-α

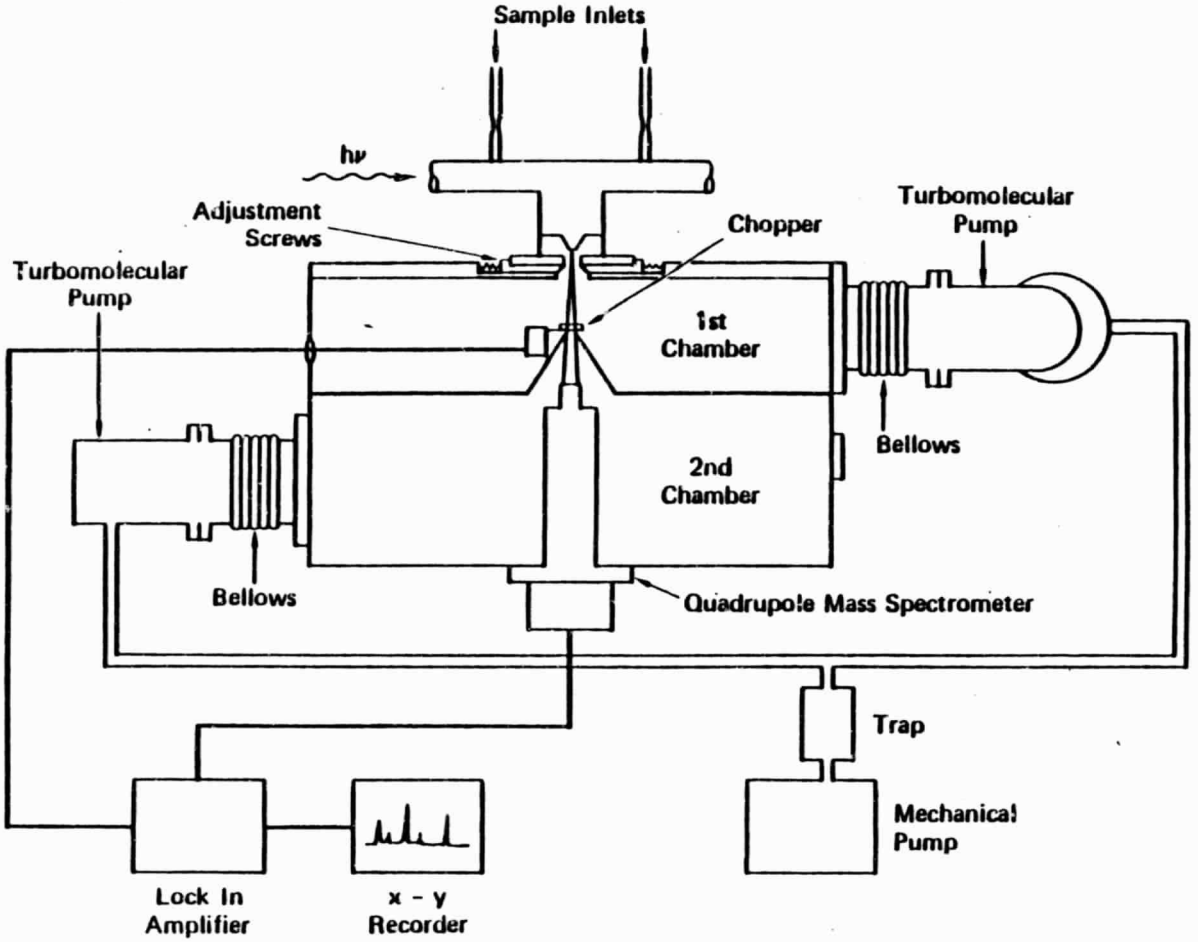

FIGURE 1 SCHEMATIC OF VERY LOW-PRESSURE PHOTOLYSIS APPARATUS

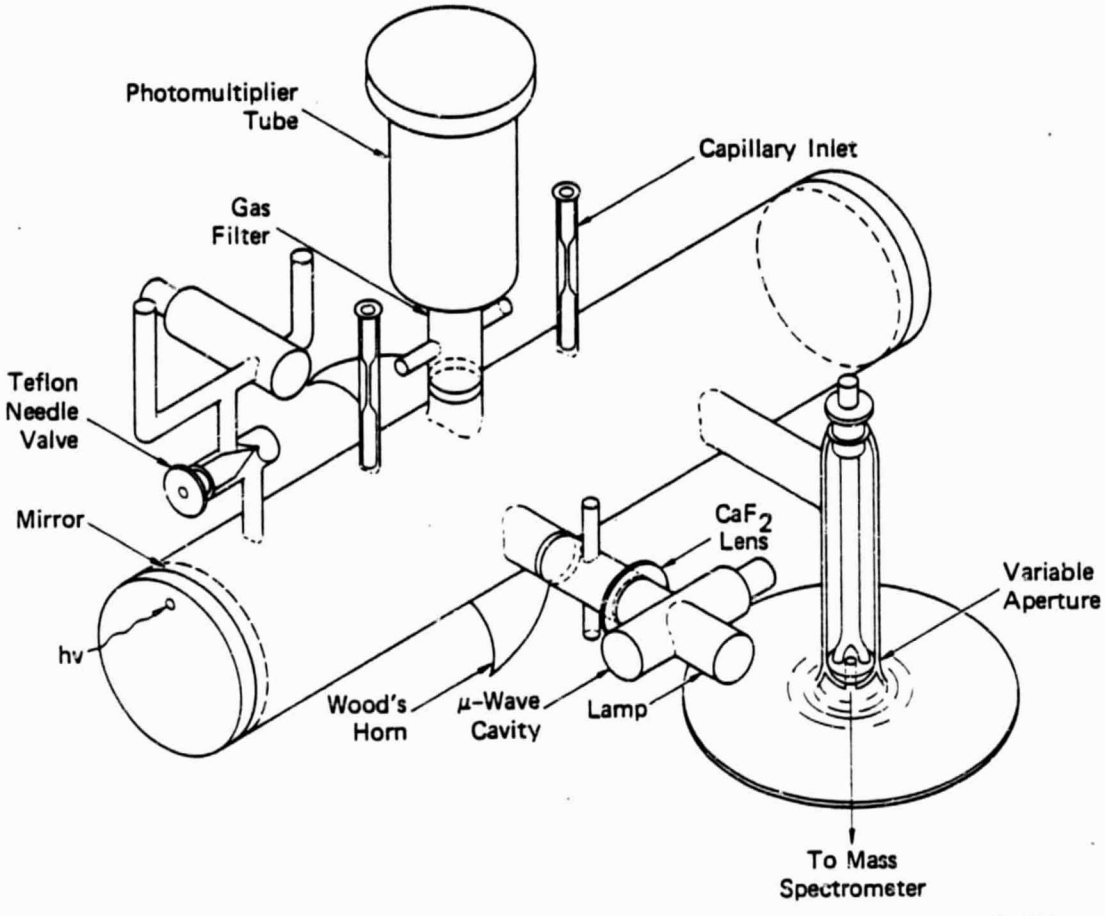

FIGURE 2 SCHEMATIC OF KNUDSEN CELL EQUIPPED WITH "WHITE-CELL" OPTICS (~50 passes)

radiation. The region between the lamp and the cell was flushed with a mixture of 1% O_2 in He in order to filter out 135 nm-175 nm light; the area between the photomultiplier tube and the cell was flushed with dry nitrogen. A CaF_2 lens (fl = 5 cm) was placed immediately in front of the resonance lamp to focus the light into the center of the cell. Single photon pulses from the photomultiplier went to an amplifier/discriminator (PRA Model 1763) whose output was stored in a multichannel analyzer (Nicolet Model 1072).

The white cell optics consisted of two mirrors (CVI Laser Corporation), 2-inch diameter, 0.3-m radius of curvature. The front optic was made from an AR-coated optosil base which was coated for high laser power at 290 nm ± 20 nm over the entire surface except for the 0.5-cm diameter laser entrance area at the very edge. The back optic was completely coated with the same high-power dielectric coating. The mirrors were carefully glued into aluminum mounts which were sealed to the cell with viton o-rings.

The laser light was aligned by eye into the cell and onto the optics in such a way as to produce the brightest, most uniform, eliptical pattern of approximately 50 multiple passes.[4] The laser output from the frequency-doubled Quantel dye laser consisted of 10 nsec, 8 mJ pulses, generated at 10 hertz. The beam was steered into the cell with four mirrors (CVI Laser Corporation) coated for high laser power at 290 nm ± 20 nm; the coated mirrors also served to filter out the undoubled laser light (570 nm). A power meter was placed in the beam immediately after the second steering optic, and the total energy did not change by any measurable amount when the undoubled light was blocked with a cutoff filter (Corning 7-54).

The reagent and titrant gases were introduced from an associated vacuum line through the capillary inlets, and the flow rates were measured using a calibrated 0.1 psi Validyne transducer. Just prior to data collection, the surface of the pyrex cell was silanized.

Photolysis of $ClONO_2$

The possible product channels involved in $ClONO_2$ photolysis at ~ 300 nm are given in Table 1. Several studies[5-8] at various wavelengths have found that path (b) is the dominant channel, while others[9,10] have concluded that path (d) is the important one. Thus, a reliable, quantitative measure of any O-atom production from the photolysis of $ClONO_2$ was an essential part of this experiment.

Table 1 $ClONO_2$ PHOTOLYSIS PRODUCT CHANNELS

Product Channel	Thermodynamic Threshold[11]
$ClONO_2 \xrightarrow{a} ClO + NO_2$	1108 nm
$ClONO_2 \xrightarrow{b} O(^3P) + ClONO$	509 nm
$ClONO_2 \xrightarrow{c} O(^1D) + ClONO$	282 nm
$ClONO_2 \xrightarrow{d} Cl + NO_3$	722 nm

The resonance fluorescence detection system was first checked by monitoring the signal from $O(^3P)$ generated on a steady-state basis. A mixture of 10% N_2 in He was dissociated in a μ-wave discharge (2450 MHz), and a fraction of this flow was metered directly into the cell. Excess NO was added to the cell and the N-atoms were converted to $O(^3P)$ ($N + NO \rightarrow N_2 + O$) very quickly.[12] The instantaneous concentration of O-atom was determined by the loss of NO observed at m/e = 30 for which the mass spectrometer was previously calibrated.

For a period of several hours, the plot of the resonance fluorescence signal intensity remained reproducibly linearly proportional to the concentration of the reacted NO; unfortunately, after longer times, the slope of such a plot changed. In order to eliminate the possibility that the instantaneous measure (Δ[NO]) of [O] was not representative of the true steady-state [O] in the cell because of complicating wall reactions, a mixture of 10% O_2 in He, instead of the N_2/He mixture, was discharged and metered into the cell.

The [O] was measured by titrating with excess NO_2 and monitoring the calibrated signal at m/e = 46 at the mass spectrometer. The decrease in the [NO_2] gave the steady-state [O] by $NO_2 + O \rightarrow NO + O_2$.[12] Although there was no major difference in fluorescence intensity, the same problem with long-term reproducibility of the resonance fluorescence signal intensity at a set [O] persisted. Not without precedent, the resonance lamp UV-output slowly varied during the day, regardless of the precautionary measures taken such as cold trapping for impurities in the makeup gases.

In order to avoid this problem in addition to calibrating the system under conditions as similar as possible to the $ClONO_2$ photolysis runs, a known concentration of NO_2 was photolyzed at 285 nm in the multipass cell ($NO_2 \xrightarrow{h\nu} NO + O$), and the time-dependent resonance fluorescence signal was averaged over many laser shots (~ 10,000), and recorded. An example of such a signal is shown in Figure 3.

At NO_2 concentrations of 3-10 x 10^{13} cm^{-3}, the decay rate of the $O(^3P)$ signal was consistent (within experimental error) with the reaction rate for $NO_2 + O \rightarrow NO + O_2$.[12] The signal was too small to be significant, without more time-averaging, when [NO_2] $\lesssim$ 3 x 10^{13} cm^{-3}. The instantaneous intensity (I_o) of the $O(^3P)$ signal was determined by extrapolation of the exponential decay to time = 0; it was then noted along with the NO_2 concentration. I_o versus

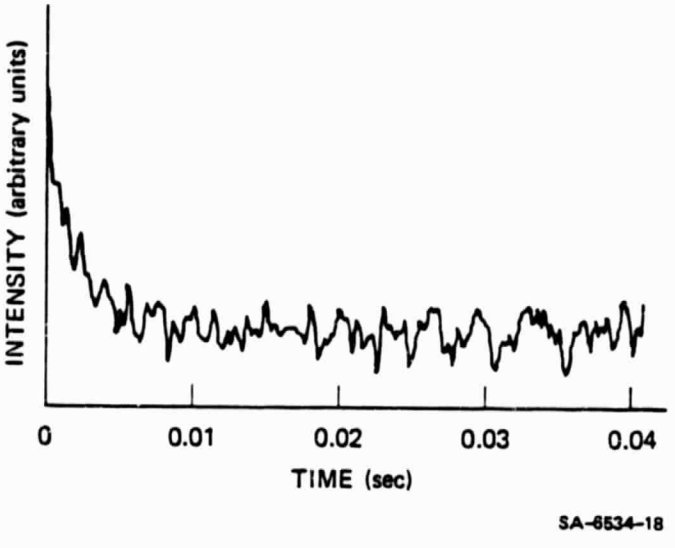

FIGURE 3 $O(^3P)$ PRODUCTION FROM NO_2 PHOTOLYSIS AT 285 nm (8192 shots)

[NO_2] was not measured over a wide concentration range due to the time limita tion on these preliminary experiments. However, there was no evidence that the resonance fluorescence signal was not well behaved. Although both the irradiated volume and the actual laser power in the cell could not be accurately measured, reasonable estimates were made and an upper limit to the instantaneous $O(^3P)$ concentration was determined using the reported value for the NO_2 absorption cross section[12] at 285 nm and a quantum yield of one.[12] No more than 1% of the NO_2 within the irradiated area was dissociated per pulse, thereby yielding $O(^3P) \leq 5 \times 10^{11}$ cm^{-3} at typical NO_2 concentrations (i.e., 5×10^{13} cm^{-3}). At those $O(^3P)$ concentrations, no significant deviation from proportional linearity was expected[3] for I_o versus [O]. Also, the steady-state dissociation of NO_2 (~ 2 %) as observed at the mass spectrometer (m/e = 46) provided a good consistency check on the above estimates.

NO_2 was photolyzed both before and after a $ClONO_2$ photolysis run was made. Thus the system was phenomenologically calibrated for determining the quantum yield of $O(^3P)$ product for any other molecule such as $ClONO_2$ whose absorption cross section[12] at 285 nm is known. Errors resulting from drift in the lamp output were minimized with this arrangement.

The $ClONO_2$ sample was prepared according to an established method.[13] Before purification, it contained substantial levels of Cl_2 (m/e = 70, 72, 74), ClO_2 (m/e = 67, 69), and Cl_2O (m/e = 86, 88, 90). After line passivation and partial purification, $ClONO_2$ (~ 5-8 $\times 10^{13}$ cm^{-3}) was introduced into the cell and photolyzed at 285 nm. A $ClONO_2$ mass spectrum (steady-state) before and during photolysis is shown in Figure 4. $ClONO_2$ had no measurable parent peak (m/e = 97,99). Several results are particularly noteworthy, even with this contaminated sample: (1) both HNO_3 (m/e = 63) and NO_3 (m/e = 62) were produced; (2) after normalizing relative to NO_2, the quantum yield for

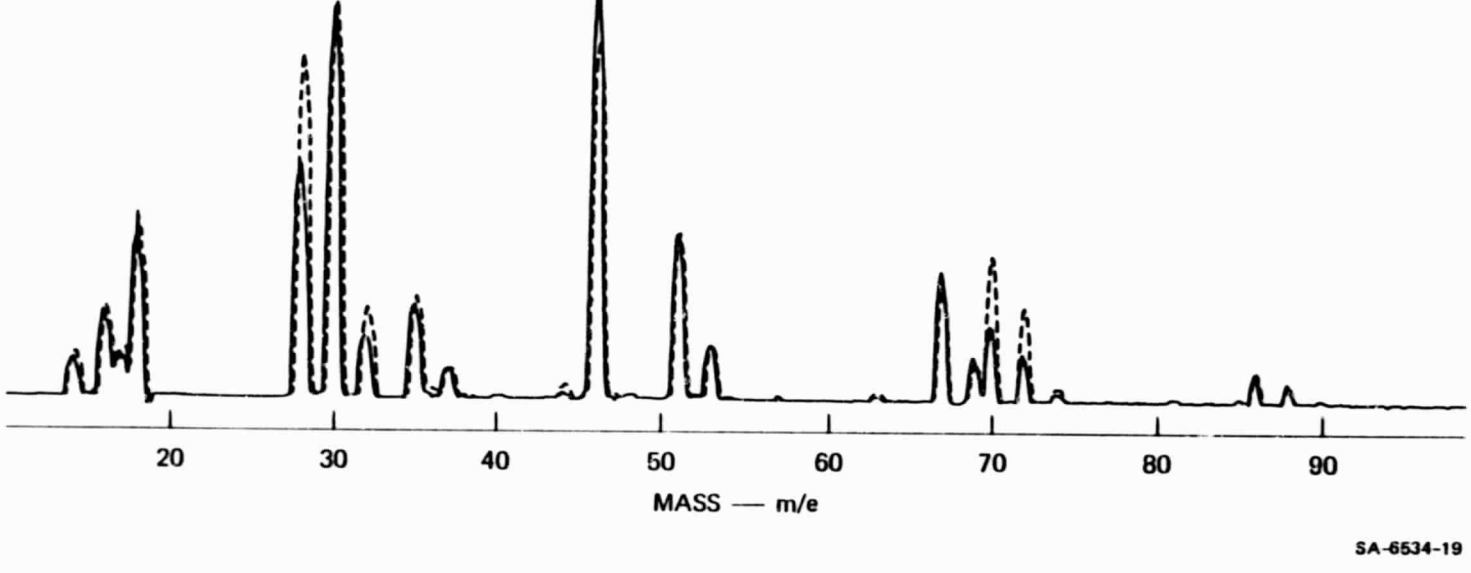

FIGURE 4 CHLORINE NITRATE (PLUS IMPURITIES) MASS SPECTRA

Solid line is unphotolyzed $ClONO_2$; dotted line is $ClONO_2$ undergoing photolysis.

$O(^3P)$ production from $ClONO_2$ appeared to be greater than one; (3) the percentage of $ClONO_2$ (m/e = 46) photolyzed was ~ 15%, instead of the anticipated 2-3%. These results certainly confirmed the ability to detect product NO_3 (m/e = 62, with time-averaging on the peak), as indicated in Figure 5. However, the photolysis of the impurities and the secondary reactions of those products with $ClONO_2$ (see Table 2) were obviously obscuring any primary product information.

Table 2 RATE CONSTANTS FOR SOME $ClONO_2$ AND IMPURITY REACTIONS

Reaction	Absorption Cross Section (T ≃ 298 K)	Ref.
$ClONO_2 + h\nu$ (285 nm) $\xrightarrow{?}$ $Cl + NO_3$	8.8×10^{-20} cm^2	12
$Cl_2 + h\nu$ (285 nm) → 2Cl	5×10^{-20} cm^2	14
$NO_2 + h\nu$ (285 nm) → NO + O	6.99×10^{-20} cm^2	12
$ClO_2 + h\nu$ (351 nm) → ClO + O	~ 1.2×10^{-18} cm^2	15
$Cl_2O + h\nu$ (285 nm) → ClO + Cl	1.1×10^{-18} cm^2	16

Reaction	Rate Constant (T≃ 298 K)	Ref.
$O + ClONO_2$ → Products	2.0×10^{-13} cm^3 molec^{-1} s^{-1}	12
$Cl + ClONO_2$ → Products	2.2×10^{-13} cm^3 molec^{-1} s^{-1}	12

The $ClONO_2$ sample was further purified by distillation at 175 K to remove the Cl_2 and by pumping at 195 K to remove the NO_2, ClO_2, and Cl_2O. The pumping at 195 K was continued until the parent peaks of the impurities were very

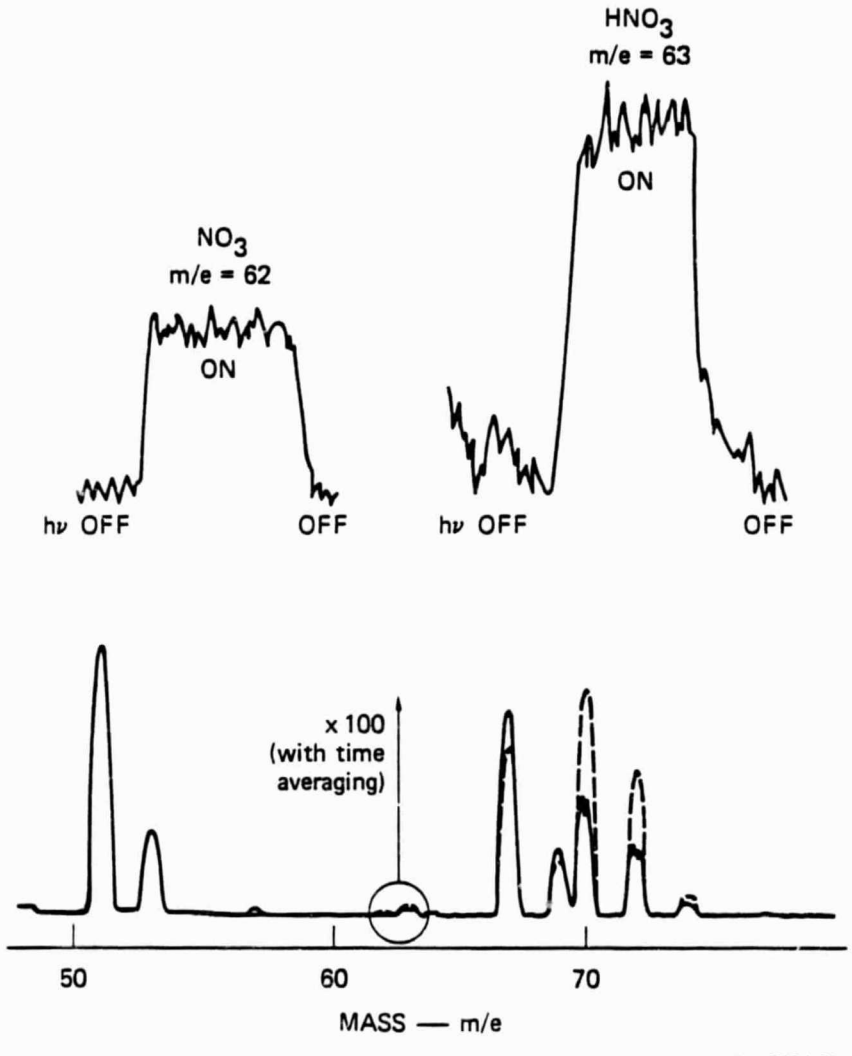

FIGURE 5 EXPANDED VIEW OF NO_3 AND HNO_3 FORMATION DURING PHOTOLYSIS

minimal and the m/e ratio of 46/51, 53, no longer changed. The $ClONO_2$ reservoir was left at 195 K (vapor pressure $\simeq$ 1 torr) for the photolysis experiments. A much cleaner sample of $ClONO_2$ ($\sim 5 \times 10^{13}$ cm^{-3}) was photolyzed, as given in Figure 6, which yielded the following results: (1) the quantum yield for $O(^3P)$ product, normalized to NO_2, was very small ($\sim$ 0.06); (2) Cl_2 (wall recombination of Cl) and a slight amount of HCl were produced; (3) NO_3 and HNO_3 were formed.

The mass spectrometer was locked onto NO_3 (m/e = 62); NO ($\sim 2 \times 10^{13}$ cm^{-3}) was added to the cell, and the NO_3 was titrated away via the reaction $NO + NO_3 \rightarrow 2NO_2$.[12] As indicated in Figure 7, this confirmed the fact that m/e = 62 was indeed due to NO_3. Prior to these experiments, the mass spectrometer had been calibrated with HNO_3, which gave an m/e ratio of 63/62 $\geq$ 100/1, where the same unit mass resolution was maintained. HNO_3 was clearly not contributing to m/e = 62, although the HNO_3 formation during photolysis (see Figure 5) may have been the result of NO_3 finding H-atoms on the cell surface, analogous to the formation of HCl when Cl is present.

Since the $ClONO_2$ purity cannot be determined to better than $\sim$ 90% by the method described above, the 0.06 $O(^3P)$ quantum yield is a conservative upper limit to path (b) and most likely is the result of the photolysis of impurities (NO_2 and/or ClO_2).

In order to eliminate the possibility that the NO_3 was being formed by the reaction $Cl + ClONO_2 \stackrel{?}{\rightarrow} Cl_2 + NO_3$, ethane was added to the cell ($[C_2H_6] \simeq 7 \times 10^{13}$ cm^{-3}) to preferentially react away Cl according to the reaction $Cl + C_2H_6 \rightarrow HCl + C_2H_5$.[12] Although the ethane reaction was not a "clean" titration reaction in that the C_2H_5 could further react in the cell, even with

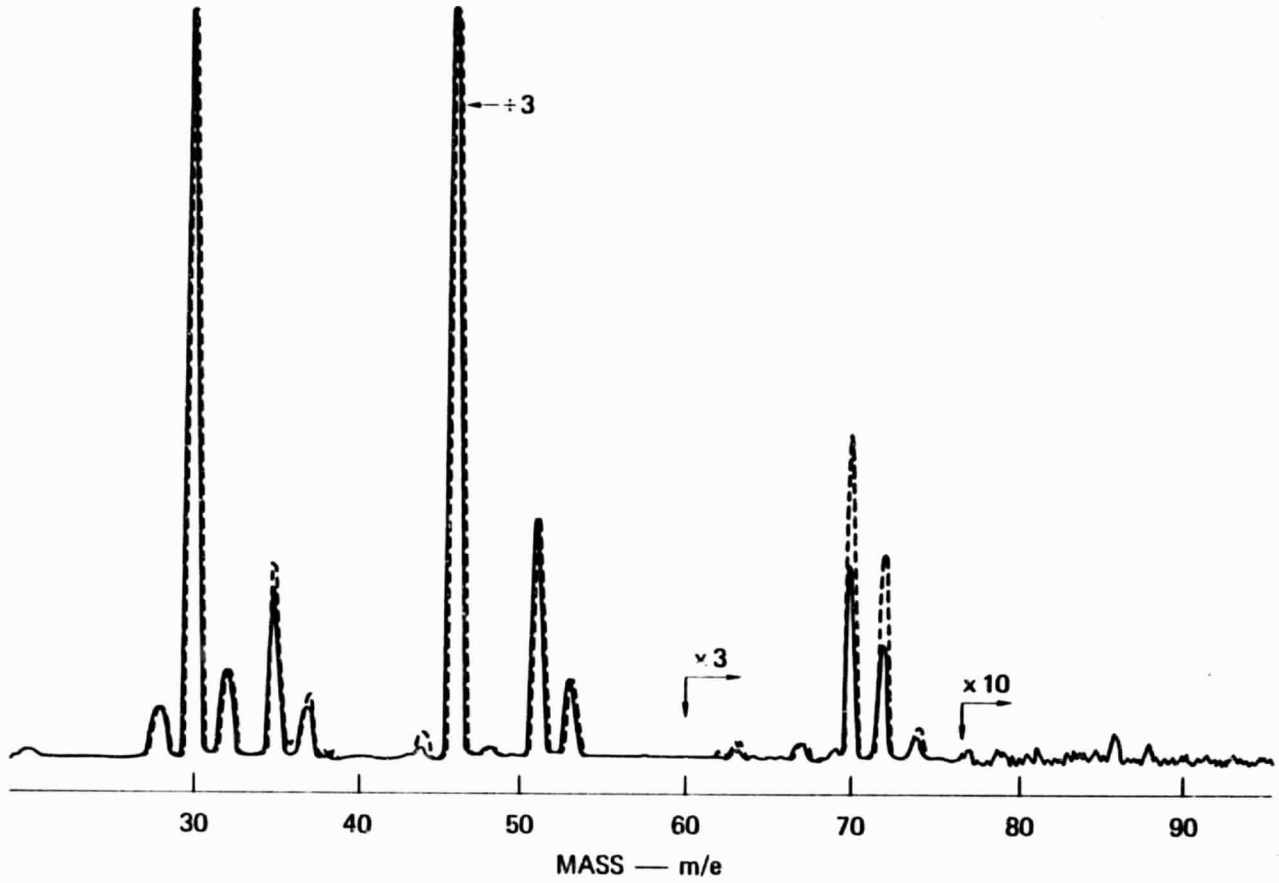

FIGURE 6 CHLORINE NITRATE MASS SPECTRA

Solid line is unphotolyzed $ClONO_2$; dotted line is $ClONO_2$ undergoing photolysis.

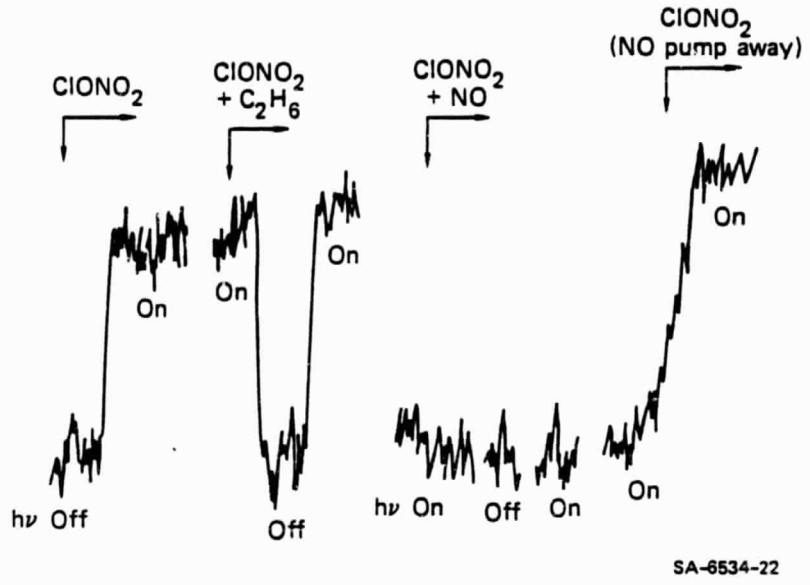

FIGURE 7 EXPANDED VIEW OF NO_3 (m/e = 62) FORMATION AND CHEMICAL TITRATION TESTS

$ClONO_2$ (k_e = 0.155 s^{-1}), Figure 7 shows that the [NO_3] remained the same, which strongly suggests that the NO_3 came directly from the photolysis of $ClONO_2$.

In summary, this preliminary study of the photolysis of $ClONO_2$ at 285 nm indicates that Cl + NO_3 is the major, if not the only, product channel.

Photolysis of N_2O_5

N_2O_5 was photolyzed at 285 nm in exactly the same manner as $ClONO_2$. The $O(^3P)$ detection sensitivity was calibrated with NO_2, as described above. The two most likely product channels for N_2O_5 photolysis at 285 nm and their thermodynamic thresholds are given in Table 3.

Table 3

Product Channel	Thermodynamic Threshold[11]
$N_2O_5 + h\nu \xrightarrow{e} NO_2 + NO_3$	1288 nm
$N_2O_5 + h\nu \xrightarrow{f} 2NO_2 + O$	393 nm

One study[17] has concluded that pathway (f) is the product channel at 254 nm. Therefore, serious efforts were again made to monitor any $O(^3P)$ product formed during photolysis.

N_2O_5 was prepared[18] by reacting NO_2 with excess O_3 and trapping the solid N_2O_5 into a pyrex vessel at 195 K. Before use, the N_2O_5 was trap-to-trap distilled and the NO_2 was pumped off at 250 K. The N_2O_5 reservoir was maintained at 250 K (vapor pressure $\tilde{=}$ 5 torr) during the experiments. N_2O_5 appeared to be very reactive on the pyrex surfaces of the vacuum line and inlets, even after hours of passivation, as previously observed by others.[19] To hasten the

passivation process and to prevent N_2O_5 from substantially converting to HNO_3, the reservoir and needle valve were moved as close as possible to the cell, with a bypass to the vacuum line only for meassuring pressure and flow rates. This procedure reduced the HNO_3 impurity level to ~ 20%; lower levels were not achieved. However, due to the low absorption cross section[12] at 285 nm for HNO_3 (8.8×10^{-21} cm^2), no complications from its photolysis products were anticipated.

The NO_2 impurity proved to be a more serious problem, since it was continually being formed from N_2O_5 decomposition.[18] After each run, the gas above the reservoir before the needle valve, and the NO_2, were pumped away at 250 K.

A mass spectrum of N_2O_5 (~ 5×10^{13} cm^{-3}) is given in Figure 8. N_2O_5 exhibited no parent peak (m/e = 108). A very small peak was meausred at m/e = 62 (m/e ratio 46/62 ≃ 900/1), which had not been previously observed.[20,21] NO (~ 3×10^{13} cm^{-3}) was added to the cell to confirm that it was a fragmentation peak from N_2O_5 and not the parent peak of the NO_3 decomposition product. At no time was there any measurable change in the intensity at m/e = 62 in the presence of NO.

The absorption cross section[22] for N_2O_5 at 285 nm (8.4×10^{-20} cm^2) is very similar to that for $ClONO_2$. Normalized to NO_2, again only 2-3% photolysis was expected. Given both the weak signal intensity at m/e = 62 from N_2O_5 and the high probability for similar mass spectral sensitivities for m/e = 62 from N_2O_5 and NO_3, any NO_3 photolysis product would probably have not been identifiably measurable mass spectrometrically, even with long time averaging. Nevertheless, the peak at m/e = 62 was carefully monitored during several photolysis runs; no significant change in the signal intensity was

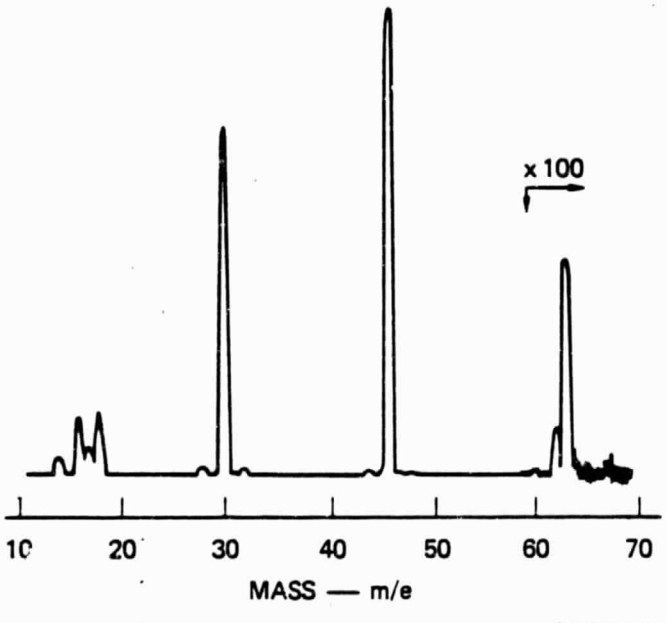

FIGURE 8 N_2O_5 MASS SPECTRUM

noted. A 2-3% change in the peak intensity would not have been measured with any certainty, given the low signal/noise. Thus, this observation was consistent with either product channel.

There was very little change in any part of the N_2O_5 mass spectrum during photolysis, which was expected because of product contributions at the major peaks. The peak at m/e = 46 was recorded (with long time-averaging), which indicated a very slight decrease ($\lesssim$ 1%) during photolysis. From prior calibrations, the mass spectrometer was found to be ~ 20% more sensitive to N_2O_5 than to NO_2 at m/e = 46. Sensitivities relative to NO_3 at m/e = 46 could not be determined or well estimated. Unfortunately, these data (or lack thereof) at m/e = 46 did not provide any confirmatory evidence as to the dominant product channel and, again, were consistent with either pathway.

Our final experimental efforts were directed at determining the quantum yield for $O(^3P)$ production. NO_2 resonance fluorescence calibration runs were conducted both before and after each N_2O_5 experiment, just as in the $ClONO_2$ study. In addition, after several of the N_2O_5 runs, steady-state [O] (~ 1×10^{13} cm^{-3}) was added to the cell from the μ-wave inlet in order to titrate any NO_2 impurity without reacting away any of the N_2O_5 (k_e = 0.147 s^{-1}).[20] In all but one titration, ~ 10% of the intensity at m/e = 46 reacted away, indicating a significant NO_2 impurity level. In one of the titrations, as much as 20% of m/e = 46 disappeared. (NO_2 was added afterwards to verify that excess [O] was still present, even in the case with high NO_2 impurity). Under these experimental conditions, an $O(^3P)$ quantum yield $\lesssim$ 0.10 would most likely be due to NO_2 photolysis rather than N_2O_5 photolysis.

After normalization, the resonance fluorescence decays, an example of which is given in Figure 9, yielded an $O(^3P)$ quantum yield $\simeq$ 0.10 (within experimental error). No single N_2O_5 run (for which the data were collected) indicated a higher quantum yield than the NO_2 impurity level; however, the purity levels were not checked on all the resonance fluorescence experiments.

The N_2O_5 concentration was not systematically varied in our data. Nonetheless, at $[N_2O_5] \simeq 5 \times 10^{13}$ cm^{-3} only minimal, if any, quenching of the photolysis as proposed by Connell[17] would have been taking place. Clearly, this is an area that requires further investigation.

In summary, since no significant $O(^3P)$ product can confidently be assigned to N_2O_5 photolysis, and, because there is no evidence to the contrary, the product channel giving $NO_2 + NO_3$ is indicated as the primary pathway for the photolysis of N_2O_5 at 285 nm.

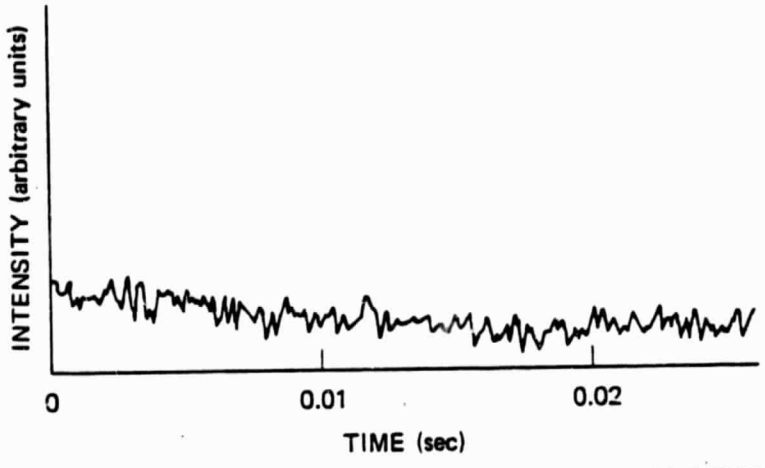

FIGURE 9 $O(^3P)$ RESONANCE FLUORESCENCE DECAY FROM N_2O_5 (~20,000 shots)

References

1. M. J. Rossi, J. R. Barker, and D. M. Golden, J. Chem. Phys., 9, 3722 (1979).

2. D. M. Golden, G. N. Spokes, and S. W. Benson, Angew. Chem. (Int'l), 12, 534 (1973).

3. M.A.A. Clyne and H. W. Cruse, JCS Faraday II, 68, 1281 (1972).

4. J. Altmann, R. Baumgart, and C. Weitkamp, Applied Optics, 20, 995 (1981).

5. S. M. Alder-Golden and J. R. Wiesenfeld, Chem. Phys. Lett., 82, 281 (1981).

6. M. J. Kurylo, Chem. Phys. Lett., 49, 467 (1977).

7. M. J. Kurylo and R. G. Manning, Chem. Phys. Lett., 48, 279 (1977).

8. W. S. Smith, C. C. Chau, and F. S. Rowland, Geophys. Res. Lett., 4, 517 (1977).

9. J. S. Chang, J. R. Barker, J. E. Davenport, and D. M. Golden, Chem. Phys. Lett., 60, 385 (1979).

10. J. J. Margitan, unpublished data, 1982.

11. J.A.N.A.F. Thermochemical Tables, Nat'l. Stand. Ref. Data Serv., U.S. Nat'l Bur. Stand., NSRDS-NBS (1971).

12. Chemical Kinetic and Photochemical Data for Use in Stratospheric Modelling, JPL Publication 81-3, W. B. DeMore, ed., 1981.

13. C. J. Schack, J. Inorg. Chem., 6, 1938 (1967).

14. D. J. Seery and D. Britton, J. Phys. Chem., 68, 2263 (1964).

15. R. T. Watson, J. Phys. Chem. Ref. Data, 6, 871 (1977).

16. C. L. Lin, J. Chem. Eng. Data., 21, 411 (1976).

17. P. S. Connell, "The Photochemistry of Dinitrogen Pentoxide," Ph.D. Thesis, University of California, Berkeley (1979).

18. G. Schott and N. Davidson, J. Am. Chem. Soc., 80, 1841 (1958).

19. E. D. Morris, Jr. and H. Niki, J. Phys. Chem., 77, 1929 (1973).

20. E. W. Kaiser and S. M. Japar, Chem. Phys. Lett., 54, 265 (1978).

21. D. L. Ames and D. W. Turner, Proc. R. Soc. Lond. A., 348, 175 (1976).

22. R. A. Graham, "Photochemistry of NO_3 and the Kinetics of the N_2O_5-O_3 System," Ph.D. Thesis, University of California (1975).

Chaapter IX

HETEROGENEOUS REACTION OF N_2O_5 AND H_2O

John R. Barker and David M. Golden

HETEROGENEOUS REACTION OF N_2O_5 AND H_2O

John R. Barker and David M. Golden
Department of Chemical Kinetics
SRI International, Menlo Park, CA 94025

INTRODUCTION

Nitrogen oxides of natural and of anthropogenic origins can interact in the stratosphere to form dinitrogen pentoxide. Once formed, N_2O_5 acts as a short-lived reservoir species, its major fate being photolysis to regenerate odd oxygen species.[1] It is known from laboratory studies that N_2O_5 hydrolyzes rapidly on surfaces and very slowly in the gas phase,[2] and it has been recognized that hydrolysis of N_2O_5 on stratospheric aerosol particles may produce nitric acid, which can rain out of the atmosphere. Because so much of the atmospheric NO_x spends short periods of time tied up in N_2O_5, a realtively minor reaction pathway to produce HNO_3 can have an important quantitative effect on stratospheric composition and the ozone distribution.

The stratospheric aerosols have been determined to consist primarily of sulfuric acid solutions in water (typically, 70-90 weight percent H_2SO_4).[3] The maximum aerosol number density occurs at about 20 km with aerosol diameters ranging from 0.01 to 1.0 μm.[4] The structure of the aerosol particles is not well characterized, but they may consist of frozen super-cooled liquid cores surrounded by a thin film of liquid.[5]

It is desirable to determine the efficiency with which N_2O_5 reacts with H_2SO_4/H_2O mixutres in order to assess whether such reactions can play significant roles in stratospheric chemistry. In a previous survey[6] by this laboratory of heterogeneous reaction involving 100% H_2SO_4 surfaces, the reaction probability (γ) of N_2O_5 was measured to be 3.8×10^{-5}, and there were indications that a small quantity of NO_2 was released as a gas-phase product. In the same study, the expected hydrolysis product, HNO_3, was found to react with $\gamma = 2.4 \times 10^{-4}$. These reaction efficiencies are too low to be important in stratospheric chemistry, but the question remained of the effect of adding water vapor to the system. This question is addressed in the present study.

EXPERIMENTAL

The experimental apparatus and technique have been described in detail elsewhere.[6,7] Briefly, the apparatus consists of a two-chamber Knudsen cell reactor (Figure 1) coupled with a modulated molecular beam mass spectrometer (MMBMS), which has been described in the literature. A regulated flow of reactant gas enters the reactor through one of the two capillary inlets and a flow of water vapor can be independently introduced through the other. Absolute flow rates are measured by timing pressure increases in calibrated volumes. The total pressure in the reactor is maintained below about 10 mtorr so that the mean-free path of the gas molecules is greater than the diameter of the escape aperture, ensuring that Knudsen

flow through the aperture controls the residence time (τ) in the reactor. The volume of the reactor is 427 cm^3 and the escape rate constant ($1/\tau$) is $k_e = 1.21/\pm M^{-1/2}$ at room temperature for species of molecular weight M. The composition of the effluent gas is monitored with the MMBMS, and the results are recorded on a strip-chart recorder or are stored in the memory of a signal averager.

The main chamber of the two-chamber reactor is isolated from the sulfuric acid surface by an externally operated valve. When the valve is opened, the H_2SO_4 surface is exposed, and the reactant gas may undergo reaction, altering the composition of the effluent gas monitored by the mass spectrometer. The mass spectrometer used in the series of experiments reported here was a Finnigan model 400 quadrupole.

Dinitrogen pentoxide was synthesized by mixing ozone generated in a stream of pure oxygen with a small amount of NO_2 and condensing the N_2O_5 at 195 K. Ozone was always present in excess and the resulting N_2O_5 was initially free of NO_2, although small amounts of HNO_3 were present, presumably due to heterogeneous reaction of N_2O_5 with traces of H_2O. The pure anhydrous nitric acid used for mass spectrometer calibration was synthesized by mixing $NaNO_3$ with concentrated H_2SO_4 and condensing the product gas at 195 K. Nitrogen dioxide was mix[illegible]ernight with a great excess of pure oxygen to convert any nitric oxide to NO_2 and was then thoroughly degassed by bulb-to-bulb distillation.

The sulfuric acid used as the heterogeneous surface was placed in a pyrex watch-glass to form a pool of circular diameter 4.8 cm. The concentrated acid was pumped at $< 10^{-6}$ torr over-night prior to use to insure that it was thoroughly degassed and as dehydrated as feasible.

RESULTS AND DISCUSSION

Typically, the freshly synthesized N_2O_5 showed little evidence of NO_2 contamination, but after 30 minutes, the mass spectrum had changed significantly. Three mass peaks were routinely monitored: m/e = 30, 46, 62/63. The sensitivity of the mass spectrometer was too low to permit unit mass resolution at m/e = 62/63 and total intensity of both peaks was measured. Since no mass 62 peak was observed for pure N_2O_5, but there was a measurable contribution from pure HNO_3, signal at this mass was indicative of the presence of HNO_3. However, the mass spectrometer sensitivity was so poor and the signal was so noisy that quantitative measures of HNO_3 could not be obtained.

In the absence of added water vapor, N_2O_5 reacted with the sulfuric acid surface in a consistent manner, such that 40 ± 10% of the N_2O_5 was lost to the surface. There was no evidence that gas was released as a product, contrary to the survey results reported earlier.

For this experiment,

$$\gamma = \frac{A_h}{A_s} \left[\frac{I_o}{I} - 1 \right]$$

where I and I_o are the mass spectrometer signal intensities without and with the sulfuric acid exposed, respectively. A_h is the effective area of

the escape aperture and A_s is the area of the sulfuric acid pool.[6,7] For the present series of experiments, $A_h/A_s = 4.5 \times 10^{-4}$. Thus, in the absence of H_2O vapor, $\gamma = 3 \times 10^{-4}$, about an order of magnitude larger than reported earlier and almost identical to the result obtained earlier for HNO_3.[6,7] This result was found to be independent of N_2O_5 concentration, and it was reproduced using several different batches of N_2O_5. The uncertainty on γ is no larger than ± 50%.

When water vapor was added to the system, a contribution was observed at m/e = 62/63, indicative of the formation of HNO_3. Unfortunately, the signal was too noisy to be of quantitative usefulness. Analysis of the results indicated that as much as 50% of the N_2O_5 was converted to HNO_3 when large amounts of H_2O vapor were introduced. Despite this complication, the loss of N_2O_5 on the H_2SO_4 surface seemed to be substantially unaffected by the presence or absence of water vapor. It was also concluded that HNO_3 is lost on the H_2SO_4 surface with about the same γ as measured for N_2O_5 (consistent with the earlier results).

The reason for the discrepancy between the present results for N_2O_5 and those reported earlier is not known, but it may be related to the way concentrations were monitored in the earlier work.[6,7] Previously, only m/e = 46 was monitored even though the system can contain N_2O_5, NO_2, and HNO_3, all of which give contributions at that mass. In the present experiments, the situation is a little better, but not completely satisfactory due to the poor sensitivity for m/e = 62/63. In future experiments on this reaction, a better mass spectrometer will be employed.

If we accept that for N_2O_5 $\gamma = (3 \pm 1.5) \times 10^{-4}$, we can estimate the effect of heterogeneous reactions on loss of N_2O_5 in the stratosphere. For

typical concentrations and sizes of stratospheric aerosols, the collision frequency of an N_2O_5 molecule with the aerosol particles has been estimated to be ~ 10^{-5} s^{-1}.[6,7] Thus, the total first-order rate of loss of N_2O_5 due to heterogeneous reaction is ~ 3 x 10^{-9} s^{-1}. This value can be compared with the photolysis loss rate for N_2O_5 at 20 km, ~ 5.3 x 10^{-5} s^{-1},[8] which is about four orders-of-magnitude faster. Unimolecular decomposition of N_2O_5 to form NO_2 and NO_3 has a rate constant of ~ 2 x 10^{-8} s^{-1} at 20 km,[8] an order of magnitude faster than the estimated heterogeneous loss rate. Thus, we conclude that heterogeneous reaction of N_2O_5 plays only a small role at night and is insignificant when photolysis is possible.

References

1. D. L. Baulch, R. A. Cox, P. J. Crutzen, R. F. Hampson, Jr., J. A. Kerr, J. Troe, and R. T. Watson, J. Phys. Chem. Ref. Data, 11, 327 (1982).

2. E. D. Morris and H. Niki, J. Phys. Chem., 77, 1929 (1973).

3. P. Hamill, O. B. Toon, and C. S. Kiang, J. Atmos. Sci., 343, 1104 (1977).

4. O. B. Toon and J. B. Pollack, J. Geophys. Res., 78, 7051 (1973).

5. G. V. Ferry and H.-Y. Lem, Second International Conference on Environmental Impacts of Aerospace Operations in the High Atmosphere, Amer. Meteor. Soc., 27 (1974).

6. A. C. Baldwin and D. M. Golden, Science, 206, 562 (1979).

7. A. C. Baldwin, in Heterogeneous Atmospheric Chemistry, Geophysical Monograph 26, D. R. Schryer, ed., American Geophysical Union, Washington, D.C., 1982, p. 99.

8. D. J. Wuebbles, private communications (1981).